TÉCNICO LISBOA

Mapping cerebrovascular reactivity using breath-hold and fMRI: Application to migraine patients and hormonal controls

Ana Beatriz Brissos Raposo

Thesis to obtain the Master of Science Degree in

Biomedical Engineering

Supervisors: Prof. Patrícia Margarida Piedade Figueiredo
Dr. Raquel Santos Gil-Gouveia

Examination Committee

Chairperson: Prof. Rita Homem de Gouveia Costanzo Nunes
Supervisor: Prof. Patrícia Margarida Piedade Figueiredo
Member of the Committee: Dr. Joana Carolina Sequeira Pinto

December 2021

Dedicated to my grandfather.

Declaration

I declare that this document is an original work of my own authorship and that it fulfills all the requirements of the Code of Conduct and Good Practices of the Universidade de Lisboa.

Preface

The work presented in this thesis was performed at LaSEEB, a research lab of ISR-Lisboa at Instituto Superior Técnico, University of Lisbon (Lisbon, Portugal), between February and December of 2021, under the supervision of Professor Patrícia Figueiredo and Doctor Raquel Gil-Gouveia from Hospital da Luz.

Acknowledgments

Firstly, I would like to express my sincere gratitude to my supervisors, Prof. Patrícia Figueiredo and Dr. Raquel Gil-Gouveia for the support and guidance through all the stages of this dissertation. Without their shared knowledge and experience, this work would not have been possible. Their enthusiasm about their work and particularly about this project was demonstrated in each and every meeting, which motivated to always give my best over the last months and inspired me for my future professional life.

Further, I would like to thank the rest of the LaSEEB team for their constant availability and friendliness, particularly to Amparo, Ana, Thanos, Catarina, Gustavo and especially Inês.

I would also like to thank the volunteers who participated in this study for their good-will, empathy and braveness.

I would like to give my warmest thanks to the colleagues who became home away from home: Inês, Gracias, Leonor, Laura, Margarida, Mariana and Rita. Thank you for teaching me so much about friendship and for making these 5 years so full of good memories. I would also like to thank my hometown friends for the constant support and nonsense laughs: Maria Beatriz, Mariana Matias, Mariana Moura, Rita and Sara. You are forever in my heart.

Finally, I want to thank my family. Mom and dad, thank you for your unconditional love and support. Brother, thank you for the programming lessons and the countless homemade dinners along with the best conversations. Thank you for always being there for me during the good and bad times, I cannot thank you enough.

Abstract

Migraine is a disabling disease that is highly complex and incompletely understood. Cerebrovascular Reactivity (CVR) measurements have the potential to detect cerebrovascular impairment and have been shown to be altered in migraine. Given this, the objective of this work was to to clarify neurovascular mechanisms by investigating CVR changes during pain (ictal) and pain-free (interictal) phases in migraine. Patients with menstrually-related migraine were selected in order to facilitate the study of the two phases. To control for the effects of hormonal variations associated with the menstrual cycle, healthy controls were studied in the premenstrual and midcycle phases. Blood-oxygenation Level Dependent-functional Magnetic Resonance Imaging (BOLD-fMRI) data were acquired during a breath-holding (BH) task and analysed using 3 methods (one PetCO_2-based and two paradigm-based) to obtain maps characterizing CVR. In the control group, increased CVR and reduced delays were detected in the premenstrual vs midcycle session (not significant). Additionally, the group delay maps showed alterations in the posterior area that included the occipital lobe region and the CVR in the occipital lobe was increased in the premenstrual vs the midcycle sessions (not significant). This suggests that alterations in the occipital region in migraineurs during the ictal phase described in previous studies are associated with alterations related to the menstrual cycle and not with the migraine. These findings contribute with new evidence to the limited literature, being the first work investigating CVR in both migraineurs and hormonal controls in a longitudinal approach.

Keywords

Cerebrovascular Reactivity, Functional Magnetic Resonance Imaging, Breath-holding, Menstrually-related Migraine, Hormonal Controls.

Resumo

A enxaqueca é uma doença debilitante altamente complexa e incompletamente compreendida. A avaliação da vasoreactividade cerebral (CVR) tem potencial para detetar disfunções cerebrovasculares e tem mostrado alterações em doentes com enxaqueca. Assim, o objetivo deste trabalho foi elucidar os mecanismos neurovasculares através da investigação de alterações na CVR durante as fases com (ictal) e sem crise (interictal) da enxaqueca. Foram selecionados pacientes com enxaqueca relacionada com a menstruação de forma a facilitar o estudo das fases. De forma a controlar para os efeitos das variações hormonais ao longo do ciclo menstrual, controlos saudáveis foram estudados nas fases premenstrual e a meio do ciclo. Dados de ressonância magnética funcional (fMRI) foram adquiridos durante uma tarefa de apneia (BH) e analisados utilizando 3 métodos (um baseado no $PETCO_2$ e dois baseados no paradigma) de forma a obter mapas de CVR. No grupo controlo, a CVR revelou estar aumentada e os atrasos na resposta diminuídos na fase premenstrual vs a meio do ciclo (não significativamente). Além disso, os mapas de atraso de grupo revelaram alterações na parte posterior que inclui o lobo occipital e a CVR no lobo occipital mostrou estar aumentada na fase premenstrual vs a meio do ciclo (não significativamente). Isto sugere que as alterações na região occipital em pacientes com enxaqueca reportadas em estudos anteriores estão associadas com o ciclo menstrual. Estes resultados contribuem com nova evidência para a reduzida literatura, tratando-se do primeiro estudo longitudinal que avalia a CVR em pacientes com enxaqueca e controlos hormonais.

Palavras Chave

Vasoreactividade Cerebral, Ressonância Magnética Funcional, Apneia, Enxaqueca relacionada com a Menstruação, Controlos Hormonais.

Contents

List of Figures

List of Tables

Acronyms

ACA Anterior Cerebral Arteries

ANOVA Analysis of Variance

ANTs Advanced Normalization Tools

ASL Arterial Spin Labelling

BA Basilar Arteries

BBR Boundary-Based Registration

BET Brain Extraction Tool

BH breath-holding

BOLD Blood-oxygenation Level Dependent

BOLD-fMRI Blood-oxygenation Level Dependent-functional Magnetic Resonance Imaging

CBF Cerebral Blood Flow

CBV Cerebral Blood Volume

CGRP Calcitonin Gene-Related Peptide

$CMRO_2$ Cerebral Metabolic Rate of Oxygen

CO_2 Carbon Dioxide

CSD Cortical Spreading Depression

COPEs Contrast of Parameter Estimates

CSF Cerebrospinal Fluid

CVR Cerebrovascular Reactivity

dHb deoxy-Hemoglobin

DOF Degrees Of Freedom

E2 Estradiol

EPI Echo-Planar Imaging

EVs Explanatory Variables

FAST FMRIB of the Brain Automated Segmentation Tool

FEAT FMRIB of the Brain Expert Analysis Tool

FILM FMRIB of the Brain Improved Linear Model

FIRST FMRIB's Integrated Registration and Segmentation Tool

FLIRT FMRIB's Linear Image Registration Tool

fMRI Functional Magnetic Resonance Imaging

FMRIB Functional Magnetic Resonance Imaging of the Brain

FNIRT FMRIB's Non-Linear Registration Tool

FSL FMRIB's Software Library

FUGUE FMRIB's Utility for Geometrically Unwarping EPI

FWHM Full Width Half Maximum

GE-EPI Gradient Echo-Echo Planar Imaging

GLM General Linear Model

GM Gray Matter

GRAPPA Generalized Autocalibrating Partial Parallel Acquisition

GUIs Graphical User Interfaces

HC Healthy Controls

HRF Hemodynamic Response Function

HbO_2 Oxy-hemoglobin

ICA Internal Carotid Arteries

ICHD-3 International Classification of Headache Disorders, 3rd edition

LSL Lab Streaming Layer

MA Migraine with Aura

MCA Middle Cerebral Arteries

MCFLIRT Motion Correction FMRIB's Linear Registration Tool

MM Menstrual Migraine

MNI Montreal Neurologic Institute

MO Migraine without Aura

MPRAGE Magnetization-prepared Rapid Gradient Echo

MRI Magnetic Resonance Imaging

MRM Menstrually-related Migraine

NO Nitric Oxide

O_2 Oxygen

P4 Progesterone

$PaCO_2$ Partial Pressure of Arterial Carbon Dioxide

PCA Posterior Cerebral Arteries

PDB Paced Deep Breathing

PEs Parameter Estimates

PET Positron Emission Tomography

$PetCO_2$ Partial Pressure of End-tidal Carbon Dioxide

PSC Percent Signal Change

RESEL Resolution Element

ROIs Regions of Interest

rs-fMRI Resting-state Functional Magnetic Resonance Imaging

SMS Simultaneous Multi-slice

SNR Signal-to-Noise Ratio

SPECT Single Positron Emission Tomography

SPG Shenopalatine Ganglion

SSN Superior Salivatory Nucleus

SUSAN Smallest Univalue Segment Assimilating Nucleus

TCD Transcranial Doppler

TD Temporal Derivative

TE Echo Time

TR Repetition Time

TTP Time-to-peak

VAS Visual Analogue Scale

VBA Vertebrobasilar Arteries

VIP Vasoactive Intestinal Peptide

WM White Matter

Chapter 1

Introduction

The study described in this dissertation is part of the MIGN2Treat project, which has the objective to study multimodal neuroimaging biomarkers in the migraine and is a result of a collaboration between LaSEEB (Evolutionary Systems and Biomedical Engineering Lab) of ISR-Lisbon (Institute for Systems and Robotics) and Hospital da Luz (Lisbon, Portugal). This dissertation specifically aims to investigate neurovascular changes of migraine by looking into differences in Cerebrovascular Reactivity (CVR) in distinct periods of this cyclic disease and of the menstrual cycle in hormonal controls. To do so, analysis of Blood-oxygenation Level Dependent-functional Magnetic Resonance Imaging (BOLD-fMRI) data acquired during a breath-holding (BH) challenge from a group of patients with (menstrually-related) episodic migraine without aura was conducted, such as from a group of hormonal healthy controls. Each participant was scanned under two different conditions: during a migraine attack (ictal headache phase) and during an attack-free period (interictal phase) in the case of patients and during the premenstrual and midcycle phases of the menstrual cycle in the case of controls. This chapter starts by describing the motivation behind this dissertation (1.1), followed by a theoretical background of migraine (1.2). Next, relevant information about the concept of cerebrovascular reactivity (CVR) is presented (1.3). Following, guidance regarding the best practices when using BH as vasoactive stimulus to measure CVR is described (1.4), followed by the state of the art where a literature review can be found 1.5. Finally, the main objectives of this dissertation (1.6) and the dissertation outline (1.7) are presented.

1.1 Motivation

Migraine is one of the most prevalent and disabling diseases on a global scale [4–9], predominantly affecting young women in their most productive life years [6, 7, 10, 11]. Moreover, migraine is a cyclic disorder composed of headache (and other associated symptoms) and headache-free periods that is thought to result from a combination of genetic and environmental factors, which makes it highly complex

and incompletely understood [10, 12–14]. Currently, there are no biomarkers used in the clinical practice to help the diagnosis process or effective treatment to end or prevent attacks [10, 13, 14].

Migraine has been associated with cerebrovascular [15–18] and cardiovascular diseases [19–21]. In recent years, it has been suggested that this vasculopathy may be related with a dysfunction in the cerebral endothelium [20]. Furthermore, in the case of menstrual and menstrually-related migraine, perimenstrual attacks seem to be triggered by the decrease of the hormone estradiol that occurs prior to menstruation [22–26]. Estradiol plays an important role in the regulation of the vascular endothelium [25], which means that the vasculopathy in migraine may be intensified near menstruation [27]. Therefore, it seems important to study and take into account the effect of menstrual cycle hormonal alterations when assessing cerebrovascular function in migraine. However, there are few studies evaluating cerebrovascular changes through the menstrual cycle and the menstrual migraine cycle.

CVR measurements have great potential as a way to detect the suspected brain vascular endothelium dysfunction. There are only few studies assessing CVR in migraine and this was commonly done using Transcranial Doppler (TCD) Ultrasound. From these, it has been suggested that CVR is impaired in the posterior circulation of migraineurs [15, 28–31]. In the last years, BOLD-fMRI has been shown to be a more promising technique to measure CVR than TCD. However, there were only two studies assessing CVR in migraine using BOLD-fMRI [32, 33]. Additionally, most studies investigated CVR in a case-control approach, assessing it in the pain-free phase of migraine. Being migraine a cyclic disorder, greater potential could be achieved by performing a longitudinal study, studying patients in both phases. This was done in a previous dissertation analysing data from a study that made use of BOLD-fMRI and a BH task, where it was shown that there is increased CVR in the occipital area of migraineurs in the pain phase, when compared to the pain-free phase [33]. However, this study did not include controls. More significant results should be achieved by taking into account the natural cerebrovascular alterations through the menstrual cycle. Additionally, although a BH task has been done, the Partial Pressure of End-tidal Carbon Dioxide ($PetCO_2$) was not recorded, which could take into account the variations in task performance and normalize CVR measurements [3, 34–36].

1.2 Migraine

Migraine affects approximately 14% of the worldwide population and is the second in years lived with disability, according to the World Health Organization. Additionally, it is associated with medication overuse headache, that constitutes itself a top cause of disability worldwide [4–8].

Until puberty, migraine incidence between women and men is similar, but after puberty the one in females increases more than in men [37]. Therefore, although being prevalent in both genders and all ages, migraine predominantly affects women, following a 3:1 ratio [11]. Specifically, it is more prevalent

among young and middle-aged women between ages 15 and 49, which usually correspond to their most formative and productive life years. In this group, migraine assumes the first place in years lived with disability, which means that no other disease is responsible for more years of lost healthy life [6, 7, 10].

Migraine is a complex disorder characterized by not only headaches with specific features, but also other associated symptoms. It is a cyclic disease as it is composed of an ictal state with attacks alternated with an attack-free interictal state. In the ictal state, four phases of the attack can be defined: the premonitory, aura, headache and postdrome [11, 14, 38]. The headache phase is the most notorious phase in migraine episodes and all the phases can appear in the mentioned sequential order or overlap [8, 11]. The migraine cycle is presented in figure 1.1, with the ictal phase consisting of a whole migraine attack, where the duration of the four phases and the main associated symptoms are shown.

The preictal or prodrome phase usually begins as early as 2 days before the headache onset and can last up to 3 days over this. This phase is experienced by 70-80% of the migraine patients in at least some of their attacks, but only a minority is able to recognize it in the majority of the attacks where it happens [38, 39]. Its symptoms include fatigue, yawning, sleep disturbances, changes in appetite, food cravings, nausea, concentration problems, mood changes, photophobia (light sensitivity), phonophobia (sound sensitivity), neck pain/stiffness, among others [8, 38, 40–45]. Some of these symptoms such as for example photophobia and sleep disturbances can be hard to distinguish from triggers (external factors that increase the likelihood of having an attack) such as bright light and changes in the sleep pattern, respectively [11, 41, 44, 46, 47]. The postdrome phase follows headache resolution up to 48 hours. Its symptoms are quite similar to the ones of the prodrome phase, generally including fatigue and lack of concentration [40].

In about 20% of migraine patients, the disorder is associated with an aura phase that begins right before and/or during the headache attack and lasts for 5 minutes to 1 hour. It is characterized by transient neurological symptoms that can be visual (most frequent), somatosensory , related with speech/language or motor disturbances [11, 12, 48].

The headache phase lasts 4-72h and is typically unilateral, located in the forehead, eye or temporally (corresponding to the first division of the trigeminal nerve), pulsating/throbbing and moderate to severe in intensity. It is accompanied with cognitive impairment, loss of appetite, nausea, vomiting, photophobia and/or phonophobia, odor, sensitivity to touch and even to movement (kinesiophobia) [10–12, 40, 48–50].

The migraine disorder is classified according to the frequency of the headache attacks. Briefly, 15 or more days a month with headache correspond to chronic migraine, while 14 or fewer days a month corresponds to episodic migraine, the latter subtype being the most common [14, 27, 40].

Currently, there are no biomarkers used in the clinical practice to help the diagnosis process or effective treatment to end or prevent attacks. Given this and the worldwide burden of this disease, it is crucial to better understand its pathophysiology - the complex workings of it and the brain regions

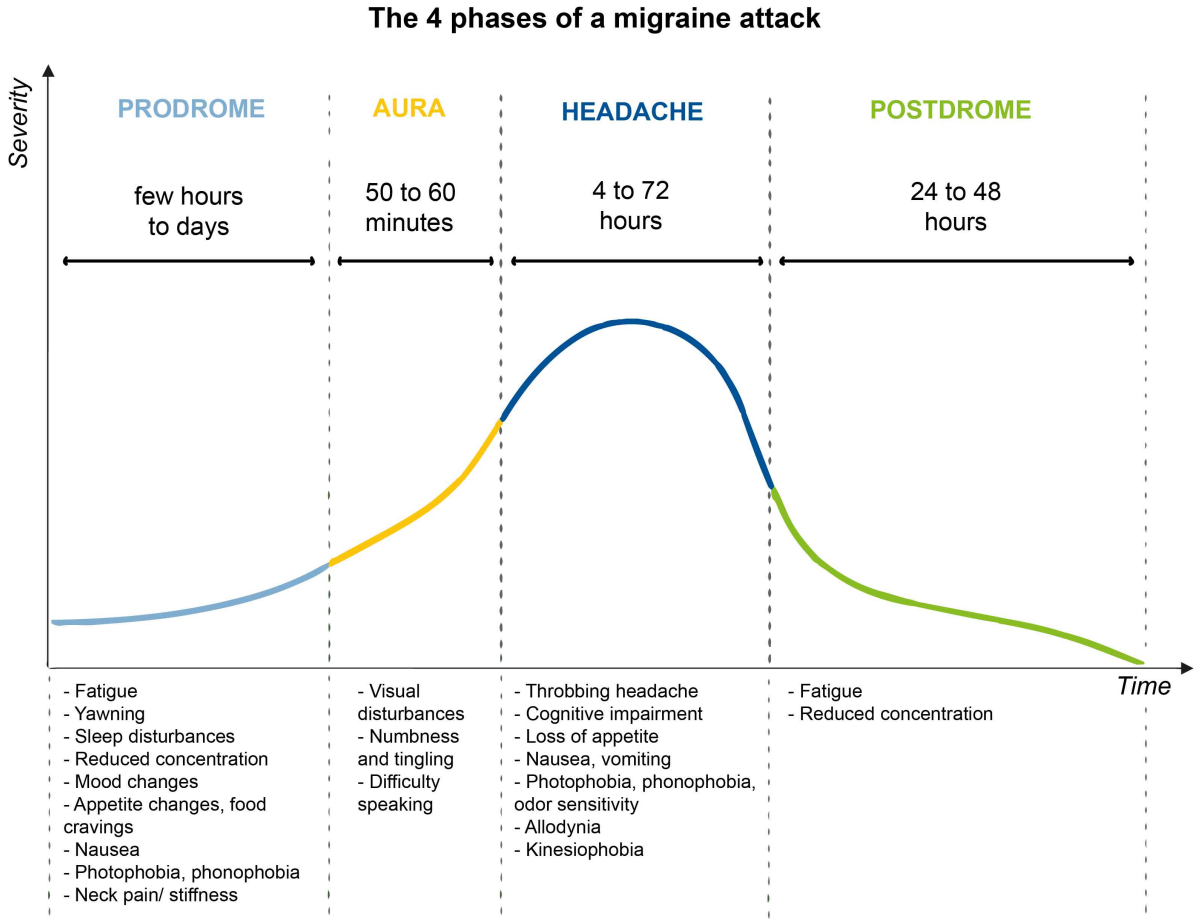

Figure 1.1: Schematic illustration of the migraine attack in the ictal phase. Within a migraine attack with aura, four phases can be distinguished: the prodrome phase, the aura phase, the headache phase and the postdrome phase. The main symptoms associated to each one of the four phases are listed. Figure based on information from [8, 10–12, 38, 40–45, 48, 50].

responsible for them [10, 13, 14].

1.2.1 Migraine pathophysiology

The pathophysiology of migraine is complex and still not fully understood. In 1940, the vasogenic theory appeared, that defended that mechanical stimulation and distension of cranial blood vessels resulted in the migraine headache. This was supported by the pulsating quality of the migraine headache [19], the fact that neuropeptides Nitric Oxide (NO) and Calcitonin Gene-Related Peptide (CGRP) were capable of trigger migraine and the vasoconstrictive therapeutic effect of triptan. However, the pulsating feature is not synchronous with the cardiac contractions and the Vasoactive Intestinal Peptide (VIP) vasodilator does not trigger migraine and so, the theory was refuted. Nowadays, migraine is commonly described as a neurovascular disease, being characterized by both neurogenic and vascular alterations [11].

The pain associated with the headache phase in a migraine attack is widely accepted to result from

the activation of the trigeminovascular system. The trigeminovascular pathway transmits nociceptive information from the meninges to the central areas of the brain and cortex that give rise to some of the associated symptoms of this phase [14].

The involvement of hypothalamus in migraine explains the symptoms that begin in the prodrome phase and last through the whole attack. In fact, the hypothalamus is responsible for maintenance of homeostasis, regulating food intake, energy balance, responses to stress and circadian rhythms, among others, thus being associated with the premonitory symptoms [37, 46, 51]. There are currently two theories that try to explain how the hypothalamus influences the trigeminal nerve pain processing signals, and thus the headache onset. The first one defends that the hypothalamus is connected to the trigeminal nerve, which communicates to the trigeminovascular system. Migraine triggers provoke the release of inhibitory and excitatory neurotransmitters and neuropeptides that modulate the response of the trigeminovascular thalamic neurons in the hypothalamus, which can then activate or inhibit the trigeminovascular system [11, 14, 38, 42, 52]. The second hypothesis is that the triggers lead the hypothalamus to induce a parasympathetic overdrive that is sent to the brainstem Superior Salivatory Nucleus (SSN) that activates the Shenopalatine Ganglion (SPG). The latter is part of the trigeminovascular system and is able to dilate the meningeal arteries and to increase the release of inflammatory molecules in the meninges that activate the trigeminovascular system, which in its turn gives rise to pain [11, 14]. Thus, the understanding of the premonitory phase of migraine involves hypothalamus functional connections with cortical, thalamic, brainstem and even limbic areas [4, 13, 41, 45, 46, 53, 54]. Particularly, during the 24h preceding an attack, altered functional connectivity between the hypothalamus and the brainstem is reported [4, 8, 42, 44].

Aura seems to be explained by a Cortical Spreading Depression (CSD), which is characterized by a slowly propagating wave of depolarization in neural and glial cell membranes followed by hyperpolarization/inhibition. This wave is also associated with an increase in local brain perfusion, followed by a prolonged neuronal refractory period [10, 13, 14, 14, 48, 55]. Animal studies support that the CSD can trigger meningeal inflammation and vasodilation and consequently activate trigeminal nociception, leading to headache occurrence. However, whether CSD can cause headache in humans remains controversial [8, 14].

Some neuropeptides have also shown to trigger migraine attacks, namely CGRP, the most potent a vasodilatory peptide that is involved in the activation and transmission of sensory stimuli within trigeminovascular pathways. Specifically, CGRP-based drugs that show a vasoconstrictive effect are now considered an effective therapeutic target for both acute and preventive treatment. This supports the view that vascular changes are involved in migraine [8, 14, 56–58].

The migraine brain has also been characterized by general neuronal hyperexcitability in response to a wide range of stimuli during the interictal state, which means that there is a lack of habituation in

response to repetitive stimulation [14]. This is then normalized during the attack [12].

Some of these mechanisms have an inherent genetic predisposition since as migraine tends to run in families and is associated with some genes related with vascular biology. In fact, migraine has been proven to have a genetic association of about 42% [19]. Thus, although vascular mechanisms do not, by themselves, explain migraine, they seem to have an important role on its pathophysiology [8, 10, 11, 14].

All in all, the pathophysiology of migraine has shown to be highly complex and thus still incompletely understood, being determined by interactions that involve genetic, environmental and other factors. Nevertheless, the consensus nowadays points towards a neurovascular hypothesis.

1.2.2 Migraine-associated vasculopathy

As presented in the previous section, vascular changes are assumed to be an important factor in the migraine pathophysiology.

Stroke is the second highest cause of death and a major cause of disability worldwide [59]. Ischaemic strokes represent 80% of all strokes and are a result of blockage or narrowing of an artery supplying blood to the brain, causing damage and death to brain tissue [17]. Migraine and ischaemic stroke have been linked for around 30 years, with reports of ischemic stroke occurring during and between migraine attacks [15]. In a case-control study from 1993 [60], a significant association between migraine and stroke was found in women aged below 45 years old, especially among the ones who smoked. In a meta-analysis of 21 observational studies of the association between migraine and stroke, migraine was independently associated with a 2-fold increased risk of ischemic stroke [59]. An association with stroke has been shown to be present predominantly in Migraine with Aura (MA). In particular, young women (typically under 45 years old) with MA are more susceptible to have ischaemic stroke, being MA an independent risk factor for ischemic stroke in young women [16, 18, 19, 21, 61, 62]. This association is enhanced if these patients present risk factors such as smoking or using oral contraceptives [21, 62–64]. The risk is even greater for those with active migraine (who had a migraine attack in the last 12 months) and higher frequency of attacks [21]. In this group of patients, migrainous infarction is more prone to happen in the posterior circulation territory of the brain, especially in the occipital cortex and cerebellum [17, 61, 62, 65]. On the other hand, Migraine without Aura (MO) might not have a direct causal relationship to lead stroke, but share genetics, risk factors and comorbidities in common with stroke [18]. Neuroimaging evidence showed a high incidence of White Matter (WM) hyperintense lesions and infarct-like lesions in migraineurs, notably in those with aura [17, 21, 61, 65]. Infarct-like lesions usually occur in the posterior circulation territory, particularly in the cerebellum and have shown to be independent of atherosclerosis or small vessel disease, showing evidence that its origin is probably associated with migraine-related hypoperfusion together with embolic events [17, 21, 65]. Other factors that may contribute to migrainous infarction can be genetic, hormonal, hypercoagulation or right

to left cardiac shunts. Additionally, antimigraine drugs, such as ergot alkaloids and triptan, cause severe vasoconstiction, which may result in the development of ischemia [16].

Besides ischaemic stroke, hemorrhagic stroke (rupture and bleeding of a blood vessel in the brain) [16–18], subclinical ischemic lesions (caused by asymptomatic cerebral infarction, also called "silent cerebral infarction") [17] and transient ischaemic attack (temporary blockage or decreased blood supply to the brain) [17, 18, 21] have been consistently found in migraineurs. Additionally, patients with migraine receiving surgery under general anaesthesia are found to have a higher perioperative stroke (stroke occurring within 30 days of surgery) risk [21]. These associations have shown to be stronger in patients with MA than in those with MO.

Moreover, migraine has been demonstrated to be a systemic vascular disorder, being not only associated with cerebrovascular, but also with cardiovascular events. There is growing evidence of an association between migraine and cardiovascular disorders, including ischaemic heart disease [19], myocardial infarction [20, 21], angina [20], arrythmia [20], hypertension [21], venous thromboembolism [21] and atrial fibrillation [21]. Once more, these connections are found to be stronger in patients who experience aura than in those without aura.

Several proposed mechanisms have been suggested to be involved in this association, such as atherosclerosis, cardiovascular risk factors and genetic risk factors. In recent years, it has been reported that the vasculopathy in migraineurs may be related with peripheral/systemic endothelial dysfunction [20]. The endothelium is the monolayer of endothelial cells lining the lumen of blood vessels. It is the key regulator of vascular homeostasis, functioning not only as a mechanical and biological barrier between the blood and vascular wall, but also being able to respond to physical and chemical signals by production of a wide range of factors. Specifically, it plays a direct role in tissue oxygen supply and metabolic demand by regulation of vessel tone and diameter [66]. Endothelial dysfunction is a systemic disorder that includes impaired endothelium-dependent vasodilation, inflammation, hypercoagulability and vascular reactivity. Consequently, endothelial dysfunction is critical in the pathogenesis of cerebrovascular and cardiovascular events and/or disorders. Migraine was demonstrated to be associated with both systemic and cerebral endothelial dysfunction. This was evidenced by decreased vasodilation [28, 67], increased thickness of the carotid intima media [28, 68] and higher levels of inflammation markers (such as blood levels of erythrocite sedimentation rate, C-reactive protein and fibrinogen) [28, 68] in migraine patients (both MO and MA) compared to healthy controls. Fewer circulating endothelial progenitor cells [69] and higher endothelial microparticles levels (vesicles that are released from activated endothelial cells and serve as a surrogate for endothelial dysfunction) [70] were also detected in migraine patients compared with healthy subjects. Importantly, while there have been uncertainty about the systemic endothelial dysfunction in migraine, cerebral endothelial function has been reported to be impaired in this disorder. A study was made assessing cerebral endothelial function in

migraneurs in the absence of systemic endothelial dysfunction that revealed impaired endothelial function restricted to the posterior cerebral circulation in migraneurs in comparison with controls. However, the reason for this was unclear since the trigeminovascular system is implicated in the pathogenesis of migraine, thus being expected for the anterior circulation arteries to be as well [29].

All in all, these results support the idea of a dysfunctional cerebral endothelium as a possible explanation for the association between migraine and cardiovascular and cerebrovascular diseases.

1.2.3 Menstrual or menstrually-related migraine

A higher prevalence of migraine in young women compared to men may imply that female sex hormones play a role in the pathogenesis of the disorder [64, 71]. Menarche, menstruation, pregnancy and menopause, and also the use of hormonal contraceptives and hormone replacement treatment influence migraine attacks occurrence. Migraine usually starts after menarche, occurs more frequently in the days before or during menstruation, and gets better in pregnancy and menopause. Therefore, throughout the reproductive years, menstruation is one of the events that shows higher association with migraine attacks [64]. In fact, more than half of female migraineurs have migraine attacks, often without aura, prior to menstruation or during ovulation [23]. The International Classification of Headache Disorders, 3rd edition (ICHD-3) defines Menstrual Migraine (MM) as migraine that occurs between 2 days before and 3 days after menstruation in at least two out of three menstrual cycles, with no attacks at any other time of the menstrual cycle. This is only reported by 10% to 20% of female migraineurs. In turn, the ICHD-3 defines Menstrually-related Migraine (MRM) as the one occurring at the previously mentioned conditions and additionally at other times of the menstrual cycle. This is prevalent in more than half of female migraineurs [23, 40, 64, 72]. In these types of migraneurs using combination oral contraceptives, attacks are more likely to occur during the pill-free week. Perimenstrual attacks are usually longer, more incapacitating, recurrent, painful and less responsive to treatment compared to attacks at other times of the cycle or to "non-menstrual" migraineurs attacks [9, 23, 24, 26, 64]. However, few studies have assessed this disorder's quality of life, disability and cerebrovascular function.

A typical menstrual cycle is represented in figure 1.2. It is 28–32 days long and starts with a follicular or proliferative phase (12–14 days) characterized by increasing Estradiol (E2) concentration reaching a pre-ovulatory peak and low Progesterone (P4) levels. A subsequent luteal or ovulatory phase (12–14 days) is characterized by a progressive increase of P4 concentrations and a lower secondary E2 peak followed by a decrease of both hormone levels in the last days of the menstrual cycle. It is thought that the ovarian hormones E2 and P4 may modulate brain structure, chemistry and function and shape the behaviour and mental health of women in their reproductive years. Thus, it is likely that neuroadaptive mechanisms arise every month to modulate brain structure and function in response to the hormonal fluctuations across the menstrual cycle [64, 73, 74].

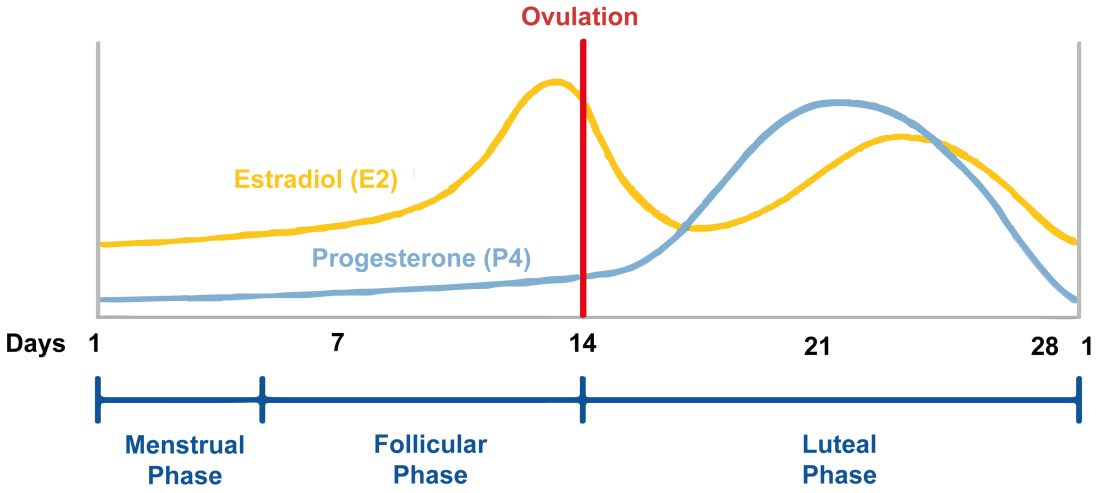

Figure 1.2: Schematic illustration of the relationship between menstrual cycle days and ovarian hormones estradiol (E2) and progesterone (P4) (considering a 28 days menstrual cycle). Figure adapted from [1].

A number of studies have demonstrated changes in cerebral artery function in postmenopausal women after longterm exposure to constant doses of exogenous E2 and P4. However, the short-term effects of these two ovarian hormones on cerebral vessels of younger premenopausal women, resulting from normal cyclic variations of these hormones across the menstrual cycle, remain largely unknown [23, 71, 75]. In fact, menstrual cycle studies become especially challenging as the spread of ovulation varies widely across one woman's cycle and between different women [71]. In fact, performing blood tests to find the hormones' concentrations in plasma seems to be the most accurate method to know the exact ovulation time and the calendar method alone is not always reliable [71].

Cerebrovascular function has been shown to differ between different phases of the menstrual cycle. Brackley et al. [73] reported higher downstream resistance to flow in the Middle Cerebral Arteries (MCA) of young healthy women during the luteal phase compared to the follicular phase. In turn, Nevo et al. [75] studied the association between ovarian stimulation and Cerebral Blood Flow (CBF) by measuring blood flow after pituitary suppression and during controlled ovarian stimulation in women. A significant correlation between increments in E2 levels and increments in CBF when the late follicular phase was compared with the ovarian suppression period was found. Mean blood flow velocity significantly increased and cerebral vascular resistance significantly decreased during the late follicular and midluteal phases compared with respective measures during ovarian suppression. Lastly, there was a significant correlation between an increase in estrogen levels and a decrease in cerebral vascular resistance when the late follicular phase was compared with the ovarian suppression period. These results imply sex hormone-associated intracranial vasodilation causing increased CBF during controlled ovarian stimulation. Additionally, Krejza et al. [71] showed that in young healthy women, blood flow velocity was increased on the right Internal Carotid Arteries (ICA) in the luteal phase, when compared to the

follicular phase and to the left ICA. As the distribution of receptors for sex hormones in the vessels of both hemispheres is most likely symmetrical, the observed unilateral pattern of cerebral blood flow velocity changes suggested intermittent interhemispheric differences in neuronal activity across the cycle. Additionally, these variations during the cycle seemed to be associated with oscillation of circulating E2 and P4. Therefore, it is thought that the cerebral blood flow varies substantially throughout the menstrual cycle along with changes in the circulating ovarian hormones [71, 73–75].

In patients suffering from MM or MRM, the perimenstrual attacks seem to be triggered by the rapid decrease of estradiol (E2) that occurs prior to menstruation. Initial evidence for the role of E2 in migraine emerged in the early 1970s, in studies evaluating the influence of exogenous E2 on female migraineurs across the menstrual migraine. Migraine attacks were correlated with declining E2 levels and independent of P4 concentrations. Additionally, E2 levels in pregnant women suffering from migraine were shown to increase through each trimester and decline postpartum, with one study reporting that 80% of the studied women with migraine did not had any attack in the third trimester. Also, it was deduced that as women enter menopause and E2 levels decline and stabilize, the prevalence of migraine attacks also declines [24]. Several other studies investigating estradiol-induced migraines followed that confirmed E2 association with migraine [22–26]. Furthermore, circulating E2 is associated with reduced stroke risk and favorable stroke outcomes, which supports the connection between migraine and vasculopathy discussed in the previous section 1.2.2 [25]. Nevertheless, no study has identified a minimal threshold of E2 concentrations at which migraine attacks are prone to occur, nor a difference in its concentrations between women with and without MM or MRM. Furthermore, migraineurs did not show any apparent correlation between the concentration of E2 and the day on which the attack occurred, or on any of the 5 preceding days [9].

Estradiol is involved in reducing inflammation, oxidative stress and cell death, thus playing a role in the health of the vascular endothelium. Therefore, the reduction of the estradiol levels before menstruation may compromise the regulation of the vascular endothelium, intensify the cerebral endothelial dysfunction and consequently trigger a migraine attack [27]. This is in agreement with the results described in the previous section 1.2.2, where the impairment of the cerebral endothelium emerged as a possible explanation for the association between migraine in young premenopausal women and cardiovascular disease. In addition, it seems likely that E2 can regulate sensitisation of trigeminal neurons by modulating the release of nociceptive vasodilator CGRP [9].

All in all, it seems to exist an association between migraine perimenstrual attacks in MM and MRM and the decrease of the ovarian hormone estradiol after ovulation. Estradiol, in turn, is thought to be involved in the regulation of the vascular endothelium and is associated with reduced stroke risk and favorable stroke outcomes. This means that the possible impairment of the cerebral endothelium in migraine may be intensified near the menstruation days. Therefore, it seems important to perform

longitudinal studies assessing brain vascular changes throughout the menstrual cycle. Furthermore, these alterations must be taken into account when studying cerebrovascular function in MM and MRM.

1.3 Cerebrovascular reactivity

This section contains relevant information about the concept of cerebrovascular reactivity (CVR), together with the neuroimaging techniques and vasoactive stimuli that can be used to assess it.

Migraine's suspected brain endothelial dysfunction leads to several changes, including CVR. CVR is an intrinsic regulatory brain mechanism that reflects the capability of its vessels to alter their calibre in response to vasoactive stimuli, whether by dilating or constricting, with the objective to increase or decrease CBF. If CVR is impaired, then CBF cannot increase when brain activity increases. Thus, CVR can be thought of as an indicator of brain's vascular health, showing to be impaired in several conditions and pathologies such as stroke [3, 76–78], arterial stenosis, brain tumours [76], obstructive sleep apnea [3] and dementia [77, 78].

To determine CVR, a challenge to the vasculature is usually applied while the CBF changes are measured simultaneously. The CVR is then calculated by the change in CBF per change in vasoactive stimulus. Thus, it is important that both of these variables are measured in a precise and standardized way within and across subjects. This is the only way to assure that, when analysing the results, the differences in CVR are exclusively linked to the condition we are studying and not due to methodological variability.

1.3.1 Neuroimaging techniques for cerebral blood flow assessment

To determine CVR, it is needed to measure the changes in CBF and for this, several neuroimaging techniques can be used. These comprise Transcranial Doppler (TCD), Positron Emission Tomography (PET), Single Positron Emission Tomography (SPECT), and Functional Magnetic Resonance Imaging (fMRI).

TCD

TCD, introduced in 1982 by Aaslid et al. [79], has been the most frequently used technique to measure intracranial CBF by taking advantage of the Doppler effect. It is usually used in large cerebral arteries such as Anterior Cerebral Arteries (ACA), Middle Cerebral Arteries (MCA) and Posterior Cerebral Arteries (PCA). TCD presents several advantages such as being non-invasive, easy to use, portable, highly available, inexpensive and presenting high temporal resolution [77, 80, 81]. However, it has low

spatial resolution, being limited to large arteries and only assesses global (rather than regional) CBF in an indirect manner (it assumes constant diameter in the insonated arteries) [27, 77, 81, 82].

PET and SPECT

Nuclear imaging PET and SPECT take advantage of the radioactive properties of the radiotracers to obtain images of their distribution in the brain, which enable to conclude about brain impairment associated to certain pathologies and conditions. Thus, it is important to choose an appropriate radiotracer to assess CBF. These techniques provide quantitative regional CBF measurements and whole-brain CVR mapping. Nevertheless, they exhibit poor spatial resolution and are both invasive and expensive, therefore being limited in availability and use [3, 77, 81].

fMRI

By overcoming the limitations of the techniques mentioned above, fMRI, particularly Blood-oxygenation Level Dependent (BOLD) and Arterial Spin Labelling (ASL), have emerged as techniques to evaluate CVR.

Since the early 1990s, fMRI, and particularly BOLD-fMRI, has been the main technique used for mapping brain activity. This is mostly due to the fact that it enables non-invasive, whole-brain scans with high spatial resolution [83, 84]. Specifically, it enables the assessment of region-specific CVR. Image contrast depends on the chosen pulse sequence parameters and on the tissues physical parameters. In fact, by choosing the adequate radiofrequency and gradient pulses and the most appropriate acquisition times Echo Time (TE) and Repetition Time (TR), it is possible to highlight different characteristics of the tissues being imaged. The most common imaging sequence used is Echo-Planar Imaging (EPI), which allows the collection of whole brain data in few seconds or less. Furthermore, contrast comes from the tissues themselves as different tissues such as Gray Matter (GM), Whitte Matter (WM), Cerebrospinal Fluid (CSF) and even damaged tissues exhibit different values for each relaxation time constant. There are three relaxation time constants that are of primary interest — T1, T2, and T2*. T2* is the transverse magnetization time constant sensitive to susceptibility differences, being the most relevant for understanding contrast in BOLD-fMRI images [85].

fMRI on BOLD contrast is based on a difference in the relative concentration of deoxy-Hemoglobin (dHb) and Oxy-hemoglobin (HbO_2) in blood, which are paramagnetic and diamagnetic, respectively. HbO_2 is diamagnetic, having the same susceptibility as the surrounding tissues and therefore has minimal impact on the measured BOLD signal, while dHb is paramagnetic and degrades the BOLD signal. This magnetic susceptibility difference, when accentuated by a decrease in oxygen saturation and consequent lower HbO_2/dHb ratio, creates a magnetic susceptibility gradient that causes susceptibility effects in the BOLD-fMRI images, such as signal loss (darker images caused by the shortening of T2*)

and geometric distortions [83–85]. Hypercapnia increases Partial Pressure of Arterial Carbon Dioxide ($PaCO_2$) with no significant changes in Cerebral Metabolic Rate of Oxygen ($CMRO_2$), which induces regional CBF increase through vasodilation in order to maintain a constant supply of Oxygen (O_2) and nutrients despite fluctuations in perfusion pressure and blood gas concentrations [86–88]. Vasodilation is thought to be induced by CO_2-mediated changes in pH levels by the mechanism represented in figure 1.3 [2, 3, 89]. In turn, this leads to regional Cerebral Blood Volume (CBV) and blood HbO_2 concentration increases. Thus, ultimately, the BOLD signal will be higher due to the measurable T2* prolongation [86–88].

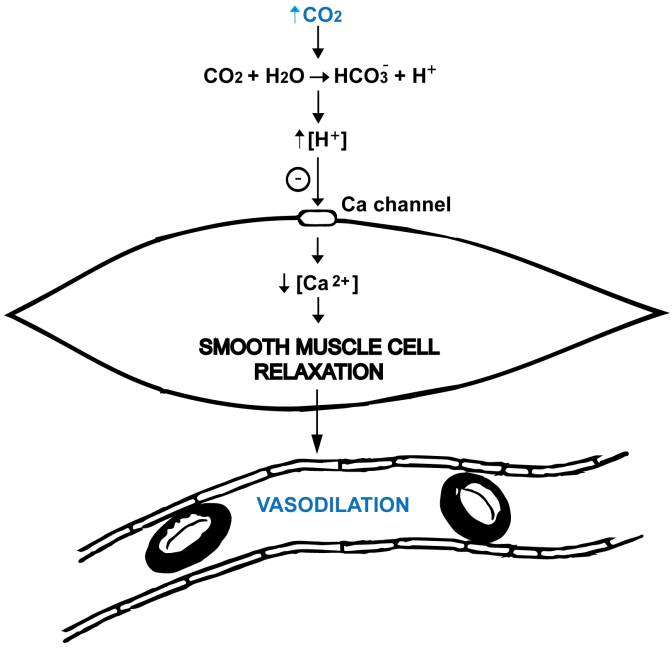

Figure 1.3: Schematic illustration of the mechanism that relates an increase in the Partial Pressure of Arterial Carbon Dioxide ($PaCO_2$) with vasodilation. Altering the $PaCO_2$ alters the extracellular pH, which leads to changes in vascular smooth muscle intracellular calcium concentration and vascular tone. Figure adapted from [2].

The precise amount by which the MRI signal intensity increases depends on the contribution from several factors. The signal is a sum of the intravascular signal that arises from the interaction of the water molecules in blood itself and with the extravascular signal that results from magnetic susceptibility differences between the blood water molecules in the vessels and the surrounding tissues [85]. It is important to notice that BOLD-fMRI only provides an indirect measure of CBF. In fact, the BOLD signal results from a complex combination of several physiological parameters, including not only CBF but also CBV and blood oxygenation, which turns it into an only semiquantitative CBF measurement technique [83–85].

Concerning ASL, it takes advantage of water protons present in arterial blood, using them as an endogenous perfusion tracer. Some arterial spins are labelled and when they reach brain regions with non-labelled spins cause tissue magnetization alterations. By subtracting labelled and control images,

perfusion images are obtained. This method is non-invasive and provides high spatial resolution images and quantitative CBF values. Nonetheless, it presents low Signal-to-Noise Ratio (SNR), which restricts its use and makes BOLD-fMRI often preferred as the fMRI technique to assess CVR [3, 36, 76, 77, 90].

Having said this, fMRI and, in particular, BOLD-fMRI, seems to be the most promising measurement technique of CVR, enabling non-invasive whole-brain scans with high spatial resolution.

1.3.2 Vasoactive stimuli

Changes in CBF can be achieved by the application of different vasoactive stimuli, such as administration of external vasodilators, inhalation of gas mixtures or execution of breathing tasks. From these, the most common vasoactive stimuli used to elicit increased CBF is hypercapnia, whereby there is an increase of the $PaCO_2$ with consequent vasodilation and increase of CBF [3, 76, 77, 82]. Alternatively, CVR can be measured using resting-state methods.

Administration of external vasodilators

Intravenous injection of external vasodilators can be used as a challenge to the vasculature. Here, acetazolamide is frequently used. Acetazolamide is the inhibitor of the enzyme carbonic anhydrase that catalyses the conversion of CO_2 to bicarbonate, inducing an extracellular and intracellular acidosis resulting in vascular smooth muscle relaxation [90, 91]. The advantages of acetazolamide are that it is usually safe and well tolerated, together with being independent of the subject's cooperation. However, it is an invasive procedure that can trigger side effects such as headache and neurological symptoms related to ischaemia that are difficult to control and terminate [36, 91]. Moreover, a standardized dose of acetazolamide does not imply a standardized stimulus, inhibiting a reproducible stimulus-response relationship [36, 77, 92].

Inhalation of gas mixtures

The induction of hypercapnia through inhalation of air can be performed using a gas mixture with approximately 5% of Carbon Dioxide (CO_2) (in comparison to the "normal" room air with 0.04% of CO_2), 21% of O_2 and balanced nitrogen. In order to better control gas concentrations, some techniques can target the precise Partial Pressure of CO_2 ($PetCO_2$), which is an accurate non-invasive surrogate of the $PaCO_2$ [3, 78]. However, the required experimental setups usually are expensive, which limits their availability, and are complex, taking additional time to prepare and requiring expertise and equipment for manipulating gas levels [3, 76, 93]. Moreover, the inhalation mask can be uncomfortable and cause feelings like claustrophobia or anxiety. Elderly and acute and severely ill patients, such as the ones suffering from significant pulmonary or cardiac disease, are advised not to perform gas challenges [36, 76, 90, 91].

Breathing tasks

Alternatively, stimuli that are based on the execution of breathing tasks, such as the Breath-holding (BH) and the Paced Deep Breathing (PDB), can also be used to elicit changes in CBF. Both tasks are completely non-invasive and simple in terms of execution and experimental setup.

The BH-task consists of short periods of breath holding that lead to hypercapnia, vasodilation and increased CBF, alternated with periods of normal breathing. However, even if performed with the same duration, BH usually leads to different rise rates of $PaCO_2$ in different people due to, for example, differences in lung size and metabolic rate, leading to an increase in intersubject variability [36, 77, 90], which should be monitored through $PetCO_2$ recording. Additionally, subjects tend to take deep recovery breaths after the BH, which can lead to severe task-correlated head motion that degrades the acquired data [94]. Also, BH has shown to provoke mild hypoxia, although this has not significantly influenced CVR results when compared to methods that control respiratory gas levels [95]. In fact, within normal physiological values, the role of arterial O_2 pressure in CBF regulation seems to be negligible, with CVR to CO_2 being approximately 60 times larger than to O_2 [91, 96]. Moreover, it can cause CBF changes associated to neuronal activation [90]. Furthermore, as it implies the cooperation of the patients, it may be difficult in the case of individuals with certain conditions such as language-comprehension problems, visual or auditory impairment, children and elderly or cognitively impaired patients (although it has been shown to produce similar results to the CO_2 inhalation technique in these type of subjects) [3, 76].

PDB or hyperventilation consists of periods with controlled and mild increase in the respiration rate or depth, leading to hypocapnia and vasoconstriction, alternated with normal breathing. It is particularly useful when further vasodilation is not possible, which occurs in some pathologies. However, PDB is associated with head motion and, when prolonged, can induce negative effects such as anxiety, dizziness, weakness and exhaustion [3, 34].

All in all, although task-based stimuli are non-invasive and simple, they present some disadvantages, as being highly dependent on the compliance of patients. In fact, if not performed well, it can affect the data quality and reliability. Additionally, it is crucial to do at least one pre-scan training, which leads to unpredictable extra time expenditure [3, 34].

Resting-state methods

Resting-state methods are developed in the context of Resting-state Functional Magnetic Resonance Imaging (rs-fMRI). They are based on the brain's intrinsic functional connectivity, exploiting low frequency spontaneous fluctuations in breathing, and thus in arterial CO_2, that contain information about CVR mechanisms [3, 34, 76]. Correlation has been proven to exist between these fluctuations and hypercapnic responses to BH. These methods do not require a task, thus being less demanding logistically and in matter of patient cooperation. Additionally, task-performance cannot be considered a confounding

factor in the resulting signal [36]. On the other hand, this approach presents limitations as needing minimal fluctuations in $PetCO_2$ for CVR assessment [3,76,93]. Furthermore, the frequency range associated with the breathing fluctuations has shown to be inconsistent in the literature and, even within this, the fluctuations might also be correlated with neuronal fluctuations and heart rate changes that mistakenly end contributing to CVR measurements. Additionally, studies comparing CVR assessed by the rs-fMRI metric resting state physiological fluctuation amplitude (RSFA) with CO_2 inhalation and BH tasks obtained contradictory results, which indicates that further investigation must be developed regarding this type of vasoactive stimuli and its CVR metrics [3, 34, 36, 76]. Inclusively, it seems that rs-fMRI produces less robust means of characterizing CVR that BH-fMRI [94].

This being said, except in the case of patients with baseline vasodilation or unable to cooperate, the BH task seems to be the most appropriate vasoactive stimulus used to measure CVR as it has been shown to be non-invasive and simple in terms of execution and experimental setup.

1.4 Cerebrovascular reactivity by breath-holding fMRI

From section 1.3, it was concluded that the BOLD-fMRI neuroimaging technique, together with the BH task as vasoactive stimulus, seem to be an appropriate noninvasive method to assess CVR. In this section, the main results from a research will be presented regarding the BH task paradigm and data modelling.

1.4.1 Breath-holding task paradigm

In task based methods such as the BH task, several parameters and options have to be considered before implementation with the objective of achieving the best possible results regarding CVR.

A BH task protocol usually follows a block design with alternated periods of not breathing and normal breathing. The parameters that are important to contemplate are the performance of the BH whether after inspiration or expiration, the duration of BH period, the duration of baseline and recovery periods, whether breathing is performed spontaneously or paced in these moments and the number of trials.

Firstly, regarding performing the BH after an inspiration (end-inspiration BH) or an expiration (end-expiration BH), end-inspiration BH exhibits a complex BOLD response (with a tryphasic shape), often hard to model. Actually, end-inspiration BH is easier and more comfortable to perform, allowing longer BH period duration, which is particularly useful in less cooperative patients. However, it increases head motion and introduces variability in the measurements as the signal will depend on the individual's depth and intrathoracic pressure of the preparatory inspiration. Contrarily, end-expiration BH produces simpler and faster responses, which means a shorter BH period can be adopted. Moreover, as the

chest position during the BH is more similar across trials following exhalation, it is a more reproducible method [3, 34–36, 87].

The BH period duration must be brief enough to be well performed and tolerated by the patient, but long enough to induce detectable hypercapnia, CBF and CVR response. In fact, higher BH duration leads to higher signal amplitude, sensitivity and SNR, such as more reproducible results. Unfortunately, it is often hard and uncomfortable and may cause increased head motion. Significant hypercapnia has been achieved with a BH period duration of 6s. The spatial extent of the BOLD response reaches a plateau at a BH period duration of approximately 20s. Thus, several studies have applied BH duration of about 15 s with successful results. [3, 34–36].

Concerning the baseline period, it must be long enough for blood gas levels to return to normal. During this interval, the breathing rhythm can be self-paced or externally-paced, but externally-paced breathing rhythm is preferred as it minimizes variability within and between individuals and prevents hyperventilation [3,35,36]. In order to perform this, it is advisable to choose a breathing rate that is the most similar possible to the subject's spontaneous breathing rate in order to achieve a normocapnic baseline state and avoid hypocapnia, being 1/3 Hz to 1/6 Hz the most common with an inspiration/expiration ratio of 1:2 [3]. When adopting an externally-paced approach in baseline, a recovery period after the exhalation following BH and before the baseline is recommended, where the subject breaths spontaneously during several seconds in order reduce possible discomfort and anxiety [3,35]. The choice regarding the baseline is important given the non-linear sigmoidal relationship between the CBF measured through the BOLD signal and the $PetCO_2$ where a distinct BOLD signal plateau is observed for low and high $PetCO_2$ levels [82, 86, 95].

Furthermore, it is necessary to define how many BH trials are carried out during the BH task. The more trials, the more averaging can be done and thus higher SNR can be achieved. However, this implies longer protocol duration that may cause fatigue, leading to more motion artifacts and worse task performance. Thus, a minimal number of 3 cycles is the recommendation to achieve reproducible results [3, 34].

Additionally, during the breathing task and the Magnetic Resonance Imaging (MRI) scanning, it is important to simultaneously measure $PetCO_2$ in order to monitor the participant's task compliance and to account for variations in task performance. Additionally, it allows to obtain normalized and quantitative CVR measures (%BOLD change per mm Hg variation in $PetCO_2$, %BOLD/mmHg) that account for the variability caused by the breathing task both between different scanning sessions of the same individual and between different individuals and allow us to compare CVR between sessions and individuals [3, 34–36]. In fact, estimating CVR by simply using the temporal fluctuation of the BOLD time series gives a good indication of how much the BOLD signal fluctuates but disregards the influence of the source of fluctuation, in this case the CO2-related BOLD fluctuations. Median CVR in GM using a BH-task with a

BH duration of 15s to 20s is referenced to be in the range of 0.15 to 0.40 %/mm Hg [34,35,88,94,97–99]. Other information and measures can also be deduced from $PetCO_2$ that are useful for further processing and analysis.

At least a practice run of the paradigm outside the scanner with simultaneous recording $PetCO_2$ must occur. This allows the assessment and optimization of the participants' compliance and the recording of their spontaneous breathing rates needed to decide about the breathing rate of the externally-paced baseline periods of the paradigm [3].

In summary, despite the existence of several options regarding the BH task paradigm and the lack of literature deriving conclusions about the best choices, the most appropriate parameters seem to be: (i) end-expiration BH with a duration of 15s followed by exhalation; (ii) baseline with externally-paced breathing with a frequency similar to the participant's spontaneous breathing rate and a duration that enables blood gas levels to return to baseline; (iii) recovery period with self-paced breathing; and (iv) at least three trials. Simultaneous recording of $PetCO_2$ measurements is advisable.

1.4.2 Breath-holding fMRI data modelling

Analysis of the BOLD-fMRI response to a BH task is easily accomplished using the General Linear Model (GLM) approach.

The GLM is a linear model for modelling an observed signal as a function of one or more regressors or Explanatory Variables (EVs). EVs consist in patterns that are expected to be found in the measured signal that can correspond to experimental conditions or confounds. Each EV has an associated scaling value or a parameter estimate. Parameter Estimates (PEs) are chosen in order to minimize the differences between the observed data and the fitted model with the scaled regressors. These differences are called residual errors or residuals. Therefore, the GLM in each voxel can be expressed in an equation as:

$$y(t) = \mu + \sum_{i=1}^{p} \beta_i X_i(t) + \epsilon \tag{1.1}$$

where y represents the measured BOLD signal timecourse at each voxel; μ represents the mean BOLD data timecourse at that voxel; X represents the timecourse of a regressor, EV; β the estimated coefficient PE for that EV; i the EV index; p the total number of EVs; and ϵ the residual error that reflects the difference between the data and the scaled regressor [100].

Usually, a GLM is performed for the data at each and every voxel. This means that the PEs corresponding to the best fit model depend on the series of data values at each voxel and consequently, are different for every voxel. Ultimately, the result of the voxelwise GLM analysis is a set of whole brain maps of PEs values, one map for each EV. Each of these maps contains one PE value per voxel. Based on the output PEs, several questions of interest can be included in the analysis by defining different Contrast of

Parameter Estimates (COPEs). A contrast is a inequality composed by a linear combination of PEs with different weights, one for each PE [100].

After voxelwise modelling, the PE maps arising from the contrasts are used for hypothesis testing. Hypothesis testing starts with the null hypothesis: the assumption that there are no signals of interest in the data, this is, that they only reflect random noise. Afterwards, a test statistic - a quantity derived from the fitted model - is chosen. The most commonly used test statistics are the t-statistics and the F-statistics. The t-statistics is essentially a ratio between the amplitude of the quantity of interest (the amplitude of the COPE) and its standard deviation. It is typically a one-sided statistical test, that is, it tests if the COPE in question is bigger than zero. Contrarily, F-statistics a two-sided test, as its alternative hypothesis if the COPE is non-zero (positive or negative). In GLM, an F-contrast is specified using a set of t-contrasts and it combines the quantities formed by them, therefore being represented by a matrix of contrast values where each row is a t-contrast [100].

If large effects of interest are present in the data, the test statistics are large (very different from zero), which leads to the null hypothesis being rejected, based on some margin. This margin is usually the p-value, also called the significance level or the false positive rate. It is chosen to be 0.05 by established convention, meaning that every individual test has a 5% chance of generating a false positive result. However, when performing voxelwise analysis in a brain image, the number of statistical tests needed to be performed is equal to the number of voxels in the image, in the range of tens of thousands to millions. With a 0.05 false positive rate for each particular test, the result would include too many false positives. Therefore, a correction to the false positive rate is needed in order to account for the large number of tests - multiple comparisons correction. There are many methods of multiple comparisons correction, among which the Gaussian random field theory. The Gaussian random field theory assumes that the signal of the image is a mixture of Gaussians and the effective voxel's size is equal to the Gaussian full width half maximum (FWHM). Therefore, an effective voxel is in fact a cluster of voxels and the significance threshold is determined based on it. In the end, any cluster of voxels larger than the effective voxel size for a specific Z survives the threshold [100].

The standard approach to model the BH vascular reactivity is using the block task timing convolved with an impulsive response function as regressor. Previous studies have shown that the canonical Hemodynamic Response Function (HRF) (a statistical parametric mapping (SPM) double gamma variate hemodynamic response function) is an appropriate choice when modelling the BOLD response to a BH respiratory task [3, 34, 87].

Due to hemodynamics, the HRF consists of a delayed and spread-out blood response representation. Fortunately, this does that BOLD-fMRI brain images can be acquired every few seconds without missing brain responses (the latter happening every hundred miliseconds, which would be impossible to acquire) [101]. All this has to be taken into account when designing and using an HRF. When performing

respiratory tasks, the BOLD signal increases after a relatively longer delay when compared to neuronal fMRI tasks [3, 102]. This is justified by the transport time of blood from the lungs to the brain and the delay of the vasculature response [87]. To accurately model CVR we must account for hemodynamic delays since there are arterial transit times as gases travel with the blood to arrive at each brain vascular region and local vasodilatory responses that impact the temporal relationship between our model of the vasodilatory stimulus and the BOLD fMRI timeseries [99].

Thus, an onset delay can be added to the BH square block paradigm (chosen by determining the delay that maximizes correlation between the global BOLD signal and the block regressor) previously to its convolution with the canonical HRF. Additionally, the regressor's Temporal Derivative (TD) can also be added to the GLM analysis to allow for a shift in time between the regressor and the BOLD signal [87]. All this allows to achieve a slightly better fit to the data, reducing unexplained noise and increasing resulting statistical significance.

As respiration-induced changes appear to be slower than neuronally-induced BOLD-fMRI signal changes (related with other tasks), as previously mentioned, the canonical HRF might not be the best impulse response function to model the signal. Thus, Birn et al. [102] derived a new impulse response function to variations in the respiration volume per time (RVT) - the Respiratory Response Function (RRF). Later, Vogt et al. [103] derived a new impulse response function to $PetCO_2$ variations during paced hyperventilation. $PetCO_2$ data convolved with this response function was more strongly and prevalently correlated to BOLD signal changes than RVT convolved with the corresponding RRF. Both have shown to be better in modelling BOLD changes induced by respiratory tasks than using the canonical HRF. Nevertheless, several other studies have shown that the canonical HRF is still an appropriate choice [3, 34, 87].

A study compared four different block regressors to model the BOLD-fMRI BH response: the standard block regressor, the block regressor along with its TD, the block regressor delayed by 9 seconds and the block regressor delayed by 9 seconds along with its TD. The latter regressor revealed to be the most appropriate of the four to model the BOLD signal in response to a BH task [87]. Average delay times found in literature range from 5s to 10s for end-expiration BH. Longer delays can be found for end-inspiration BH [87, 104]. Nevertheless, arterial CO_2 increases over time during the BH period and so the $PaCO_2$ stimulus most certainly does not match a simple square block [87].

Therefore, another study used ramp regressors assuming a linear increase in the BOLD signal with time in response to a BH task. However, these did not achieve acceptable repeatability and did not fully account for subject variability in BH performance. [35].

Using paradigm-based models to model the data resulting from the BH-task such as the ones making use of the block and ramp regressors, it is assumed that: (1) participants follow task instructions and (2) increases in $PaCO_2$ due to BH do not differ between subjects nor within subjects. However, this is

most certainly not true, especially in difficult patient populations (e.g. subjects with baseline vasodilation, clinical populations or children/elderly).

In order to avoid these assumptions and account for variability in the BOLD-fMRI data analysis, $PetCO_2$-based models that use the $PetCO_2$ measured during the fMRI scan are used [3, 34, 35, 87, 102]. This data, convolved with a canonical HRF, results in a $PetCO_2$ regressor that provides more reproducible findings than with the use of a ramp regressor [35]. A study compared different $PetCO_2$-based regressors: $PetCO_2$ only, $PetCO_2$ along with its TD, $PetCO_2$ convolved with the canonical HRF and $PetCO_2$ convolved with the canonical HRF along with its TD. It was concluded that the latter provided the most effective model based on $PetCO_2$ [87]. It is possible to correct for the temporal hemodynamic delay by adding it to the regressor. The optimal hemodynamic delay is usually obtained from maximizing the cross-correlation between the $PetCO_2$ physiological regressor and a mean BOLD-fMRI regressor, e.g. a global, GM or even a specific ROI mean time course [35, 97].

$PetCO_2$-based models account for variability across and within subjects. Inclusively, in difficult patient populations, individuals can end breath-holds prematurely since they exhale before going back to normal breathing. The use of $PetCO_2$ also allows for the normalization of CVR units, which enables a better comparison of CVR values obtained in different sessions and in different subjects, making cohort comparisons and longitudinal studies more accurate [3, 35, 87]. However, as mentioned before, $PetCO_2$ models also present disadvantages, as recording $PetCO_2$ requires the additional use of a nasal cannula which may cause some discomfort, and participants need to be instructed and execute at least one practice run for proper measurement, which requires extra time expenditure. In addition, synchronization between $PetCO_2$ recording and fMRI scanning is crucial, which may pose an extra problem [34]. Ultimately, changes in $PaCO_2$ during the BH are measured through $PetCO_2$, which is not a direct measure [3, 87].

All of the above modeling strategies use a single fixed, or preoptimized, delay and this is used to explain the BOLD signal across the whole brain. However, it has been suggested that the response to vasoactive stimuli may exhibit different temporal dynamics in different brain regions, not only in patients with cerebrovascular diseases, but also in healthy subjects [3, 88, 98, 105]. Thus, the hemodynamic delay must be modelled on a voxelwise basis [3, 98, 99]. Characterizing hemodynamic lag at voxel level is challenging, but necessary for correct physiologic interpretation of the data, which improves local CVR estimates otherwise underestimated. [97, 99].

The most common approach to achieve this is by determining the optimal time lag within a certain time interval using cross-correlation between between each voxel time series and a reference time series, e.g. the $PetCO_2$ regressor [3, 105].

A cross-correlation between a mean BOLD-fMRI time series (as the global signal or the signal in GM) and the $PetCO_2$ regressor can also be done in order to obtain a general hemodynamic delay - bulk

shift. From this, it is possible to achieve a voxelwise analysis by performing a lagged GLM fitting using shifted regressors (downsampled to the fMRI TR). Here, the delay between the fMRI and the $PetCO_2$ time series is allowed to vary on a voxelwise basis (from the bulk shift, varying negatively and positively by a certain interval within a certain limit and with a certain increment) to account for slower or faster regional hemodynamic responses by constructing a GLM for each shifted $PetCO_2$ regressor. In the end, for each voxel, the delay at which the GLM explained the most variance in that voxel is chosen as the optimal delay [3, 94, 98, 106].

A voxelwise analysis can also be achieved through the use of a sine–cosine model, which is a linear combination of sine and cosine waves at the BH task frequency. This model takes advantage of the approximately sinusoidal BOLD signal - periodic at the paradigm frequency in response to a BH task in which there are alternating periods of task and baseline (assuming similar duration of each period). Its inherent phase flexibility allows for different time delays across the brain, thus being able to model variations of the BOLD signal across brain regions. Additionally, a great advantage of the sinusoidal modelling is that it only requires the BH task frequency as input parameter, automatically performing delay estimation, thus avoiding time lag assumptions and optimizations. In a study, Murphy et al. [87] concluded that the sine–cosine model explained more variance than any global block model and that there was no significant difference in the variance explained by the most effective model based on $PetCO_2$ ($PetCO_2$ trace convolved with the canonic HRF along with its TD) [34, 87]. Considering the complex shape that the BH BOLD response may have (especially in end-inspiration BH, as referred in 1.4.2), it has been reported by Pinto et al. [88] that the inclusion of harmonics could improve the sine-cosine modelling of the BH BOLD response, by allowing more flexibility to the amplitude, phase and shape of the model. When comparing linear combinations of sine-cosine pairs at the BH task frequency and its successive harmonics, it was found that the second order model (sine-cosine linear combination at the task frequency with its first two harmonics) explained significantly more variance, produced a greater number of responsive voxels, did not underestimate CVR amplitude, and showed better test-retest reproducibility than lower order methods for the BH protocol used. Therefore, one can infer that the sine-cosine pair at the BH task frequency and its first two harmonics provide the most suitable sine-cosine model for BOLD-fMRI response to a BH task if a similar BH protocol is used (especially regarding the duration of BH and baseline periods). Despite the multiple advantages presented by the sine-cosine model, it is still a paradigm-based model, thus presenting the previously mentioned assumptions of these type of models, which reveals limitations especially in the case of difficult patient populations.

This being said, voxelwise characterization of the CVR is important, this way taking into account the different regional hemodynamic delays across the brain that happen even in healthy subjects. This can be achieved whether by using, for example, $PetCO_2$-based models or paradigm-based models.

1.5 State of the art

A literature review was handled regarding CVR in migraine in 1.5.1, menstrual cycle in 1.5.2 and menstrual and menstrually-related migraine in 1.5.3. The present study is done recurring to BH BOLD-fMRI and employing a longitudinal approach focused on menstrually-related episodic migraineurs without aura (in their ictal and interictal phases of the migraine cycle) and hormonal controls (in their premenstrual and midcycle phases of the menstrual cycle). Nevertheless, studies that used other measurement techniques, vasoactive stimuli and approaches (e.g. cross-sectional approaches) were also included in this review. The same was done regarding studies that incorporated patients with other subtypes of migraine, such as the ones that were chronic and with aura. The reasons for this are that these are still relevant to compare to our study and that there are few studies that analysed CVR in migraine. Contrariwise, studies that did not comprise episodic migraine patients without aura in their cohort and the ones that did not evaluate CVR were excluded.

1.5.1 Migraine and CVR

A literature review was conducted looking for studies associating migraine and CVR, which is depicted in table 1.1. Among the 24 researched studies, most included patients both with and without aura and 7 focused on migraine without aura. All studies employed TCD as technique to measure CBF (lacking regional information) apart from two that handled fMRI and another one that used SPECT. Regarding the main arteries studied through TCD, these are the middle cerebral artery (MCA), posterior cerebral artery (PCA) and Basilar Arteries (BA). As regards the vasoactive stimulus, the majority resorted to BH to induce hypercapnia; 6 made use of CO_2 inhalation; 5 measured CVR in response to hypocapnia induced by hyperventilation and two other applied infusion of chemical substances (acetazolamide and L-arginine). All studies assessed migraineurs during the interictal phase (in a case-control approach) except from 7 studies that acquired data in both interictal and ictal phases (in a longitudinal approach).

The findings from these studies revealed to be inconsistent. Nevertheless, studies comparing the ictal with the interictal phases in patients with migraine consistently found lower ictal than interictal reactivity [107–110]. Furthermore, recently, the CVR of the PCA has been consistently reported to be reduced in migraineurs when compared to controls [15, 29, 31].

The most recent study was developed by Cotrim et al. [33] in LaSEEB, the same research lab where the present work was developed. BH BOLD-fMRI data from patients with episodic migraine without aura acquired during ictal and interictal phases from a previous project was processed and analysed. Whole-brain activation maps were obtained using a sine-cosine GLM analysis, and the amplitude metric CVR and delay metric Time-to-peak (TTP) were computed in each voxel. Group-level analysis was also performed to identify differences in CVR and TTP between the ictal and interictal phases. From this,

increased CVR and TTP were found in the occipital region during the ictal compared with the interictal phases. Despite the longitudinal approach being considered the best method having in mind the cyclic nature of migraine, a control group was missing in this study, which is important to confirm the veracity of the results. Furthermore, the direct cause of the vascular response and BOLD signal changes is the change in $PaCO_2$ associated with the BH challenge. Measuring $PetCO_2$ could provide a more accurate CVR characterization, being used as regressor in the GLM analysis instead of the sine-cosine GLM model. At the same time, it would reduce inter- and intrasubject variability caused by respiratory and BH-task compliance differences. In addition, it would be possible to obtain a quantitative measure of CVR if the BOLD Percent Signal Change (PSC) was normalized by the $PetCO_2$.

Table 1.1: Cerebrovascular reactivity studies in migraine, presented in chronological order (most recent first).

Study	Cohort (N,gender)	CBF measurement technique	Vasoactive stimulus	Acquisition phase	Main findings
Cotrim (2020) [33]	MO (14, F)	fMRI	BH	Interictal and ictal	In ictal, compared to interictal: Inreased CVR in the occipital regions.
Harris (2020) [111]	MO (26, F; 4, M) HC (20, F; 10, M)	TCD	BH and hyperventilation	Interictal	In MO, compared to HC: Reduced CVR of the MCA ipsilateral to the headache.
Chan (2019) [32]	Episodic MO (3, M) Episodic MA (2, F; 1, M) HC (5, F)	fMRI	Inspired CO_2 (4-8 mm Hg above the subject's resting $PetCO_2$)	Interictal	In MO, compared to HC: Similar CVR at cortical and WM. In MO, compared to MA and HC: Reduced (or even negative) CVR at the red nucleus of the midbrain.
Lee (2019) [15]	Episodic and chronic MO (168, F; 38, M) Episodic and chronic MA (33, F; 9, M) HC (61, F; 19, M)	TCD	BH	Interictal	In MO and MA, compared to HC: Reduced CVR of MCA, PCA and BA.
Podgorac (2018) [112]	Episodic MO (71, F; 29, M) Episodic MA (61, F; 9, M) HC (13, F; 17, M)	TCD	BH	Interictal	In MA, compared to MO and HC: Increased CVR of the bilateral MCA. In MO, compared to HC: Similar CVR in bilateral MCA.
González-Quintanilla (2016) [28]	Episodic MO (12) Episodic MA (25) Chronic MO (13) Chronic MA (22) HC (41)	TCD	BH	Interictal	In chronic, compared to episodic and HC: Reduced CVR of the MCA. In episodic and chronic, compared to HC: Reduced CVR of the MCA.
Rajan (2014) [29]	Episodic MO (30) Episodic MA (15) HC (44)	TCD	BH	Interictal	In MO and MA, compared to HC: Reduced CVR of bilateral PCA and BA; Similar CVR of the bilateral MCA.
Perko (2011) [31]	MO (16, F; 4, M) MA (16, F; 4, M) HC (16, F; 4, M)	TCD	Intravenous infusion of 100 ml of 30% L-arginine	Interictal	In MO and MA, compared to HC: Reduced CVR to of the PCA; Similar CVR of the MCA.
El-Khawas (2010) [113]	MO (12, F; 2, M) MA (11, F; 2, M) HC (9, F; 5, M)	TCD	Hyperventilation	Interictal	In MO and MA, compared to HC: Reduced CVR of the MCA. In MA, compared to MO and HC: Reduced CVR of the MCA.
Arjona (2007) [114]	Episodic MO (26, F; 10, M) HC (25, F; 19, M)	TCD	BH	Interictal	In MO, compared to HC: Similar CVR of the bilateral MCA.
Silvestrini (2004) [115]	MO (15, F) MA (15, F) HC (15, F)	TCD	BH	Interictal	In MA, compared to MO and HC: Reduced CVR of the BA. In MO, compared to HC: Similar CVR of the BA. In MA and MO, compared to HC: Similar CVR of the MCA. No side-to-side differences in CVR.
Dora (2002) [116]	Episodic MO (22, F; 1, M) HC (9, F; 1, M)	TCD	BH	Interictal	In MO, compared to HC: Increased CVR of the bilateral MCA. "Headache side" compared to the "non-headache" revealed increased CVR.

Kastrup (1998) [117]	Episodic MO (18) Episodic MA (2) HC (17, F; 13, M)	TCD	Inhalation of carbogen (95% O2, 5% CO2)	Interictal	In MO and MA, compared to HC: Increased CVR of the ACA, MCA and PCA. "Headache" side compared to the "non-headache" revealed increased CVR.
Totaro (1997) [118]	MO (28, F; 2, M) MA (26, F; 4, M) HC (27, F; 3, M)	TCD	Inhalation of carbogen (95% O2, 5% CO2)	Interictal	In MO, compared to HC: Reduced CVR of the MCA.
Silvestrini (1996) [30]	MO (13, F; 2, M) MA (11, F; 4, M) HC (15)	TCD	BH	Interictal	In MO and MA, compared to HC: Similar CVR of the MCA; No side-to-side differences in CVR of the MCA.
Valikovics (1996) [119]	MO or MA (12, F) HC (19, F)	TCD	Intravenous administration of acetazolamide	Interictal	In MO and MA, compared to HC: Similar CVR in bilateral MCA.
Silvestrini (1995) [107]	MO (10, F; 6, M) HC (10, F; 6, M)	TCD	BH	Interictal and ictal	In MO, in interictal phase, compared to HC: Similar CVR in bilateral ACA, MCA and PCA. In MO, in ictal phase, compared to interictal phase: Reduced CVR of the ACA, MCA and PCA. No side-to-side differences in CVR, both in interictal and ictal phases.
Fiermonte (1995) [120]	MO (10, F; 5, M) MA (9, F; 6, M) HC (8, F; 7, M)	TCD	Hyperventilation	Interictal	In MA, compared to MO and HC: Increased CVR of the MCA.
Thomsen (1995) [121]	MO (12) MA (8) HC (30)	TCD	Hyperventilation	Interictal and ictal	In MA, in interictal phase, comparedto MO and HC: Increased CVR of the MCA. In MO, in interictal phase, compared to HC: Similar CVR of the MCA. In MO, in interictal phase, comparedto ictal phase: Similar CVR of the MCA. No side-to-side differences in CVR of MCA, both in interictal and ictal phases.
Zwetsloot (1992) [122]	Episodic MO (17, F; 6, M) HC (26, M; 22, M)	TCD	Hyperventilation	Interictal and ictal	In MO, in ictal state, comparedto interictal phase: Similar CVR of the VBA.
Zwetsloot (1991) [123]	MO (48) HC (10, F; 7, M)	TCD	Hyperventilation	Interictal and ictal	In MO, in ictal phase, comparedto interictal phase: Similar CVR of the MCA and BA. In MO, compared to HC: Similar CVR of the MCA and BA.
Harer (1991) [109]	MO or MA (21, F; 9, M) HC (21, F; 9, M)	TCD	Inhalation of carbogen (95% O2, 5% CO2)	Interictal and ictal	In MO and MA, compared to HC: Ictal phase: Reduced CVR of the MCA. Interictal phase: Nearly double CVR of the MCA ipsilateral to the headache.
Thomas (1990) [80]	MO or MA (7, F; 3, M) HC (3, F; 7, M)	TCD	Inhalation of carbogen (95% O2, 5% CO2)	Interictal	In MO and MA, compared to HC: Increased CVR of the MCA.
Sakai (1979) [108]	MO (32, F; 5, M) MA (13, F; 5, M) HC (26, M; 22, M)	SPECT	Inhalation of carbogen (95% O2, 5% CO2)	Interictal and ictal	In MO and MA, compared to HC: Prodrome and headache phases: Reduced CVR; no side-to-side differences. Interictal phase: Excessive CVR; "headache" side showed increased CVR compared to the "non-headache".

CBF = Cerebral Blood Flow; MO = Migraineurs without Aura; MA = Migraineurs with Aura; HC = Healthy Controls; TCD = Transcranial Doppler; fMRI = Functional Magnetic Resonance Imaging; BH = Breath-holding; O_2 = Oxygen; CO_2 = Carbon Dioxide ; $PetCO_2$ = Partial Pressure of End-tidal Carbon Dioxide; CVR = Cerebrovascular Reactivity; WM = White Matter; ACA = Anterior Cerebral Arteries; MCA = Middle Cerebral Arteries; PCA = Posterior Cerebral Arteries; BA = Basilar Arteries;

1.5.2 Menstrual cycle and CVR

As regards CVR in menstrual cycle, 3 studies have been done as far as we know and these are presented in table 1.2. All of them used TCD to measure CBF. The first study [124] used inhalation of carbogen as vasoactive stimulus to induce hypercapnia and indomethacin administration to inhibit the production of progesterone in healthy women and men and thus simulate the hormonal levels of the follicular (pre-ovulation) phase of the menstrual cycle. Reduced CVR of the MCA was found after pro-

gesterone production inhibition. On the other hand, the two most recent studies [25, 71] used the natural menstrual cycle of healthy women. From these, one [71] recurred to intraveneous administration of acetazolamide and measured CBF during the early follicular, late follicular and late luteal phases of the menstrual cycle. It was suggested that the CVR of the brain parts supplied by the right ICA varied significantly during specific phases of the menstrual cycle and that these variations seem to be associated with the circulating levels of the ovarian hormones estradiol (E2) and progesterone (P4). The other one [25] used inhalation of a gas mixture with CO_2 and assessed CBF during the early and late follicular phases. However, no difference in CVR between these phases was verified. Therefore, the results from the literature review concerning CVR and the menstrual cycle revealed to be incongruent.

Table 1.2: Cerebrovascular reactivity studies in menstrual cycle, presented in chronological order (most recent first).

Study	Cohort (N, gender)	CBF measurement technique	Vasoactive stimulus	Acquisition phase	Main findings
Peltonen (2016) [25]	HC (11,F)	TCD	40% O_2 and 3% CO_2 gas mixture	∼day 3 and day 14 of the cycle	Day 3 compared to day 14: Similar CVR of the MCA.
Krejza (2013) [71]	HC (19, F)	TCD	Intravenous administration of acetazolamide	Days 5, 13 and 26 of the cycle	Day 26 compared to day 13: Higher CVR of the right ICA. Day 26: Higher CVR of the right ICA compared to the left ICA.
Kastrup (1999) [124]	HC (11, F; 11, M)	TCD	Inhalation of carbogen (95% O2, 5% CO2)	Before and following indomethacin administration	Women compared to men: Higher CVR of the MCA before indomethacin administration. In men and woman, after indomethacin administration compared to before: Reduced CVR of the MCA. Similar CVR of the right and left MCA.

CBF = Cerebral Blood Flow; HC = Healthy Controls; TCD = Transcranial Doppler; O_2 = Oxygen; CO_2 = Carbon Dioxide; CVR = Cerebrovascular Reactivity; MCA = Middle Cerebral Artery; ICA = Internal Cerebral Artery.

1.5.3 Menstrual and menstrually-related migraine and CVR

To the best of our knowledge, there were no studies associating menstrually-related migraine and CVR and only 2 studies related menstrual migraine and CVR, which are presented in table 1.3. Both used TCD to measure CBF, which does not provide regional information of the brain. The first employed a longitudinal approach studying patients with menstrual migraine and included Healthy Controls (HC) without specifying the migraine or the menstrual cycle phase, respectively. CVR of the MCA was found to be reduced during the menstruation period when compared to the period after menstruation and CVR of the MCA and PCA was detected to be reduced when compared to controls. In the most recent one, menstrual migraineurs were assessed during the interictal state and both these and the HC were not menstruating at the time of the acquisition. However, the migraineurs recruited for this study were not a clinical sample (they were not patients of a migraine or neurology clinic nor diagnosed by a neurologist). No differences in the CVR of the MCA were found [23]. Nevertheless, the cross sectional nature of the study may have precluded to prove an association between MM and impaired CVR.

Table 1.3: Cerebrovascular reactivity study in menstrual migraine, presented in chronological order (most recent first).

Study	Cohort (N, gender)	CBF measurement technique	Vasoactive stimulus	Acquisition phase	Main findings
Dzator (2021) [23]	MM (50) HC (29)	TCD	Inhalation of carbongen (95% O_2, 5% CO_2)	Interictal and not menstruating (for MM); Not menstruating (for HC).	In MM, compared to HC: Similar CVR of the MCA; Negative correlation between headache frequency and CVR of the MCA.
Tasdemir (2013) [72]	MM (23) HC (20)	TCD	BH	Days 3 and 10 of the menstrual cycle (for MM); Any day of the menstrual cycle (for HC).	In day 3, compared to day 10: Reduced CVR of PCA. In MM, compared to HC: Reduced CVR of the MCA and PCA.

CBF = Cerebral Blood Flow; MM = Mentrual Migraineurs; HC = Healthy Controls; TCD = Transcranial Doppler; O_2 = Oxygen; CO_2 = Carbon Dioxide; CVR = Cerebrovascular Reactivity; BH = Breath-holding; MCA = Middle Cerebral Arteries; PCA = Posterior Cerebral Arteries.

1.6 Dissertation objectives

The main goal of this study is to investigate the CVR changes through the analysis of BH BOLD-fMRI data from menstrual or menstrually-related migraine patients and hormonal controls. In order to successfully accomplish this, specific objectives were defined to be achieved in the a sequential order:

1. To develop and optimize a BH task paradigm and its experimental setup (that inclusively enables to acquire the expired CO_2 data).

2. To collect the BOLD-fMRI and CO_2 data at Hospital da Luz following a longitudinal approach: from a group of migraine patients during an attack and in an attack-free period and from a group of hormonal healthy controls with a regular menstrual cycle during the premenstrual and midcycle phases of their menstrual cycle.

3. To compare different models for the voxelwise analysis of the BH BOLD-fMRI data: a $PetCO_2$-based method (that uses the $PetCO_2$ regressor) and two paradigm-based methods (that used the breathing task timings).

4. To identify brain regions showing altered CVR and delays in patients during the ictal and interictal phases of the migraine cycle; in controls during the premenstrual phase when compared to the midcycle phase of the menstrual cycle by conducting a group-level analysis.

1.7 Dissertation outline

This dissertation is organized in 4 main chapters. The first and current chapter consists in an introduction to this work and starts with the motivation behind this work in 1.1, followed by a theoretical description of migraine in section 1.2 that includes its pathophysiology, associated vasculopathy and the specific case of menstrual migraine. Section 1.3 contains relevant information about the concept of cerebrovascular reactivity (CVR), together with the neuroimaging techniques and vasoactive stimuli that can be used to assess it. Following, section 1.4 comprises guidance regarding the best practices when using

breath-holding as vasoactive stimulus to measure CVR, namely when designing the task paradigm and modelling the acquired data. Section 1.5 consists in state of the art, where a literature review can be found, focusing on previous studies assessing CVR in migraine, in menstrual cycle and in menstrual migraine, directly or indirectly related to the present work. Chapter 2 starts with a description of the BH task used in this study, namely its paradigm, experimental setup and experimental optimization in section 2.1. The following section 2.2 exhibits a description of the participants recruited for this work, the study design and the acquired imaging and expired CO_2 data. Next, section 2.3, describes how the CO_2 was processed, using information about the participant's breathing rate and the acquisition delay to produce the $PetCO_2$ regressor. Next, section 2.4 presents the methodology applied in order to achieve this dissertation' objectives: starting with an explanation of the preprocessing and registration steps and ending with a description of the processing of the breath-holding BOLD-fMRI data using different analysis methods and including a final region-of-interest analysis. Chapter 3 focuses on the description of the results achieved regarding $PetCO_2$, motion and cross-correlation analysis in section 3.1, cerebrovascular reactivity and delay maps in section 3.2, whole brain analysis (at both subject- and control group-level) in section 3.3 and region-specific (control group-level) analysis in section 3.4. Simultaneously, these are discussed and interpreted along with their comparison with findings from literature. This dissertation ends with chapter 4, where the main conclusions are presented, together with the relation of these with the literature in section 4.1 and its main limitations and suggestions for future work in section 4.2.

Chapter 2

Material and methods

This chapter details the material and methods used to achieve this dissertation's objectives. It starts with a description of the breath-holding (BH) task used in this study, explaining the paradigm and experimental setup, such as their optimization (2.1). Next, a description of the participants recruited for this work, the study design and the acquired images and expired CO_2 data are presented (2.2). Following, a description of how the CO_2 was processed and analysed is presented (2.3). Finally, the methodology applied in order to process and analyse the BOLD-fMRI data, starting with the preprocessing and registration steps and ending with the processing of the BH BOLD-fMRI data using different analysis methods and including a final regions-of-interest analysis, is described (2.4).

2.1 Breath-holding task

2.1.1 Paradigm design

The paradigm design followed the parameters that seemed to be the best according to the research presented in 1.4.1, although the lack of literature deriving conclusions about the best choices. These parameters included end-expiration BH followed by exhalation, BH duration of 15s, baseline period with externally-paced breathing with a frequency similar to the participant's spontaneous breathing period and a duration that enables blood gas levels to return to baseline, recovery period with self-paced breathing and at least 3 trials.

Therefore, the task comprised a 30s initial baseline of externally-paced breathing and four 58.5s cycles (resulting in a total duration of 269s, approximately 4.5 minutes taking into account a 5s fixation cross). Each cycle consisted of a 15s end-expiration BH followed by a 1.5s quick exhalation of residual air, a subsequent 12s recovery period with self-paced breathing and finally a return to 30s baseline of externally-paced breathing. The paradigm and its corresponding parameters is illustrated in figure 2.1.

Regarding the 30s baseline periods (both the initial baseline and each trial's baseline), these were externally-paced at a breathing period that was the most similar to the subject's spontaneous breathing period to achieve normocapnic baselines and avoid hypocapnia. Based on literature, it was concluded that the most common spontaneous breathing periods ranged from 1/3 Hz to 1/6 Hz with an inspiration/-expiration ratio of 1:2. Therefore, four paradigms were created that differed in inspiration and expiration duration and consequently in the number of breathing cycles in each baseline. For the breathing rates of 1/3z, 1/4 Hz, 1/5 Hz and 1/6 Hz, each baseline inspiration/expiration were chosen to have 1s/2s, 1.5s/2.5s, 2s/3s and 2.5s/3.5s and consequently 10, 7.5, 6 and 5 cycles (in 30s), respectively. This is represented in table 2.1. In the case of the of the breathing rate of 1/4 Hz, in order to achieve the 7.5 cycles, the baseline started with an expiration instead of an inspiration. One of these four paradigms was chosen for each subject according to his/her measured breathing period.

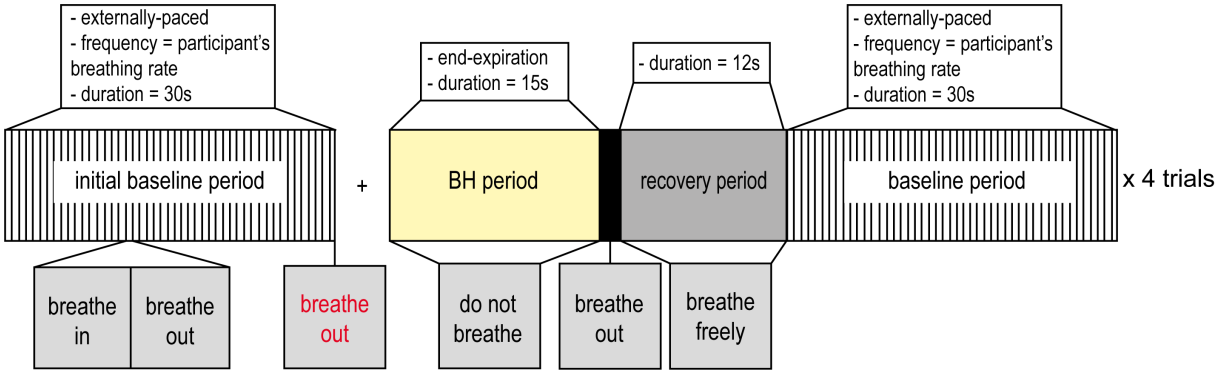

Figure 2.1: Schematic illustration of the breath-holding task paradigm with the corresponding parameters. Figure adapted from [3].

Table 2.1: Inspiration and expiration durations in seconds and number of breathing cycles in the baseline period, for each breathing period paradigm.

Breathing rate (Hz)	Inspiration/expiration duration (s)	No. of breathing cycles in baseline
1/3	1/2	10
1/4	1.5/2.5	7.5
1/5	2/3	6
1/6	2.5/3.5	3

2.1.2 Experimental setup

The experimental setup is illustrated in figure 2.2. Regarding the breath-holding (BH) task, participants were cued to proceed by a series of written instructions presented on a screen, similarly to several CVR studies that used a BH-task [3, 94, 98]. The Neurobehavioral Systems Presentation software (https://www.neurobs.com/) was used to program these written instructions. Presentation is a stimulus delivery and experiment control program for neuroscience that delivers auditory, visual and multimodal

stimuli with sub-millisecond temporal precision. The instructions were written in Portuguese and without abbreviations to avoid interpretation doubts. To control for the potentially strong neuronal activation induced by visual instructions, brightness levels remained similar across the whole task [3, 117] and all the instruction were given in black letters over a gray background, except for one. In fact, the expiration instruction before the BH period was red for the participants to know what was coming next and thus to avoid the initiation of the next inspiration, following the sequence up to that point. Additionally, according to what was explained in the previous section 2.1.1, four sets of instructions were programmed in Presentation with slightly different inspiration and expiration durations and consequently different number of breathing cycles in each baseline. From these, one was chosen for each subject according to his/her measured natural breathing period and the Presentation visual stimuli in the computer (Presentation computer) were projected on the googles mounted on the head radiofrequency coil.

Measurement of CO_2 levels of expired air data was carried out throughout the MRI scan session using the Medlab CAP10 capnograph (https://www.medlab.eu/english/products/capnographs/cap10) and a nasal cannula as the one shown in the top of figure 2.2. Additionally, due to the logistics of the MRI environment, a long sampling line (e.g. small sampling lines connected between each other) had to be used to connect the capnograph in the control room to the participant's nasal cannula in the scanner room. This introduced a delay between CO_2 exhalation inside the scanner and CO_2 recording outside the scanner.

CO_2 data from the capnograph was recorded in a computer (the recording computer) by connecting the two through the analog to digital converter Arduino UNO (https://store.arduino.cc/products/arduino-uno-rev3/). In the recording computer, the inhouse code written in MATLAB (https://www.mathworks.com/products/matlab.html) was used to detect and real-time plot the CO_2 signal. The Presentation computer was also connected to the recording computer through an ethernet cable. This enabled to send the codes relative to the written instructions while these were being displayed to the subject inside the scanner. For this, the Lab Streaming Layer (LSL) system was used. LSL is a system for the synchronized collection of streaming data for live analysis or recording. In this case, the LSL received streaming data from the capnograph and Presentation and the LabRecorder LSL recording program recorded it in an .xdf (Extensible Data Format) file. LabRecorder records a collection of streams, including all their data (time-series/ markers, meta-data) into a single .xdf file, the default file recorder for use with LSL. The .xdf format is a general-purpose format for time series and their meta-data that was jointly developed with LSL to ensure compatibility. The MATLAB importer for .xdf files (xdf-Matlab code) was used to import the files into MATLAB. In MATLAB, the CO_2 signal and the Presentation codes could be analysed in a single plot. Further processing of CO_2 will be described in a further section.

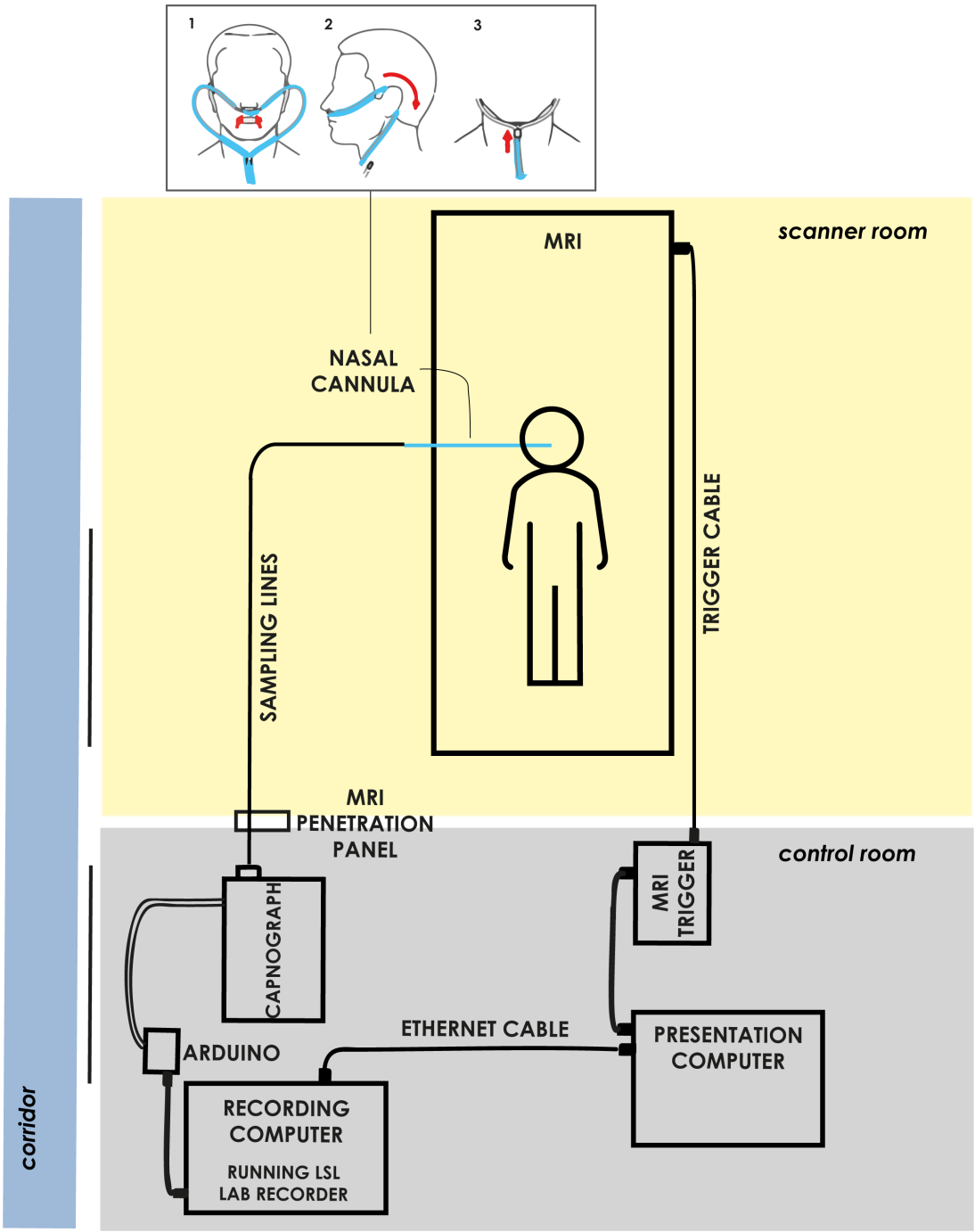

Figure 2.2: Schematic illustration of the breath-holding task experimental setup. The visual stimuli in Presentation computer are projected on the googles mounted on the head radiofrequency coil inside the scanner. Measurement of CO_2 levels of expired air data is carried out using the Medlab CAP10 capnograph and a tubing system (composed of a nasal cannula and sampling lines connected to each other). The codes relative to the written instructions being displayed to the subject and the CO_2 data being acquired in the capnograph (passing through the analog to digital converter Arduino UNO) are both sent to the recording computer.

2.1.3 Experimental optimization

In order to optimize the BH task, both the experimental paradigm and setup were tested at the research lab LaSEEB (Evolutionary Systems and Biomedical Engineering Lab) of ISR-Lisbon (Institute for Systems and Robotics) (Lisbon, Portugal) in may 2021. The volunteers were 7 female gender adults aged from 20 to 55 years that were professors, investigators or students. Additionally, a pilot study was performed in the same month at Hospital da Luz (Lisbon, Portugal) with one of these volunteers to test the BH task along with the fMRI scan.

Breathing rates between 1/3 Hz and 1/5 Hz were registered, what was according to the most common spontaneous breathing rates found in literature (1/3 Hz to 1/6 Hz) [3].

As concerns the paradigm, a first draft was made that consisted of a 30s initial baseline of externally-paced breathing and three 90s cycles (resulting in a total duration of 302s, approximately 5 minutes taking into account a 2s fixation cross). Each cycle consisted of a 15s end-expiration BH followed by a 3s quick exhalation of residual air, a subsequent 12s recovery period with self-paced natural breathing and finally a return to 60s baseline of externally-paced breathing.

At the lab, the Presentation program to be displayed on the computer screen was chosen according to the calculated breathing period. The volunteer then performed the BH task while the CO_2 signal was being visualized in a real-time MATLAB plot and simultaneously recorded through LabRecorder. Signals were then analysed in MATLAB to check if the signal's shape was the expected one (e.g. the post-BH CO_2 peaks were higher than the pre-BH CO_2 peaks or the baseline was regular). Additionally, it was asked to the volunteer if she had found it hard to perform in general, e.g. had felt tired in general, had found the task too long, had found hard to sustain the breath during the BH period, to exhale after the BH, or to breath according to the instructions during the externally-paced baseline period. If the signals did not have the expected shape or if the person had found the task hard to perform considering the mentioned questions, the task was repeated with a Presentation program corresponding to another breathing period (usually a higher one). Once more, the signal was analysed and the same questions were made to the volunteer. This allowed the assessment and optimization of the participants' compliance.

Still considering the answers to the questions asked in the end of the task, volunteers revealed that the post-BH exhalation was often hard to perform, and so this parameter was reduced to half, resulting in 1.5s of post-BH exhalation.

From the analysis of the acquired CO_2 and fMRI data in the pilot experiment performed in Hospital da Luz, the fixation cross time period revealed itself short for the subject to calm her spontaneous breath and focus on the task, so this was extended to a 5s duration. Additionally, it was concluded that both signals returned to baseline in a time period of 30s, and so, the 60s baseline duration was reduced to 30s. This also brings advantages in the data analysis, namely when recurring to the sine-cosine

model to model the data, since a better model can be achieved when the baseline period duration is more similar to the BH period duration, as explained in section 1.4.2. Finally, as mentioned in section 2.1.1, the more BH trials are performed, the more averaging can be done and thus higher SNR can be achieved. Unfortunately, this usually implies longer protocol duration that may lead to patient fatigue and thus more motion artifacts and worse task performance. However, in this case the resulting paradigm resulting from changing the fixation cross time period, the baselines' duration and the number of trials remained with similar total duration. Additionally, as there were no motion artifacts in the fMRI data resulting from the pilot experiment, then the number of trials was changed to 4.

Therefore, as mentioned in section 2.1.1, the final task paradigm comprised a 30s initial baseline of externally-paced breathing and four 58.5s cycles (resulting in a total duration of 269s, approximately 4.5 minutes taking into account a 5s fixation cross). Each cycle consisted of a 15s end-expiration BH followed by a 1.5s quick exhalation of residual air, a subsequent 12s recovery period with self-paced natural breathing and finally a return to 30s baseline of externally-paced breathing.

Once more, lab experiments were made with the same volunteers and all of them revealed to feel evenly or more comfortable with the new paradigm execution.

Considering the tubing system (connected nasal cannula and sampling lines), this introduced a delay between CO_2 exhalation inside the scanner and CO_2 recording outside the scanner, as it was mentioned in section 2.1.2. Therefore, tests with nasal cannulas and sampling lines of different lengths and widths were made with different volunteers at the lab. From this, it was concluded about which kind of tubing system was more comfortable and introduced a smaller delay, being better in terms of time optimization. This constituted the best tubing system for the hospital acquisitions (although it was not always possible to have the same tubing system for all the acquisitions due to logistics issues). Afterwards, at the pilot acquisition, it was inferred about how many tubes were necessary to reach the volunteer in the scanner, in the scanner room, from the capnograph, in the control room. The expected delay from this latter tubing system was calculated and taken into account by recording an extra time period of data at the end of the acquisition.

A preprocessing filtering of the recorded signals was being done in MATLAB. However, it was concluded to be deteriorating the signals, namely the post-BH signal peaks that were really important for the analysis, as it will be further explained in the next section. Therefore, it was chosen not to apply any preprocessing to the signals and then, the signal recorded corresponded to the signal being visualized in the real-time MATLAB plot. For time optimization, it was chosen to inspect the signals' shape in the latter during the hospital acquisitions.

2.2 Participants and data acquisition

2.2.1 Participants

A longitudinal study was conducted in the Imagiology Center of Hospital da Luz (Lisbon, Portugal) in the period from May to October 2021. The cases comprised 3 female gender adults aged from 29 to 46 years old with a diagnosis of menstrually-related episodic migraine without aura according to the International Classification of Headache Disorders (ICHD-3) criteria. These cases were otherwise healthy, defined as not having any disease that was currently preventing an active productive life nor with a life expectancy below 5 years. The cases recruited were patients from the Hospital da Luz outpatient clinic already diagnosed according to the criteria previously described. As control group, 6 healthy (following the previous criteria) (mean age = 25.50$\pm$3.08 years old) women who had no history of migraine or any other type of headache and had regular menstrual cycles were included. The controls were recruited among social media, migraine groups, academic groups and internal mailing lists. Both cases and controls could be using hormonal contraception during the study provided that they still had menstruation and were able to track their menstrual cycle.

Volunteers were excluded if they had a neurologic medical record, a current psychiatric disorder, were being treated with psychoactive drugs (including anxiolytics, anti-depressives, anti-epileptics and migraine prophylactic) or if they had any contraindication for performing MRI, as it is the case of women with ferromagnetic metallic implants, non-removable piercings, tattoos near the head, claustrophobia or currently breast-feeding, pregnant or trying a pregnancy. The former was done with the aim of avoiding neurological confounds or pharmacological interference and the latter to ensure safety during acquisition.

The study was approved by the Comissão de Ética para a Investigação Clínica of Hospital da Luz, and all the participants filled a written informed consent form. Subjects who satisfied the inclusion criteria and agreed to participate were included in the study after signing informed consent. None of the volunteers received any contribution for participating in the study and could quit at any stage with no consequences for future treatments at the institution.

Table 2.2 presents cases' demographic data together with several clinical parameters regarding their usual migraine attacks: migraine age of onset, usual attack frequency (number of attacks per month), usual duration of the attack (in hours) and the intensity of some of its associated symptoms: headache, nausea, photophobia, phonophobia, motion intolerance and concentration levels (assessed on a 0-10 Visual Analogue Scale (VAS), where 0 corresponds to "non-existing" and 10 to "very strong"). The usual headache localization was also registered.

For both cases and controls, it was registered whether they were taking any hormonal contraception and which it was. Additionally, all volunteers were asked about their average menstrual cycle duration

Table 2.2: Demographics and clinical parameters, averaged across patients.

Parameters	**mean $\pm$ s.d.**
Age (years)	35.3 ± 9.3
Age onset (years)	16.7 ± 5.8
Usual attack frequency (no. of attacks/month)	1.3 ± 0.6
Usual attack duration (hours)	56.7 ± 13.3
Usual headache intensity (0-10 VAS)	7.7 ± 0.3

(in days).

2.2.2 Study design

This study consisted of a longitudinal study.

Each patient was scanned in two different phases of migraine: ictal (headache) and interictal. The acquisition of each one of the phases was managed to be programmed as the migraine cycle in these patients was associated with the menstrual cycle.

Regarding the ictal (headache) phase scanning session, it was performed during an eligible migraine attack, as indicated by the patient. Eligible attacks are defined as perceived by the patient as migraine attacks (including at least one accompanying symptom, either photophobia, phonophobia, mental slowing, nausea or aggravation by movement); pain intensity on VAS $\geq$ 4/10; untreated or treated previously with a migraine specific drug (triptans or ergots) more that 12 h before or treated with a non-steroidal anti-inflammatory drug or analgesic more that 6 h before; and being able to come to the hospital.

Several clinical parameters were reported during the ictal (headache) session, including the attack/-pain duration (time from the beginning of the migraine attack until data acquisition onset), the headache intensity of the ongoing attack and other ictal phase associated symptoms (using a 0-10 VAS). This information is presented in table 2.3. Further headache characterization, including its localization, was also performed.

Table 2.3: Clinical parameters characterising the ongoing attack in the ictal session, averaged across patients.

Parameters	**mean $\pm$ s.d.**
Attack/Pain duration (h)	14.50 ± 17.68
Headache intensity (0-10 VAS)	3.50 ± 0.71
Nausea (0-10 VAS)	0 ± 0
Photophobia (0-10 VAS)	1.00 ± 1.41
Phonophobia (0-10 VAS)	1.00 ± 1.41
Motion intolerance (0-10 VAS)	1.00 ± 1.41
Concentration level (0-10 VAS)	3.50 ± 2.12

Scanning of controls happened in two sessions: in the premenstrual phase and in the post-ovulation phase of the menstrual cycle, denominated midcyle. The premenstrual phase was considered to be 1 to 4 days before menstruation onset and the midcycle phase 1 to 4 days after ovulation (ovulation being

forecasted by natural menstrual cycle monitoring through the calendar method and sometimes using basal temperature measurement; and in day 14 of the menstrual cycle for the participants taking the pill, then having a 28 days duration menstrual cycle).

The two sessions (for both patients and controls) were performed with a minimal interval of 15 days. However, in some cases, it was not possible to acquire both session of a volunteer. This was due to the inherent unpredictability of the migraine (concerning the patients) and to hospital logistics issues, the latter having been exacerbated by the COVID pandemic. Therefore, only 2/3 patients and 5/6 controls concluded the two planned sessions within the duration of the work leading up to this dissertation.

In one of the sessions of the volunteer (whether being a patient or a control), functional, structural and fieldmap data were acquired. In the other session, only the functional and fieldmap images were obtained. Additionally, in the interictal (in the case of patients) and midcycle (in the case of controls) scans, concomitant MR-compatible EEG acquisition was performed during the functional sequences (data not analysed in the scope of this work). Brief neuropsychological evaluation was conducted before each one of the scans.

A breath-holding (BH) challenge scan was performed in each session in order to investigate for CVR changes in migraine. The imaging protocol comprised several other functional and structural images. Only the ones directly related with the study of CVR performed in this work are described in this dissertation.

2.2.3 Data acquisition

Two types of data were acquired for each participant, for each acquisition: brain images and the expired CO_2.

2.2.3.1 Image data

All images were acquired with a 3 Tesla Siemens MAGNETOM Vida MRI scanner using a 64-channel receive radio-frequency coil.

The structural anatomic T1-weighted images were collected using a Magnetization-prepared Rapid Gradient Echo (MPRAGE) sequence with 1 mm of isotropic resolution.

Functional images were collected using a T2*-weighted 2D Gradient Echo-Echo Planar Imaging (GE-EPI) sequence, accelerated with a Simultaneous Multi-slice (SMS) acceleration factor of 3 and an in-plane Generalized Autocalibrating Partial Parallel Acquisition (GRAPPA) acceleration factor of 2, with the following parameters: TR=1260ms; TE=30ms, effective EPI echo spacing 0.31ms and 2.2mm isotropic resolution. The number of acquired volumes was 213, yielding a total acquisition time of 268.38s, which corresponds to approximately 4.5 minutes.

As concerns B0 fieldmap images, these were collected using a GE-EPI, with TE1/TE2 = 4.92/7.38 ms and otherwise similar geometry to the functional images.

2.2.3.2 CO_2 Data

During the BOLD imaging of the BH task described in section 2.1.1, the expired CO_2 was simultaneously acquired using the experimental setup described in section 2.1.2.

To assure that the BH task was well executed and that the CO_2 was properly measured once inside the scanner, the participants' preparation outside the scanner was crucial. Consequently, all the experimental setup described in 2.1.2 was put together in a preparation room located near the scanner, in a stainless steel hospital utility cart and it was checked that the whole recording system was fully operational.

Still in the preparation room, the breathing task paradigm was explained to the participants recurring to a visual scheme, enhancing the importance of always breathing through their noses and not to inspire during the BH period. After this, each participant's spontaneous breathing period was measured by recording the expired CO_2 during approximately one minute while the participant was resting with eyes opened. The breathing period was calculated in MATLAB and, according to it, the corresponding Presentation paradigm was displayed on the Presentation computer screen and a practice run was performed with live visualization of the CO_2 signal in MATLAB in the recording computer. If the signal's shape was not the expected one (e.g. the post-BH CO_2 peaks were not higher than the pre-BH CO_2 peaks) or if the participant found the task hard to perform, then a new practice run was performed and likewise analysed with the Presentation program corresponding to a slower breathing period (e.g. breathing period 4s instead of 3s).

After the preparation finished, the participant was directed to the scanner room. Meanwhile, the stainless steel hospital utility cart with the experimental setup was taken to the control room and the tubing system was passed from the control room to the scanner room according to the setup illustrated in figure 2.2. Additionally, the Presentation visual instructions in the Presentation computer were projected on the googles mounted on the head radiofrequency coil. By doing this, it was possible to record the expired CO_2 and the codes corresponding to the Presentation instructions being displayed in the recording computer at the same time the fMRI images were being acquired throughout the BH task.

2.3 CO_2 data processing and analysis

Processing and analysis of the CO_2 signal acquired were conducted using the MATLAB software (https://www.mathworks.com/products/matlab.html).

2.3.1 Breathing period

First of all, the custom MATLAB peak detection algorithm was applied to the acquired breathing period CO_2 data in order to detect the end-tidal peaks - level of CO_2 released at the end of exhalations. The output was manually checked for every dataset to ensure that each end-tidal peak was detected and to remove incorrectly identified ones (e.g. in the case of partial breathing through the mouth and not fully through the nose, not resulting in a true end-tidal peak). Two manners of deducing the spontaneous breathing periods were implemented (that produced similar results): (1) calculating the average period between end-tidal peaks and (2) dividing the recorded time duration by the number of end-tidal peaks.

2.3.2 Delay

Each capnograph stream output in the .xdf file was purposefully slightly longer than the length of the fMRI acquisition: an additional time period of at least 30s of data before and after each acquisition were included in the exported data. This time value was chosen based on the tests performed at both the lab and the pilot acquisition referred in section 2.1.3.

The time period after each BH acquisition made it possible to correct for the recording delay between CO_2 exhalation inside the scanner and CO_2 recording outside the scanner due to the long tubing system. In fact, the first step of the CO_2 processing was to apply a negative time shift in order to manually align each marker from the Presentation stream referring to the beginning of post-BH exhalation and the capnograph CO_2 signal right before this started increasing as a representation of the post-BH exhalation.

On the other hand, the time period added before was due the delay between the CO_2 pressure change in the blood and the fMRI signal change caused by the vascular transit time and vasodilatory dynamics. This will be useful in further data processing.

2.3.3 PetCO$_2$ data extraction and analysis

The CO_2 data corrected for the recording delay was similarly processed to the breathing periods CO_2 data in order to detect the end-tidal peaks.

The $PetCO_2$ trace was produced by using a piecewise cubic interpolation between the detected end-tidal peaks to the capnograph sampling interval. On each subinterval, this interpolation used a cubic Hermite interpolating polynomial that was shape preserving, which means that the slopes were chosen to preserve the shape of the data and respect monotonicity (on intervals where the data in monotonic, so is the polynomial and at points where the data has a local extremum, so does the polynomial).

For each subject and session, the mean baseline $PetCO_2$ and the mean $\Delta PetCO_2$ were calculated. The mean baseline $PetCO_2$ was obtained by calculating, for each baseline period, the mean across the number of breathing cycles in that baseline corresponding to the paradigm that was run for that

subject according to her spontaneous breathing rate (presented in table 2.1) and averaging across the four cycles. For the breathing period of 4s, as the number of corresponding breathing cycles in the 30s baseline was 7.5, the number of breathing cycles used to do this calculation was 7. The mean $\Delta PetCO_2$ was calculated by subtracting, for each task cycle, the value of the post-BH $PetCO_2$ by the mean baseline $PetCO_2$ of the previous baseline period and averaging across the four cycles.

Finally, a $PetCO_2$ regressor was created by convolving the $PetCO_2$ trace with the canonical HRF [3, 34, 87].

2.4 BOLD-fMRI data processing and analysis

Processing and analysis of the BOLD-fMRI was conducted using both the Functional Magnetic Resonance Imaging of the Brain (FMRIB) Software Library (FSL, https://fsl.fmrib.ox.ac.uk/fsl/fslwiki/) and the MATLAB software. The FMRIB's Software Library (FSL) built-in tools were run both from the command line and Graphical User Interfaces (GUIs).

2.4.1 Preprocessing and registration

2.4.1.1 Preprocessing

fMRI data consists of 3D images composed of groups of 3D voxels whose values are repeatedly collected over time. Thus, fMRI data is a 4D data in which time corresponds to the fourth dimension. The performance of BH tasks typically causes task-correlated motion in this high amount of data [94]. Hence, it is crucial to perform some preprocessing steps to remove unwanted artifacts. Furthermore, to preprocess the fMRI data, both anatomical and fieldmap data were needed, so it was necessary to previously prepare them.

Regarding the **structural** images, the methods used and respective tools were the following:
(i) Reorientation of the image, using fslreorient2std (https://fsl.fmrib.ox.ac.uk/fsl/fslwiki/Orientation$%$20Explained). This tool applied 90, 180 or 270 degree rotations around the different axes as necessary to get the labels in the same position as the standard template (Montreal Neurologic Institute (MNI) 152) for visualization purposes.
(ii) Removal of non-brain tissues, using the Advanced Normalization Tools (ANTs) (https://andysbrainbook.readthedocs.io/en/latest/ANTs/ANTs_Overview.html). It used a template with the skull and a brain probability mask to eliminate voxels that were not part of brain, such as the ones in the skull.
(iii) Segmentation of the brain, using the FMRIB of the Brain Automated Segmentation Tool (FAST) (https://fsl.fmrib.ox.ac.uk/fsl/fslwiki/FAST). It segmented the brain into different tissues including the grey matter (GM), white matter (WM) and cerebrospinal fluid (CSF).

Concerning the **fieldmap** images' preparation, the methods used and corresponding FSL tools were the following:

(i) Removal of non-brain tissues, using Brain Extraction Tool (BET) (https://fsl.fmrib.ox.ac.uk/fsl/fslwiki/BET). This tool used the mean volume of the data, created a brain mask and applied it to all the other volumes in order to eliminate voxels of no interest, such as all non-brain voxels and any voxels with only a small partial volume contribution. Afterwards, a mask was manually created and applied to the BET output in order to exclude the remaining non-tissue voxels.

(ii) Normalization of the phase image to get a fieldmap image in the desired units (rads/s), using the Fsl_prepare_fieldmap GUI (https://fsl.fmrib.ox.ac.uk/fsl/fslwiki/FUGUE/Guide#SIEMENS_data). As the B0 field can be measured in Tesla, Hz or rad/s in MRI, it is important to convert it to rad/s for future fMRI preprocessing.

Finally, to preprocess the **functional** image, the methods and respective FSL tools were the following:

(i) Distortion Correction or B0 unwarping, using the FMRIB's Utility for Geometrically Unwarping EPI (FUGUE) tool (https://fsl.fmrib.ox.ac.uk/fsl/fslwiki/FUGUE). Some of the most noticeable artifacts in the fMRI data are geometric distortions and signal losses that are originated by magnetic B0 field inhomogeneities. These inhomogeneities are mainly caused by neighbouring tissues' differences in magnetic susceptibility (particularly near air-bones and air-tissue boundaries). It is possible to partially correct for these artifacts through a method called B0 unwarping, which is based on a fieldmap image characterizing the location of field inhomogeneities. The FUGUE tool made use of the previously preprocessed fielmap image to determine the geometric distortions and partially compensate for these artifacts [125].

(ii) Motion correction, using the Motion Correction FMRIB's Linear Registration Tool (MCFLIRT) (https://fsl.fmrib.ox.ac.uk/fsl/fslwiki/MCFLIRT). Head motion occurs in all fMRI data acquisition scans. It leads to the mismatch between the location of subsequent images in the time series, which results in an incorrect spatial correspondence between voxels and anatomical areas over time. To fix this, volume registration is performed, resulting in one subject volumes' realignment. MCFLIRT starts by defining a common reference volume (the middle volume) and realigns each one of the other volumes according to it. For each volume, 6 motion parameters (3 rotations and 3 translations along the x, y and z axis) were estimated and a rigid body geometrical transformation based on these is applied in order to align every single volume with the template [125, 126].

(iii) Spatial smoothing, also known as spatial filtering, using the Smallest Univalue Segment Assimilating Nucleus (SUSAN) tool (https://fsl.fmrib.ox.ac.uk/fsl/fslwiki/SUSAN) [127].

This consists in the application of low-pass spatial filters to the image in order to reduce the high-frequency spatial components (e.g. physiological noise). However, with the spatial smoothing, there is

consequent loss of spatial resolution (especially needed to detect the activation of smaller brain regions). Thus, although this preprocessing step worsens spatial resolution, there are two reasons to perform it: (1) it improves SNR and (2) allows to use the Gaussian random field theory method in later statistics as a method of multiple comparison correction (to control for false positive active voxels) [126]. The spatial smoothing is carried out on each volume of the fMRI data separately and assumes that the signal in each voxel is a mixture of Gaussians with a Full Width Half Maximum (FWHM) in which the effective independent voxel - the Resolution Element (RESEL) (that corresponds to a cluster of voxels) - has the width equal to the FWHM. In later statistics, the significance threshold is determined based on the RESEL size.

In the case of this work, the spatial smoothing was undertaken by convolving for each volume of the fMRI data the signal in each voxel with a 3D Gaussian kernel with a FWHM equal to 3.3mm. This value corresponds to 1.5x the voxel dimension, which constitutes the minimum value that satisfies the previously explained trade-off: increasing SNR without loosing the anatomical definition of smaller regions of activity [125].

(iv) High-pass temporal filtering, using FMRIB of the Brain Expert Analysis Tool (FEAT) (`https://fsl.fmrib.ox.ac.uk/fsl/fslwiki/FEAT`).

Temporal filtering is a method that suppresses signals based on their known or expected frequencies. Low frequency artifactual signals commonly found in fMRI are typically driven by scanner drifts ($<$0.01 Hz) from instrumentation imperfections. These changes often appear as near linear increases or decreases in absolute signal over the experiment and can be extremely problematic for fMRI experiments. The most commonly used filters to address this issue in task-based fMRI are high-pass filters, with a cutoff value that must not be set lower than the maximum stimulation period (e.g. the time interval between one trial start and the next one) to avoid removing the signal of interest [126, 128].

The cutoff frequency used in this work was 0.01 Hz, which succeeded in eliminating scanner-related drifts from the signal without eliminating the signal of interest (with a trial duration of 58.5s, corresponding to a frequency of approximately 0.02Hz).

Nuisance regressors of motion parameters and motion outliers were introduced together with the regressors of interest during the BH BOLD-fMRI analysis that will be further discussed in section 2.4.2.

(v) Nuisance regression of motion parameters, using the MCFLIRT (`https://fsl.fmrib.ox.ac.uk/fsl/fslwiki/MCFLIRT`). Motion induces additional changes and artifacts in the signal that cannot be removed by the motion correction spatial transformations (3 rotations and 3 translations along the x,y and z axis) mentioned in (ii) alone. Therefore, corrections for these motion artifacts were implemented in addition to motion correction by adding motion parameters to the GLM. The 6 motion parameters (3 rotation and 3 translation parameters) were added as nuisance regressors, which means that they were regressors that did not contribute to the signal of interest but were included in the GLM to account for the

extra introduced variability. Thus, the found fMRI signal that corresponds to these regressors was left out, resulting in a more ”clean” signal of interest [126]. The nuisance regressors were not orthogonalized in relation to the regressors of interest, which means that they were not completely independent of each other. Moreover, the nuisance regressors were extended by their derivatives and squared versions of their derivatives to account for signal changes that are not linearly related to the amount of motion or do not happen instantaneously.

(vi) Nuisance regression of motion outliers using the fsl_motion_outliers tool (https://fsl.fmrib.ox.ac.uk/fsl/fslwiki/FSLMotionOutliers). The nuisance regression of motion parameters described in (ii) only accounts for signal changes induced by small motion. In order to account for artifacts induced by larger head motion, nuisance regression of motion outliers was performed. The fsl_motion_outliers detects timepoints in the fMRI dataset that have been corrupted by large motion. It starts by performing motion correction, followed by the calculation, for each timepoint, of the metric root mean square intensity difference to the reference volume (the middle volume), that indicates how much that time point is affected by motion. Afterwards, these values are thresholded (using the 75th percentile + 1.5x the interquartile range value) to look for outliers. From this, a confound matrix is generated, with a separate column for each outlier timepoint, which means that within each column, the values are all zeros except for the timepoint that is detected to be the outlier, whose value is one. This confound matrix is added to the GLM to account for the introduced variability caused by large motion. Thus, the effect of these timepoints is removed from the estimation the effects of interest.

2.4.1.2 Registration and normalization

Registration of the subjects' functional images to the structural space and normalization to the standard space were also performed. This is a crucial step in the analysis pipeline. In fact, the position of the subject's head and the field of view and resolution of the images typically vary between different subjects, acquisitions and within the volumes of one acquisition. Therefore, it is important to align the different images between each other so that posterior analysis steps are valid. Otherwise, sensitivity is lost and the false negatives and false positives rates are higher.

The registration of each subject's functional image to the matching structural space was performed using the FMRIB's Linear Image Registration Tool (FLIRT) Boundary-Based Registration (BBR) (https://fsl.fmrib.ox.ac.uk/fsl/fslwiki/FLIRT_BBR). This registration is performed by mapping the white matter boundaries (that were previously defined by the structural T1-weighted image segmentation) to the functional image. This is done by using a linear rigid-body transformation with 6 Degrees Of Freedom (DOF) (such as in the motion correction step of the fMRI preprocessing).

In turn, the normalization from the structural space to a common space is performed using the FMRIB's Non-Linear Registration Tool (FNIRT) (https://fsl.fmrib.ox.ac.uk/fsl/fslwiki/FNIRT).

When there is a substantial difference in anatomy, or any form of local geometric change, it is necessary to move from linear to non-linear transformations. A non-linear transformation is technically any transformation with more than 12 DOF, including at least zoom and shear operations besides the translations and rotations included in linear transformations. The ones most commonly used typically have thousands to millions of DOF (usually describing local geometric changes, such as vectors associated with grid points in the image, which indicate how that point and its neighbours are displaced). These local deformations typically perform better than linear registrations [126]. In this work, the standard space used was the default MNI 152 standard space T1-weighted average structural template image (2mm). Besides this, the cost function to be minimized used by FNIRT was the sum-of-square difference, and the intensity values between grid points were interpolated using a trilinear approach.

Lastly, the two transformations (registration and normalization) were combined, defining a single transformation from the functional to the standard space.

2.4.1.3 Definition of regions of interest

When looking for CVR in migraine, an initial approach may consist of a whole-brain voxelwise analysis, meaning that significant differences will be searched for across all brain voxels. However, it may also be relevant to focus the analysis into specific brain regions with the objective of identifying impaired areas. Bearing this in mind, three different categories of Regions of Interest (ROIs) were defined: cortical lobes, arterial flow territories and subcortical structures. For this, brain masks were created that consisted of whole-brain images with a value of 1 in voxels that belonged to the ROIs, and 0 in voxels that did not.

Cortical lobes

First, the ROIs analysis was focused on cortical cerebral lobes: frontal, temporal, parietal and occipital lobes. Masks of these regions had been previously obtained for another project from the Harvard-Oxford structural atlas, which already comes with FSL. This atlas is normalized to the MNI 152 standard space and the brain is segmented into different labelled brain regions. The intensity in each voxel corresponds to its probability of belonging to a specific brain structure. In order to obtain a binary mask (of 0's and 1's), it was needed to apply a threshold to the probabilistic map at a certain probability value (using the FSL tool Fslutils, `https://fsl.fmrib.ox.ac.uk/fsl/fslwiki/Fslutils`). A value of 10% was chosen, implicating that every voxel with $>10\%$ probability of belonging to the cerebral lobe being masked was included in the binary mask. The masks are presented in figure 2.3.

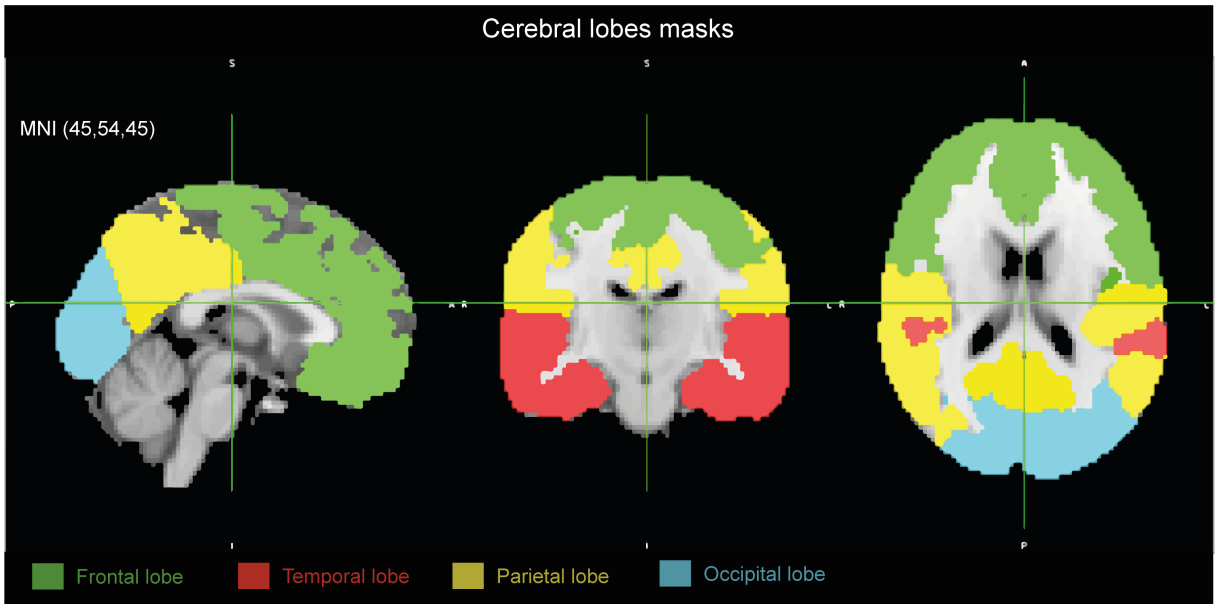

Figure 2.3: Cerebral lobes masks used for the ROI analysis: frontal, temporal, parietal and occipital lobe masks. The masks were defined in the standard MNI 152 space. All masks are represented in the sagittal, coronal and axial planes (left to right) for better representation. A and P mark the anterior and posterior sides in the sagittal and axial representations. R and L mark the right and left sides in the coronal and axial representations. S and I mark the superior and inferior directions in the sagittal and coronal representations.

Arterial flow territories

Focusing the attention on arterial flow territories, two ROIs were defined: the internal carotid arteries (ICA) and the Vertebrobasilar Arteries (VBA) flow territories. The reason for this was to obtain distinct masks for the anterior and posterior cerebral circulations: the ICA flow territory mask represents the anterior cerebral circulation, thus including more anterior regions of the brain as well as regions supplied by the ACA and MCA; the VBA flow territory mask represents the posterior cerebral circulation, thus including posterior brain regions as well as the regions supplied by the PCA (that had been shown to be impaired in migraine [15, 29, 31]). Similarly to the lobes masks, these masks had already been created in the standard space for another project, this time from ready-to-use arterial flow territory probability atlas available online [129]. The intensity in each voxel represents the probability (0-1) of that particular voxel belonging to the artery flow territory. In order to obtain a binary mask, the threshold chosen for the ICA territory was 30%, meaning that every voxel with $>30\%$ probability of belonging to the arterial flow territory was included. Regarding the VBA territory mask, the threshold was 10%, meaning that every voxel with $>10\%$ probability of belonging to the arterial flow territory was included in the masks. ICA and VBA masks are presented in figure 2.4.

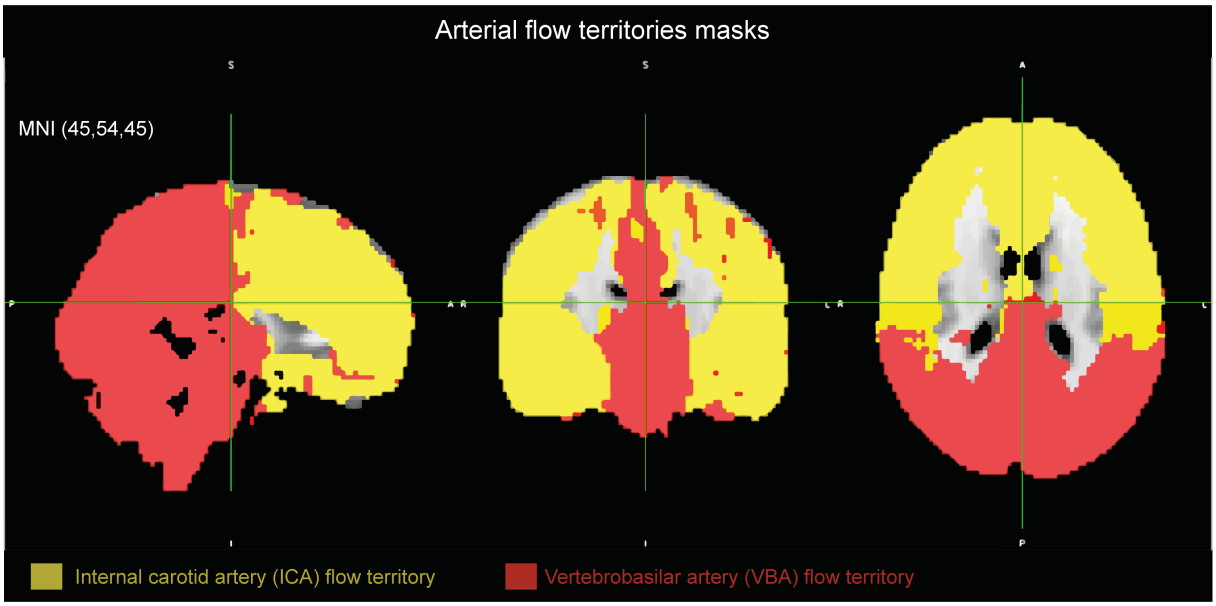

Figure 2.4: Arterial flow territories masks used for the ROI analysis: internal carotid arteries (ICA) flow territory and vertebrobasilar arteries (VBA) flow territory masks. The masks were defined in the standard MNI 152 space. All masks are represented in the sagittal, coronal and axial planes (left to right) for better representation. A and P mark the anterior and posterior sides in the sagittal and axial representations. R and L mark the right and left sides in the coronal and axial representations. S and I mark the superior and inferior directions in the sagittal and coronal representations.

Subcortical structures

In order to be more specific in the investigation, it was decided to assess if there were CVR differences in some subcortical structures. Specifically, the brainstem, thalamus, pallidum, putamen, hippocampus and caudate were analysed. To do so, masks of these structures were created by using the FMRIB's Integrated Registration and Segmentation Tool (FIRST) (`https://fsl.fmrib.ox.ac.uk/fsl/fslwiki/FIRST`). This tool is a model-based tool that segments and registers brain images in some of its subcortical structures. The models used in FIRST are constructed from manually segmented images provided by the Center for Morphometric Analysis, Boston. Based on the learned models, it searches through linear combinations of shape modes of variation for the most probable shape instance given the observed intensities in the input brain-extracted T1-weighted structural image. Thus, the subcortical regions' maps given by FIRST are in the structural space. The intensity in each voxel represents the probability (0-1) of that particular voxel belonging to the subcortical region. In order to obtain a binary mask, the threshold chosen was 50%, meaning that every voxel with $>50\%$ probability of belonging to subcortical regions was included in the masks. The obtained subcortical masks for one of the subjects are presented in figure 2.5.

Afterwards, the created masks in the standard and structural spaces (for the cortical lobes and arterial flow territories; and subcortical structures, respectively) were transformed to each subject and

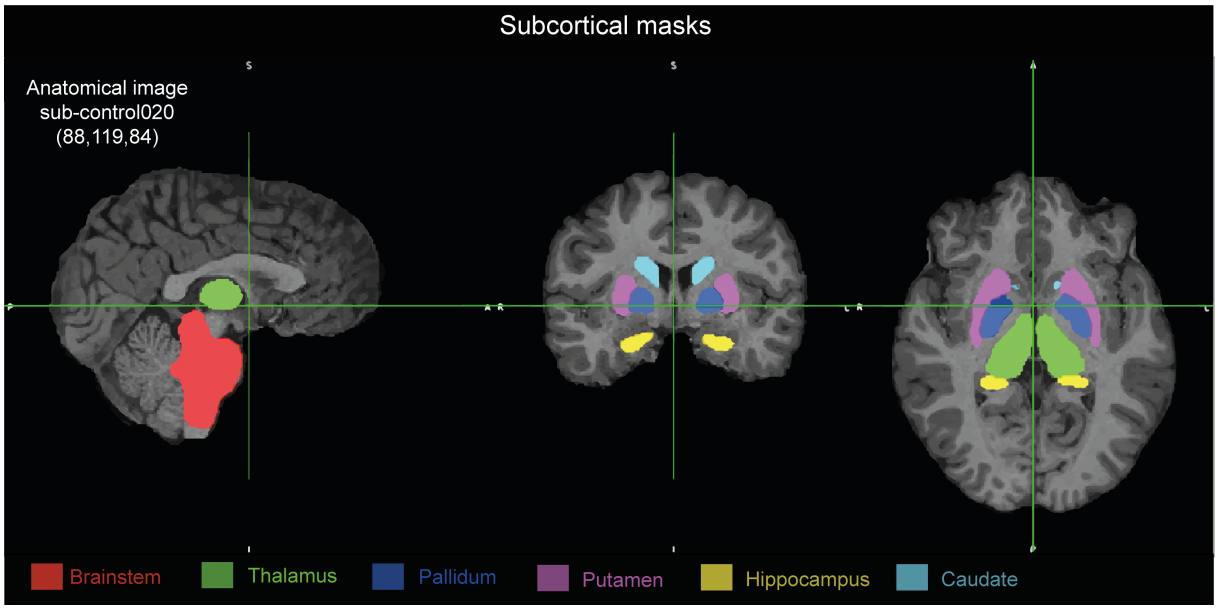

Figure 2.5: Subcortical structures masks masks used for the ROI analysis: brainstem, thalamus, pallidum, putamen, hippocampus and caudate masks for an example subject in the respective structural image space. The masks were defined in the structural space of each subject. All masks are represented in the sagittal, coronal and axial planes (left to right) for better representation. A and P mark the anterior and posterior sides in the sagittal and axial representations. R and L mark the right and left sides in the coronal and axial representations. S and I mark the superior and inferior directions in the sagittal and coronal representations.

session's functional space (using the FSL tool FNIRT, https://fsl.fmrib.ox.ac.uk/fsl/fslwiki/FNIRT/). The masks in the functional space were once more binarized by applying the same threshold that had been applied in the standard/structural space as the spatial transformation might have impacted the binarization.

In addition, they were only assigned non-zero values for voxels belonging to the gray matter (GM). The reason for this was that, within the brain, the distribution of blood flow is heterogeneous. GM is a much more vascularized area, that receives several times more flow than white matter (WM) (in an amount comparable to that in the heart muscle, the most energetic organ in the body) [130]. Additionally, in BH-CVR studies, greater BOLD signal change is usually seen in GM while nonsignificant changes are usually observed in WM [36, 131]. A study assessing CVR using hypercapnia-induced vasodilation through a breathing device observed a three times higher BOLD-fMRI signal change in GM when compared to WM, with a strong linear correlation with $PetCO_2$. In addition, this study revealed a hemispherically symmetrical and homogeneous distribution of CVR over the entire GM [132]. Therefore, it was decided to obtain these masks only within the GM. To do so, whole-brain GM masks in the structural space were created for each subject from the tissue segmentation performed in the preprocessing of the structural data in section 2.4.1.1. Voxel values of these images represent the probability that a particular voxel belongs to the GM. These images were thresholded at a probability value of 0.5 and binarized, meaning that only voxels with $>50\%$ probability of belonging to GM were given a value

of 1 (elsewhere being 0) and included in the mask. Then, they were registered to the subjects's functional space in each session (once more using the FSL tool FNIRT) and again binarized using the same threshold.

Finally, each subject's binary masks of the ROIs were intersected with the corresponding binary GM masks, both in the functional space. The resulting binary masks were imported to MATLAB and used as a template to create the regions-of-interest maps for each subject and session.

2.4.2 Breath-holding BOLD-fMRI data analysis

Concerning the BH BOLD-fMRI data analysis, this is usually performed using the General Linear Model (GLM) in FEAT ((https://fsl.fmrib.ox.ac.uk/fsl/fslwiki/FEAT)), a software tool contained in FSL for high quality model-based fMRI data analysis. Furthermore, CVR characterization must be performed on a voxelwise basis, since the hemodynamic response may exhibit different temporal dynamics in different brain regions that in turn affect CVR estimation, as explained in section 1.4.2. Taking all this into consideration, the analysis was performed using a $PetCO_2$-based method (the iteratively shifted $PETCO_2$ regressors GLM) and two paradigm-based methods (the iteratively shifted block-design regressors GLM and the sine-cosine GLM).

2.4.2.1 $PetCO_2$-based analysis

Iteratively shifted $PetCO_2$ GLM

The $PetCO_2$-based voxelwise analysis used the $PetCO_2$ regressor (that resulted from the CO_2 preprocessing described in section 2.3.3). This means that this method accounted for the variability in the BH task performance and in the resulting $PaCO_2$ levels, whether across subjects, sessions or even trials.

Before performing a voxelwise analysis, the first step was to perform an initial global gross alignment. This was obtained by maximizing the cross-correlation between the mean global gray matter (GM) BOLD time-course linearly up-sampled to the capnograph sampling frequency and the $PetCO_2$ regressor that overlapped the fMRI acquisition timing. This was done in MATLAB using the built-in cross-correlation function. A normalization was executed so that each regressor's autocorrelations at zero lag were equal to 1. The resulting delay value - the bulk shift - was used as a reference value for further voxelwise $PetCO_2$-based analysis.

To account for a voxelwise delay, the iteratively shifted $PetCO_2$ regressors GLM method was used. The first step was to create 61 fine shifted $PetCO_2$ regressors relatively to the predetermined bulk shift value, up to a maximum shift of $\pm$9s, with an increment of 0.3s, based on previous literature [94, 99] and downsampled to the fMRI sequence TR (using once more a piecewise cubic Hermite interpolation). For each of these shifted $PetCO_2$ regressors, a GLM was constructed (including its temporal derivative, TD).

Motion parameters and motion outliers (described in section 2.4.1.1) were also included in the model as regressors of no interest. An example of the design matrix and contrasts used for a specific subject, session and shifted $PetCO_2$ regressor is represented in figure 2.6. The first and second EVs correspond to the shifted $PetCO_2$ regressor and its temporal derivative, respectively. The contrast C1 (with a 1 for EV1 and 0 for EV2) tests for voxels where activation follows the $PetCO_2$ regressor (activation of interest); C2 (with a -1 for EV1 and 0 for EV2) tests for voxels where activation follows the negative version of $PetCO_2$ regressor; and C3 (with a 0 for EV1 and 1 for EV2) tests for voxels where activation follows the $PetCO_2$ regressor temporal derivative. Additionally, two F-tests were constructed: F1 included only the contrast C1 in order to test for voxels where activation follows the $PetCO_2$ regressor or its negative version; F2 combined the contrasts referring to the $PetCO_2$ regressor and its TD.

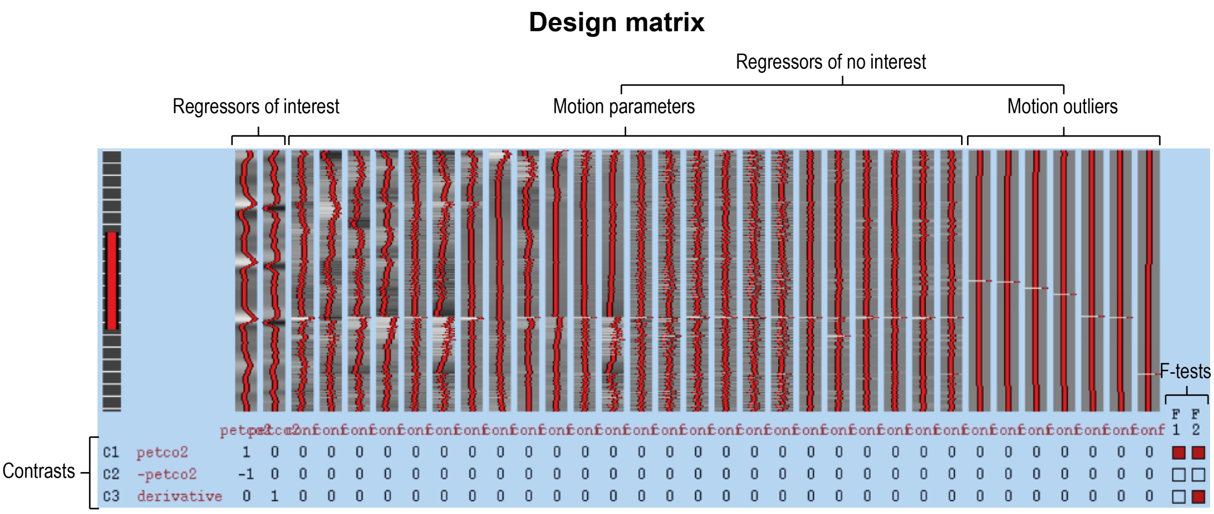

Figure 2.6: Representative design matrix and contrasts used in GLM to assess brain activation in response to the breath-hold task for one illustrative subject, session and shifted $PetCO_2$ regressor

For each shifted regressor, the GLM was fitted to the data in each voxel. The method that FEAT uses to do this on first-level data is FMRIB of the Brain Improved Linear Model (FILM). Among the outputs there are several Z statistic maps, one for each contrast and F-test. The result consisted in 61 GLMs, each one fitting a different shifted $PetCO_2$ regressor.

The next step of the analysis was to obtain the voxelwise maps depicting the CVR. For this, CVR in PSC was calculated for each one of the 61 models, following the formula:

$$\text{CVR in PSC} = \frac{PE1 * 100}{meanfunc} \quad (2.1)$$

where PE1 is the parameter estimate image that informs about how strongly the $PetCO_2$ regressor (EV1) fits the data at each voxel and *mean func* is the mean data over time at each voxel.

It is important to notice that the $PetCO_2$ regressors given to the model were not normalized auto-

matically by FEAT and consequently, EV1 was also not normalized. Therefore, the PE1 maps resulting from FEAT are per change in expired CO_2 (mm Hg) and consequently, vascular reactivity was defined as CO_2-related BOLD percent signal change (PSC) per mm Hg change in CO_2 (%/mm Hg).

The resulting 3D maps from each one the 61 models were then merged (using the FSL Fslutils tool, https://fsl.fmrib.ox.ac.uk/fsl/fslwiki/Fslutils), resulting in a 4D image (with 61 volumes) that characterized the CVR. On a voxelwise basis, the delay at which the CVR was highest in that voxel (which corresponds to the highest PE1 value and thus to the shifted regressor that better fits the data) was chosen as the optimal delay, resulting in a map of delays (s). The same was done to obtain a map of CVR (%/mm Hg). This was done for all the sessions in which a valid CO_2 signal was acquired.

2.4.2.2 Paradigm-based analysis

The models used in paradigm-based analysis are a representation of what is expected to be observed in the data: changes in BOLD hemodynamic response in response to a certain stimulus. A perfect performance is assumed, as well as similar BH effects on the $PaCO_2$ within and between subjects. Thus, the EVs given to the models were derived from the timings of BH-task paradigm presented to each subject in each MRI scanning session.

Iteratively shifted block GLM

The first method used to achieve a paradigm-based voxelwise analysis was the iteratively shifted block regressors GLM. Similarly to the iteratively shifted $PetCO_2$ regressors GLM method, the first step was to perform an initial global alignment. This was obtained by maximizing the cross-correlation between the global GM mean time-course linearly up-sampled to a sampling interval of 0.02s (having this value been chosen in order to maintain a good temporal resolution) and the block regressor - a square box function with an amplitude of 1 during the four BH periods and 0 during the baseline and recovery periods, convolved with the canonical double gamma HRF.

61 fine shifted block regressors (downsampled to the fMRI TR) were created relative to the bulk shift delay value, up to a maximum shift of $\pm$9s, with an increment of 0.3s. For each regressor, a GLM was constructed (including its TD). Motion parameters and motion outliers (described in section 2.4.1.1) were also included in the model as regressors of no interest. An example of the design matrix and contrasts used for a specific subject, session and shifted block is represented in figure 2.7. The first and second EVs correspond to the block regressor and its temporal derivative, respectively. The contrast C1 (with a 1 for EV1 and 0 for EV2) tests for voxels where activation follows the block regressor (activation of interest); C2 (with a -1 for EV1 and 0 for EV2) tests for voxels where activation follows the negative version of the block regressor; and C3 (with a 0 for EV1 and 1 for EV2) tests for voxels where activation follows the block regressor TD. Additionally, two F-tests were constructed: F1 included only the contrast

C1 in order to test for voxels where activation follows the block function or its negative version; F2 combined the contrasts referring to the block function and its TD.

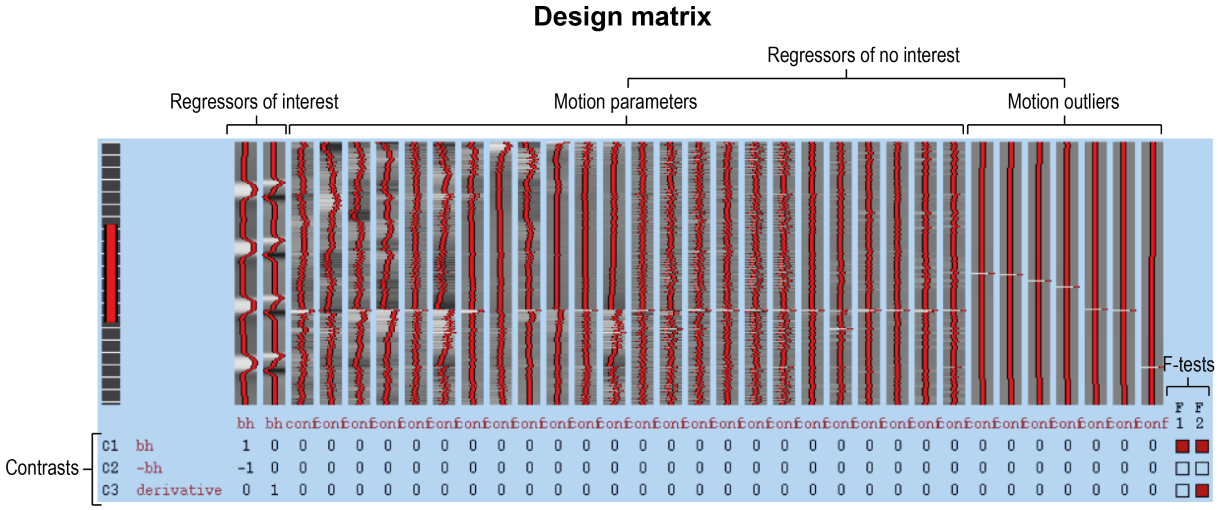

Figure 2.7: Representative design matrix and contrasts used in GLM to assess brain activation in response to the breath-hold task for one illustrative subject, session and shifted block regressor.

For each shifted regressor, the GLM was fitted to the data in each voxel. In order to create the CVR (in BOLD PSC, %) and the corresponding delay maps (in seconds), the same process that had been done in the iteratively shifted $PetCO_2$ regressors GLM method was done. However, this time, the block regressor (EV1) given to the model was automatically normalized by FEAT and thus, the 61 resulting CVR maps and the final CVR maps were presented in PSC (%).

Sine-Cosine GLM

The other voxelwise paradigm-based method used was the sine-cosine GLM consisting of a sine-cosine pair at the BH task frequency and its first two harmonics (second order sinusoidal model) [88]. As explained in section 1.4.2, this model's inherent phase flexibility allows for different time delays across the brain without the need to make assumptions or optimizations and thus only one GLM is needed (in contrast to the 61 GLMs performed for the iteratively shifted regressors GLM methods). In the present work, the BH protocol consisted of four cycles of 58.5s of alternating periods of apnea, natural breathing (recovery) and externally-paced breathing (baseline). Thus, the sinusoidal regressors consisted in sine and cosine waves at the task period (58.5s) and their first and second harmonics based on previous work optimizing the number of harmonics [88]. Motion parameters and motion outliers (described in section 2.4.1.1) were also included in the model as regressors of no interest. Furthermore, as the task cycles only begin after 35s (5s of fixation cross plus 30s of initial baseline) of task performance, this model has an initial skip with this duration (as it was concluded that this improved model fitting in comparison to the sine-cosine model beginning at time t=0s). An example of the design matrix and contrasts used for

a specific subject and session is represented in figure 2.8. The first and fourth EVs correspond to the sine and cosine waves at task frequency, the second and fifth to their first harmonics and the third and sixth to their second harmonics, respectively. The last seven regressors represent the motion outliers detected, and the remaining ones the motion parameters. As an example, the contrast C1 (with a 1 for EV1 and 0 elsewhere) tests for voxels where activation follows the sine waveform. Additionally, five different F-tests were constructed: F1 combined the sine wave and its first and second harmonics (C1, C2 and C3); F2 combined the cosine wave and its first and second harmonics (C4, C5 and C6); F3 combined the contrasts referring to the sine and cosine waves (C1 and C4); F4 combined the sine and cosine waves and their first harmonics (C1, C2, C4 and C5); and finally, F5 combined all the defined regressors of interest - sine and cosine waves and their first and second harmonics (C1, C2, C3, C4, C5 and C6).

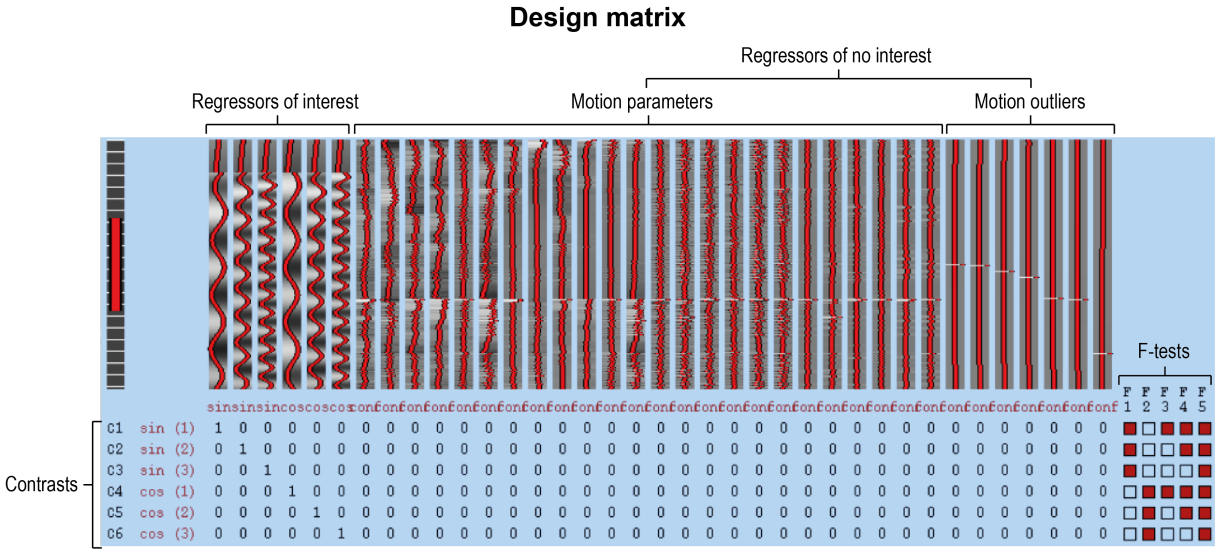

Figure 2.8: Representative design matrix and contrasts used in the sine-cosine GLM to assess brain activation in response to the breath-hold task for one illustrative subject and session

From the GLM resulting from FEAT, a representation of the BOLD response resembling the sine-cosine model was obtained. As a single GLM resulted from this analysis and it already accounts for voxelwise variations, voxelwise CVR and delay maps were constructed differently from the two previous methods. Here, CVR (in BOLD PSC, %) was calculated as the amplitude of the model's maximum relative to the average initial baseline signal multiplied by 100 and the delay under the form of TTP was calculated as the time of the model's maximum relative to the beginning of the BH (in seconds). To achieve this, the six regressors of interest (sine and cosine waves and their first and second harmonics) and respective parameter estimates values were imported into MATLAB and used in order to create the GLM of the BOLD response at each voxel (excluding the motion parameters and motions outliers regressors of no interest). The GLM recreates the BOLD response of a particular voxel to the entire BH

protocol. In order to obtain just one CVR and TTP value per voxel, an averaged model of the four BH trials was obtained and the CVR and TTP computed from it.

In order to be able to compare the CVR maps resulting from the paradigm-based methods (in $\%$) with the maps resulting from the iteratively shifted $PetCO_2$ regressors GLM method (in $\%$/mm Hg), the latter were multiplied by the previously $\Delta PetCO_2$ and the values were compared in $\%$BOLD.

On the other hand, CVR in $\%$/mm Hg accounts for the variability caused by the breathing task between different sessions of the same subject and between subjects, thus allowing to quantitatively compare CVR between sessions and individuals (as mentioned in 1.4.2). Therefore, CVR maps obtained through the paradigm-based methods (in $\%$) were divided by the corresponding $\Delta PetCO_2$ (in mm Hg) for that subject and session in order to obtain normalized CVR measures ($\%$/mm Hg) and be able to compare them with the results from the $PetCO_2$-based model.

2.4.2.3 Regions-of-interest analysis

In order to perform a ROIs analysis of the voxelwise maps obtained through the three different methods described in section 2.4.2, both the obtained CVR and delay maps and the binary GM, cortical lobes, arterial flow territories and subcortical structures ROIs masks (whose construction was described in 2.4.1.3) were imported into MATLAB. In MATLAB, a regional analysis was performed by assigning, for each ROI, only the voxels of the CVR and delay maps that belonged to it.

Firstly, CVR characterization associated with BH fluctuations was executed across voxels in the whole-brain GM for each subject, session and analysis method. On a second phase, CVR characterization for the ROIs corresponding to cortical lobes, arterial territories and subcortical structures within GM was developed.

Chapter 3

Results and discussion

The main goal of this work was the analysis of BH BOLD-fMRI data from menstrual or menstrually-related migraine patients and hormonal controls. With this purpose, both CO_2 and BOLD-fMRI data acquired during a BH task from 3 migraine patients and 6 hormonal controls who underwent fMRI sessions (ictal headache and interictal for patients and premenstrual and midcycle for controls) was processed and analyzed using three different methods. This resulted in CVR and delay maps. The analysis of these maps enabled to compare the different analysis methods. A group analysis was also performed that allowed for the detection of CVR differences between the different menstrual cycle phases, methods and even ROIs, but only for controls due to the reduced number of patients.

3.1 PetCO$_2$, motion and cross-correlation analysis

All subjects successfully completed the respiratory protocol with no major difficulties reported, verified by the increase in the mean GM BOLD time course in the periods after the BH (illustrative example of the mean GM BOLD signal, as well as the respective CO_2 signal example from one representative dataset is presented in figure 3.1). However, datasets C1-S2, P1-S1 and P3-S1 (where C represents controls, P patients, S1 the premenstrual/ictal session and S2 the midcycle/interictal session, although these were performed in a random order) revealed low quality CO_2 traces (see appendix A for all CO_2 plots). This may have been caused by periods of exhalation through the mouth, impairing the measurement of the $PetCO_2$ especially its increase after BH. This seems more prone to happen with patients in their ictal phase (that constitute 2 out of the 3 problematic CO_2 datasets). In these cases, the $PetCO_2$ method of CVR analysis was not performed and $PetCO_2$ normalised CVR measurements were not obtained.

Statistics about the $PetCO_2$, motion and bulk shifts of the $PetCO_2$ and block regressor, for each subject and session are presented in table 3.1. A mean $PetCO_2$ baseline of 36.4$\pm$4.5 mm Hg across participants was observed, which is in general agreement with other BH CVR studies [86, 87, 97]. Ac-

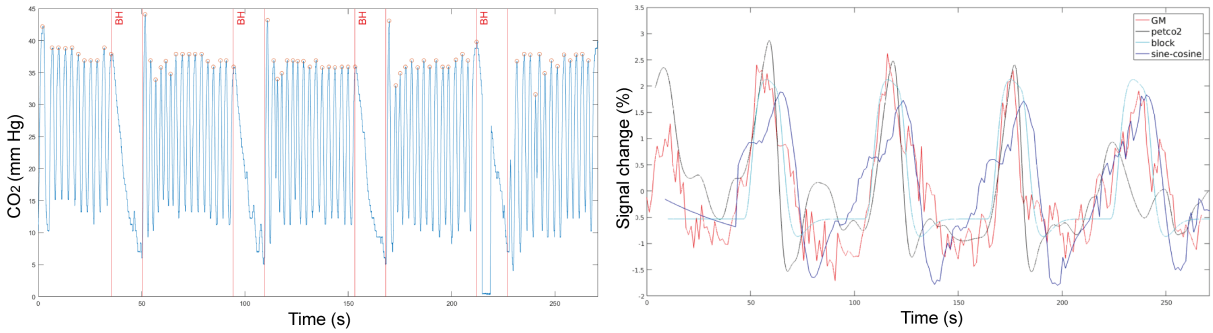

Figure 3.1: CO_2 signal (mm Hg) recorded during the BH BOLD-fMRI corrected for the delay introduced by the tubing system (lines in red represent the BH periods according to the instructions' timings given and red circles indicate the $PetCO_2$ values after each exhalation) (left) and regressors $PetCO_2$ and block and the mean sine-cosine model aligned with the GM BOLD-fMRI mean time course according to the maximum correlation between each regressor and the GM (GM in red, $PetCO_2$ in black, block in cyan and sine-cosine in blue) (right) from one representatitve dataset.

cording to Tancredi et al. [95], this value is within the range of 30 to 45 mm Hg which assures that CVR is measured over the linear range of the CBF-CO_2 dose–response curve, avoiding hypocapnic conditions [95]. Furthermore, a mean $\Delta PetCO_2$ of 5.4$\pm$1.9 mm Hg across participants was calculated, which is in general agreement with other similar BH CVR studies [86, 87, 97, 99]. However, one of the four BH trials were excluded for the calculation of the $\Delta PetCO_2$ in acquisitions C1-S1 and P2-S2, due to automatic calibration of the capnograph during that one BH, which interfered with the correct CO_2 signal acquisition.

Regarding the mean displacements calculated by the MCFLIRT tool, the mean absolute displacements averaged across subjects was 0.39$\pm$0.29 mm, while the mean relative displacements across subjects was 0.11$\pm$0.06 mm. The highest values of mean absolute and relative displacements were verified to be related with task performance.

The delay introduced by the tubing system was of around 10s in all the acquisitions, except in C1-S1 and P1-S1, in which the delay was different because the used tubing system were different (shorter and wider, respectively), due to hospital logistics' issues. However, it was possible to estimate these two different delays previously to the measurements because of the previous tests performed at the lab referred in 2.1.3 and thus to account for a proportional extra period of time at the end of the acquisitions (to record the whole CO_2 signal expired during the BH task).

Finally, regarding the bulk shifts obtained by maximizing the cross-correlation between the unshifted $PetCO_2$ regressors and the mean GM BOLD signal time course for each acquisition, this was 5$\pm$1 s on average across subjects, which is according to the range of from 5s to 10s for average delay times found in literature [87, 104]. As concerns the bulk shift corresponding to the block regressor calculated following the same procedure, the average across subjects was 10$\pm$2 s. This was expected since the block model is created using the timings of the presentation of the stimuli through visual instructions and

the $PetCO_2$ changes occur as a consequence of the performance of these instructions, that naturally happens afterwards. Nevertheless, besides the acquisitions with low quality $PetCO_2$, the bulk shifts for both the $PetCO_2$ and the block regressors were also not calculated for the datasets C4-S2 and P3-S2 due to logistics' issues during the acquisitions that impeded the synchronous presentation of the stimuli with the fMRI scanning, thus interfering with the hemodynamic delay estimation. In these cases, the shifted regressors were calculated from the other acquisitions' mean bulk shift.

Cross-correlation analysis between the mean sine-cosine model time-course and the mean GM BOLD-fMRI signal time course was also performed for each session. This was done by importing the six regressors of interest (sine and cosine waves and their first and second harmonics) and respective parameter estimates values into MATLAB and recreating the GLM of the BOLD response at each voxel (excluding the motion parameters and motions outliers regressors of no interest). From this, the mean model time-course was calculated. From the plots (presented in figure 3.1 from one representative dataset and in appendix A for all the datasets) showing the regressors aligned with the GM according to the maximum correlation between each regressor and the GM, it could be seen that, in most datasets, the sine-cosine model did not present a good fit of the mean GM time course.

Table 3.1: Statistics about the $PetCO_2$, motion and bulk shifts of the $PetCO_2$ and block regressor, for each subject and session. C: controls; P: patients; S1: premenstrual/ictal session; S2: midcycle/interictal session (for controls/-patients)

Subject	Session	Tubing delay (s)	Breathing period (s)	Mean baseline PETCO2 (mm Hg)	Mean delta PETCO2 (mm Hg)	Absolute mean displacement (mm)	Relative mean displacement (mm)	$PetCO_2$ bulk shift (s)	Block bulk shift (s)
C1	S1	8.0	3	37.8±0.4	2.1±0.7	0.47	0.10	7	8
	S2	10.0		-	-	0.11	0.05	-	12
C2	S1	10.0	3	37.1±0.8	4.8±3.1	0.31	0.10	4	10
	S2	10.0		33.2±0.4	4.8±1.0	0.27	0.08	6	11
C3	S1	10.5	4	37.0±1.4	8.1±2.7	0.50	0.20	5	9
	S2	10.0		33.0±0.7	4.7±1.1	1.19	0.22	4	7
C4	S1	10.5	3	35.6±2.7	6.6±2.5	0.71	0.11	4	9
	S2	10.0		38.8±1.7	4.4±1.9	0.61	0.08	-	-
C5	S1	10.5	4	33.8±1.2	5.5±2.1	0.26	0.10	4	8
	S2	10.0		34.7±1.3	4.9±3.2	0.15	0.05	6	11
C6	S1	10.5	4	47.4±1.0	5.8±0.7	0.33	0.08	7	10
P1	S1	50	5	-	-	0.54	0.21	-	-
P2	S2	10.0	3	28.8±1.0	9.5±2.1	0.23	0.08	4	10
P3	S1	10.0	4	-	-	0.13	0.07	-	12
	S2	10.0		39,1±0.3	4.0±1.2	0.08	0.06	-	-
Mean±s.d.		*12.7±10.3*	*4±1*	*36.4±4.5*	*5.4±1.9*	*0,39±0.29*	*0,11±0.06*	*5±1*	*10±2*

3.2 Cerebrovascular reactivity and delay maps

Regarding the CVR and delay maps, maps obtained from one representative dataset and average maps across controls are shown in figures 3.2 and 3.3, respectively. Maps presented the expected contrast between GM and WM: GM presented increased CVR values and decreased delay values when compared to the WM. These results were not surprising since GM is a highly vascularized area within the brain and in most CVR studies, GM presents a large signal change [36, 88, 130, 131]. Due to these observations, further CVR characterization presented in the next sections focuses on the GM. In addition, for the $PetCO_2$ and block methods, the posterior area of the brain presented increased delays when compared to the anterior one, which is according to the results described in literature [3, 88, 94]. On the other hand, the sine-cosine method did not present this delay pattern and resulted in a noisier map, showing not to be an appropriate method in the present study, as it will be discussed below.

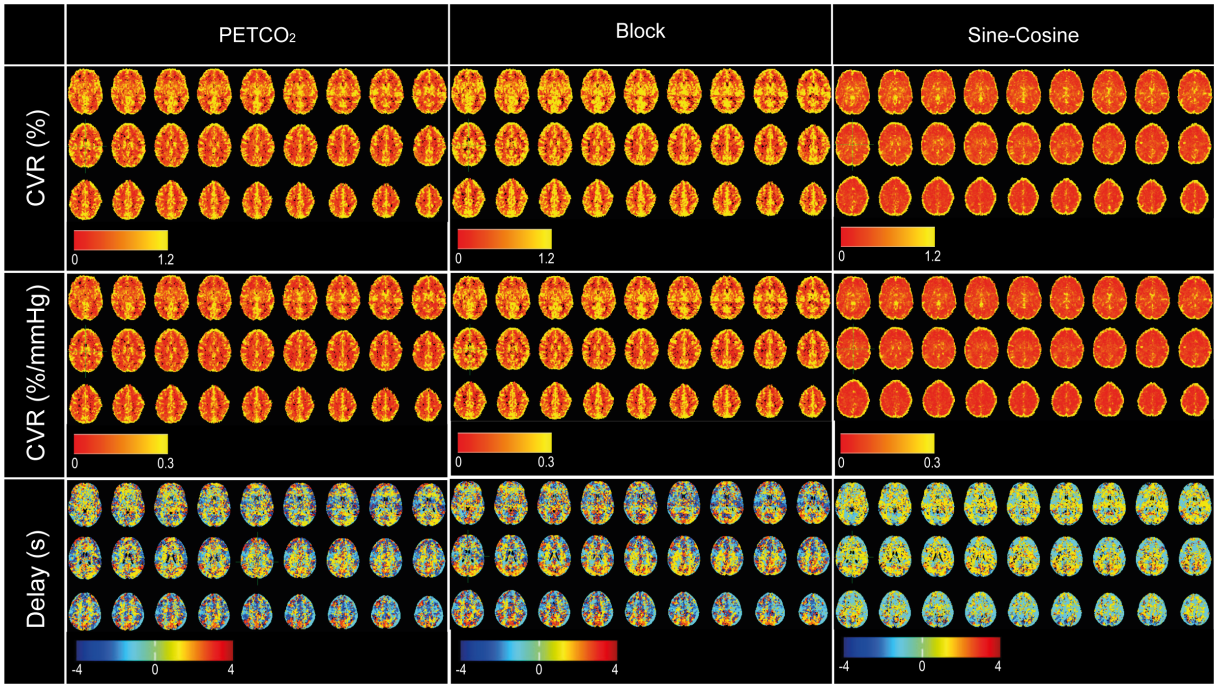

Figure 3.2: Illustrative example from one representative dataset: CVR (%), CVR (%/mm Hg) and delay (s) maps (top to bottom) obtained through $PetCO_2$, block and sine-cosine methods (left to right). The maps are represented in the standard MNI152 space.

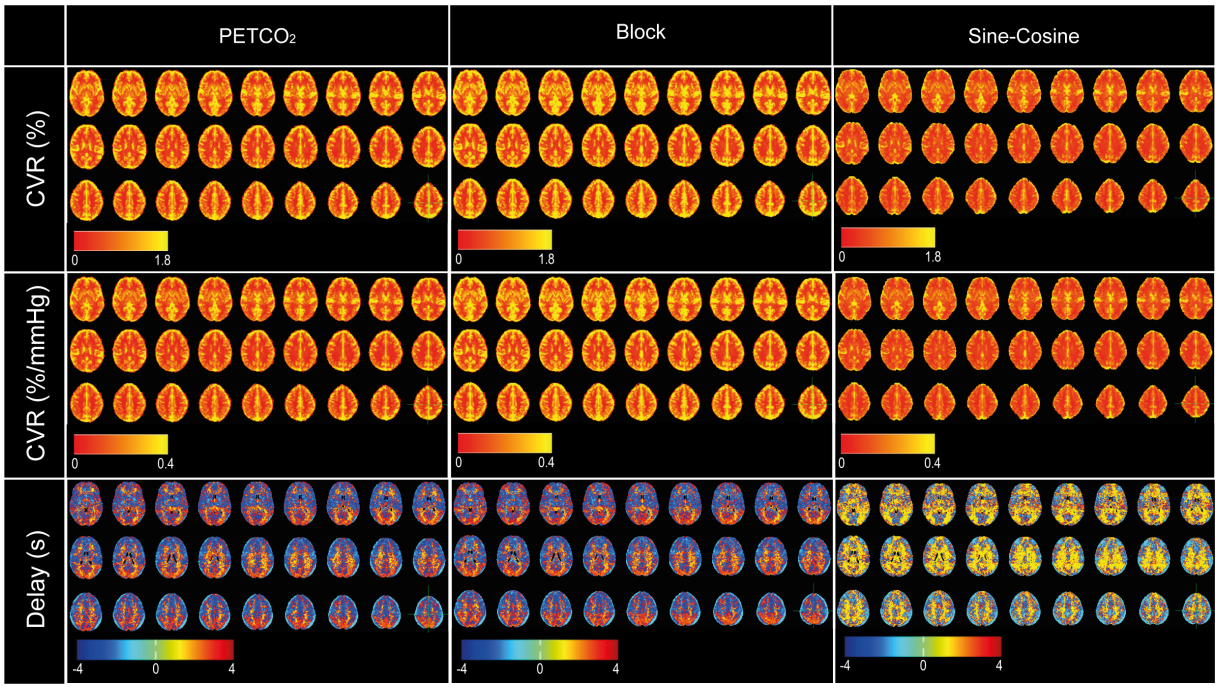

Figure 3.3: Controls' group average: CVR (%), CVR (%/mm Hg) and delay (s) maps (top to bottom) obtained through $PetCO_2$, block and sine-cosine methods (left to right). The maps are represented in the standard MNI152 space.

3.3 Whole-brain analysis

3.3.1 Subject-level analysis

Barplots with the calculated number of voxels with detected CVR in % (with a CVR in $\% > 0.3$) and the median CVR in %, CVR in %/mm Hg and delay in seconds across brain in GM for each subject, session and method, are displayed in figures 3.4 3.5, 3.6 and 3.7, respectively. Furthermore, these results, together with the averaged values across all participants for each method are displayed in table 3.2. Once more, the median CVR in %/mm Hg was not calculated for C1-S2, P1-S1 and P3-S1 because in these cases the $PetCO_2$ analysis was not performed (due to invalid CO_2 signal recording).

The iteratively shifted block-design regressors GLM method showed to be the most effective of the three methods in modelling BH BOLD-fMRI data as, besides producing the highest percentage of voxels with detected CVR, it resulted in the highest CVR amplitude estimates in GM averaged across participants (which is not true in the case of CVR amplitude estimates averaged across patients in 3.5 and 3.6, but this is probably influenced by the low number of subjects in this cohort). These results suggested that relative underestimation of the two other models occurs due to their poorer fit.

As regards the $PetCO_2$ model, this produced a percentage of voxels with detected CVR and CVR amplitude estimates averaged across participants higher than the ones using the sine-cosine model.

This is according to Murphy et al. [87], that concluded that the $PetCO_2$ model leads to a better model fit the sine–cosine, but not in all brain regions. On the other hand, it produced lower estimates than the block model. This was not expected since this type of models accounts for variability across and within subjects [35]. This result seems to be due to incorrect CO_2 acquisition caused by experimental setup issues, namely to the use of an exclusively nasal cannula that did not get the expired CO_2 from mouth (which seems to have frequently occurred even though subjects were instructed to breath as most as possible through their noses). In fact, in the cases where an increase in the expired CO_2 was not recorded, an increase in the mean GM BOLD time course in the periods after the BH was still observed, which means that an increase in $PaCO_2$ occurred although this was not fully detected by the capnograph. This could be addressed by using a mask rather than a nasal cannula [99].

Finally, the second order sine-cosine model produced the lowest percentage of voxels with detected CVR and estimates of CVR, this way showing to be the worst model in explaining the BH BOLD-fMRI data. From literature, the sine-cosine model had shown to explain more variance than any global block model (even when the latter included the regressor's temporal derivative and the time delay that maximised correlation between the global BOLD signal and the block regressor) and no significant difference in comparison with the variance explained by the global $PetCO_2$ model (with its temporal derivative) [87]. This makes sense since the sine-cosine model has an inherent phase flexibility that allows to model different time delays across the brain, thus being an intrinsic voxelwise model. However, it is important to notice that the block and the $PetCO_2$ models used in this work have also included a voxelwise lag optimization, so the results are not expected to be similar to the mentioned ones. Furthermore, the second order sine-cosine model (with its first two harmonics) that was used in this work has been shown to explain significantly more variance, produce a greater number of responsive voxels, not underestimate CVR amplitude and show a better test-retest reproducibility than lower order methods [88]. However, this was proven for a BH task with cycles' duration of 75s. In our case, with a task with cycles with 58.5s duration, the second order model may not be the most appropriate, e.g. the use of more harmonics would perhaps improve the sine-cosine model fitting. The optimal number of harmonics would have to be estimated specifically for our protocol (which was not done in this dissertation).

The normalization of CVR units is crucial as it allows to make an accurate comparison of CVR values between different subjects and sessions. Furthermore, CVR in $\%$/mm Hg has shown to result in more statistically active voxels in task-related analyses at the group level [87]. However, the $\Delta PetCO_2$ used for the normalization is inherently an unstable measure that can easily be skewed by outliers in the $PetCO_2$ trace such as erroneous readings and partial breaths, which may introduce some errors in the results presented in normalized CVR units [87]. This seems to have happened in C1-S1, in which the CVR values were higher than the ones obtained in all the other sessions probably due to the low $\Delta PetCO_2$ caused by incorrect CO_2 recording (probably related to mouth breathing). Moreover, the normalization

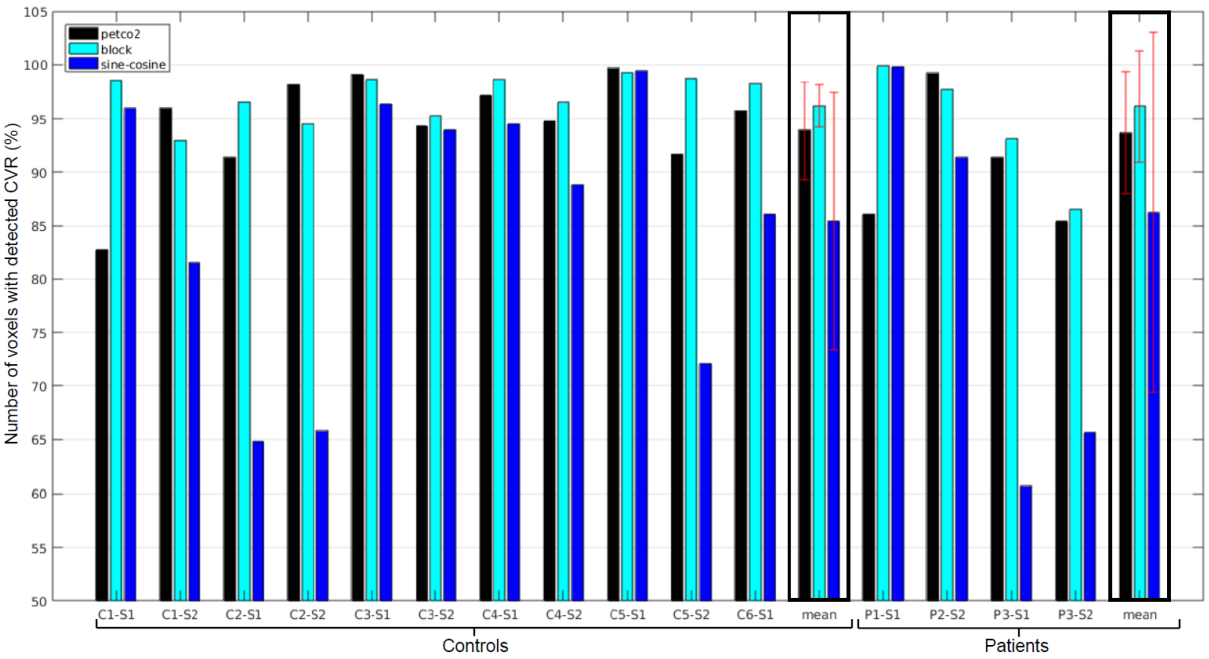

Figure 3.4: Barplots representing the number of voxels with detected CVR (%) in GM obtained for all the sessions and the methods ($PetCO_2$ in black, block in cyan and sine-cosine in blue). The group mean CVR and the respective error bars corresponding to the mean standard deviation is also represented for for both controls and patients. C: controls; P: patients; S1: premenstrual/ictal session; S2: midcycle/interictal session (for controls/patients)

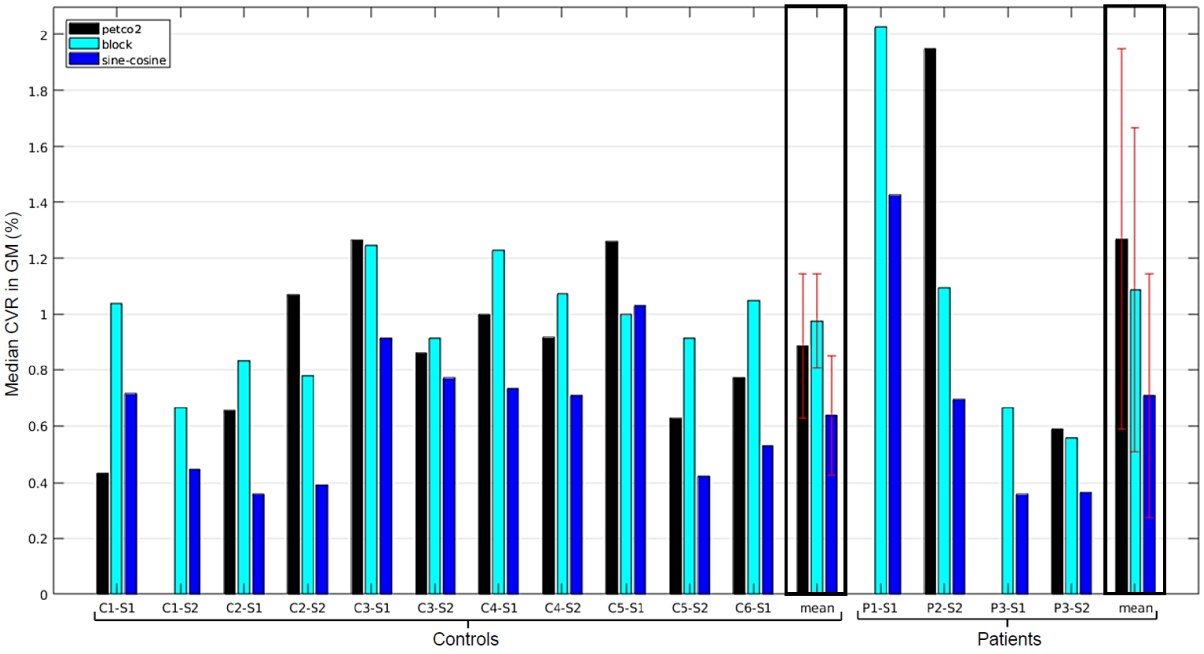

Figure 3.5: Barplots representing the median CVR (%) in GM obtained for all the sessions and the methods ($PetCO_2$ in black, block in cyan and sine-cosine in blue). The group mean CVR and the respective error bars corresponding to the mean standard deviation is also represented for for both controls and patients. C: controls; P: patients; S1: premenstrual/ictal session; S2: midcycle/interictal session (for controls/patients)

may be an oversimplification of the true interrelation between CVR and $PetCO_2$ as it also depends on the baseline $PetCO_2$ with nonlinear behavior at maximal vasodilation [3,82,86,95]. Thus, the normalized results obtained may not be completely trustworthy.

Nevertheless, the mean median CVR in GM obtained from the $PetCO_2$ and block models, 0.18±0.04 %/mm Hg and 0.20±0.10 %/mm Hg, respectively, were according to the literature (reporting a range from 0.15 to 0.40 %/mm Hg). As concerns the sine-cosine model, the median CVR values obtained through its use were lower than the ones reported in literature, which was probably caused by the use of an inadequate number of harmonics [34,35,88,94,97–99].

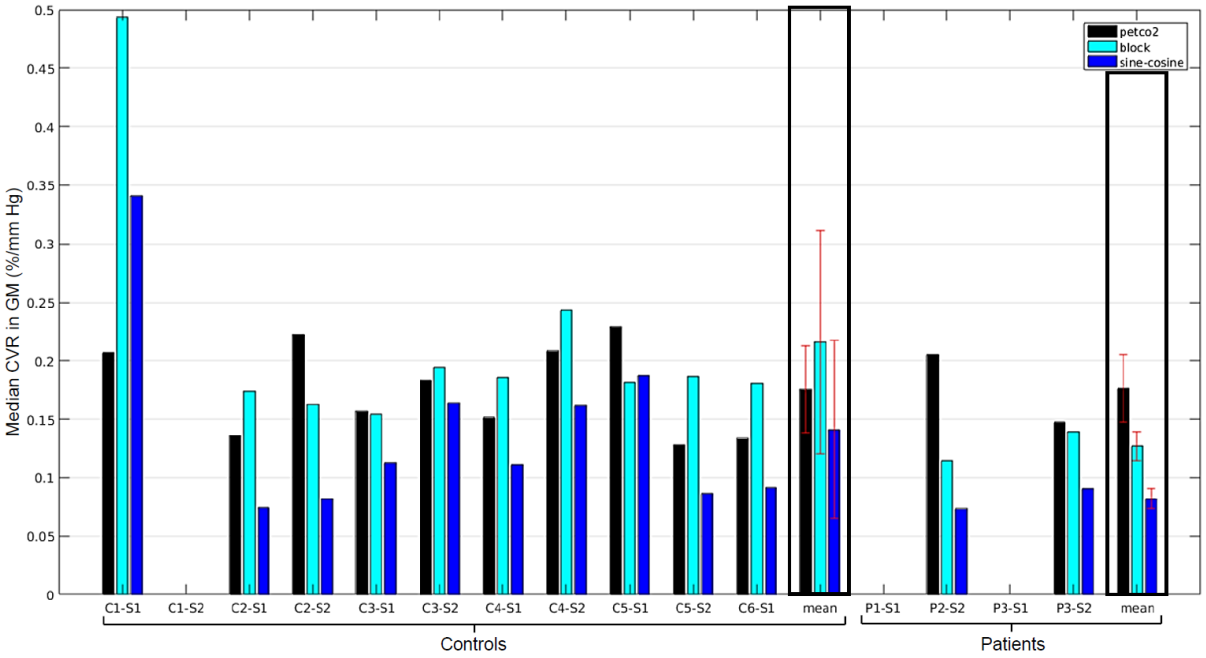

Figure 3.6: Barplots representing the median CVR (%/mm Hg) in GM obtained for the performed sessions who achieved valid $PetCO_2$ traces, for all the methods ($PetCO_2$ in black, block in cyan and sine-cosine in blue). The group mean CVR and the respective error bars corresponding to the mean standard deviation is also represented for both controls and patients. C: controls; P: patients; S1: premenstrual/ictal session; S2: midcycle/interictal session (for controls/patients)

Regarding the delays estimated on a voxelwise basis in the different sessions, their medians were generally higher for the block model in comparison to the ones obtained through the $PetCO_2$ model. This was expected due to their origin (timing of the presentation of the stimuli in block model versus timing of the reaction towards the stimuli in $PetCO_2$). Furthermore, they were similar to the previously estimated bulk shifts for the two methods, the values being closest in the case of the block model. In respect to the delays obtained through the sine-cosine model, these were obtained using a different CVR temporal metric, TTP, that is the time of the model's maximum relative to the beginning of the BH, thus being intrinsically higher than the previous two. However, TTP has been reported to be 31s for 15s end-expiration BH and between 30s and 40s for 20s end-expiration BH [33,88]. Therefore, the TTP

seems to have been underestimated in the present study, which may have been caused once more due to an incorrect number of harmonics.

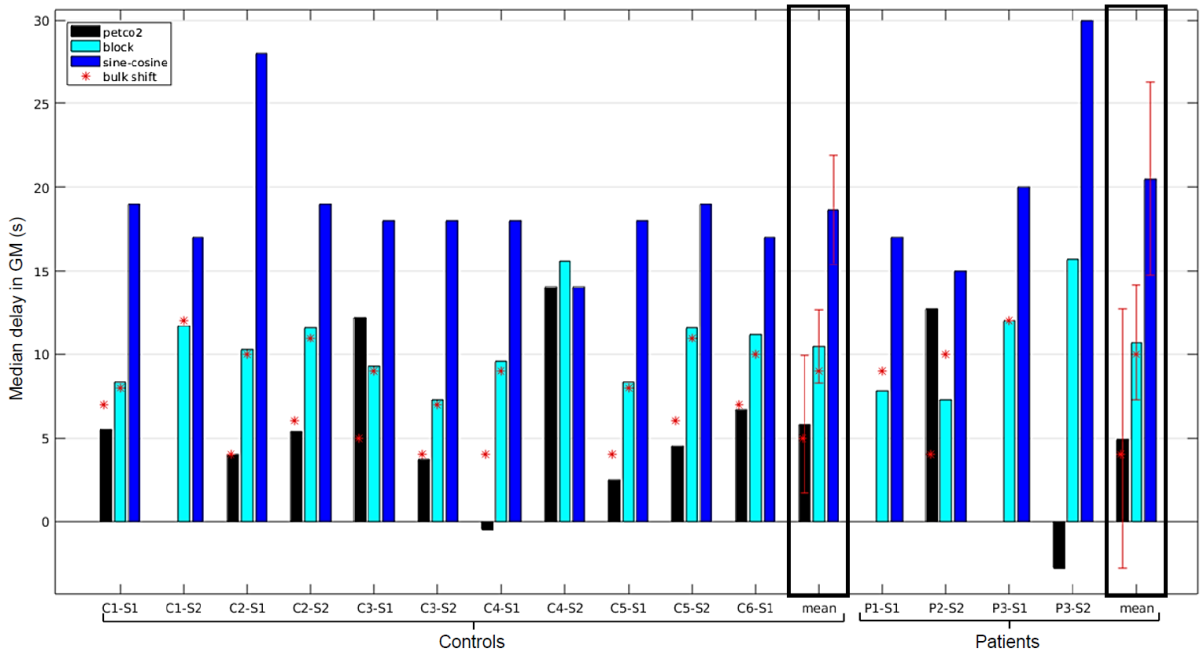

Figure 3.7: Barplots representing the median delay (s) in GM obtained for all the performed sessions, for all the methods ($PetCO_2$ in black, block in cyan and sine-cosine in blue). The bulk shifts calculated for the $PetCO_2$ and block methods are represented in red stars on the respective bars. The group mean delays, the respective error bars corresponding to the mean standard deviation and mean bulk shifts are also represented for both controls and patients. C: controls; P: patients; S1: premenstrual/ictal session; S2: midcycle/interictal session (for controls/patients)

Table 3.2: Statistics about the active voxels (in %), CVR (in % and %/mm Hg) and delay (in s) across brain in GM, for each method, subject and session. C: controls; P: patients; S1: premenstrual/ictal session; S2: midcycle/interictal session (for controls/patients)

Subject	Session	Voxels with CVR (%) >0.3 in GM (%)			Median CVR in GM (%)			Median CVR in GM (%/mm Hg)			Median delay in GM (s)						
		$PetCO_2$	Block	Sinusoidal	$PetCO_2$	Block	Sinusoidal	$PetCO_2$	Block	Sinusoidal	$PetCO_2$	Bulk shift	Difference from bulk	Block	Bulk shift	Difference from bulk	Sinusoidal
C1	S1	75.97	95.57	93.79	0.43	1.04	0.72	0.21	0.49	0.34	5.5	7	-1.5	8.3	8	0.3	19
	S2	-	88.3	75.14	-	0.67	0.45	-	-	-	-	-	-	11.7	12	-0.3	17
C2	S1	87.45	91.57	60.17	0.65	0.84	0.36	0.14	0.17	0.07	4.0	4	0.0	10.3	10	0.3	28
	S2	95.38	92.05	66.89	1.07	0.78	0.39	0.22	0.16	0.08	5.4	6	-0.6	11.6	11	0.6	19
C3	S1	97.33	97.14	95.95	1.27	1.25	0.91	0.16	0.15	0.11	12.2	5	7.2	9.3	9	0.3	18
	S2	90.07	93.03	92.63	0.86	0.91	0.77	0.18	0.19	0.16	3.7	4	-0.3	7.3	7	0.3	18
C4	S1	94.61	96.01	91.35	1.00	1.23	0.73	0.15	0.19	0.11	-0.5	4	-4.5	9.6	9	0.6	18
	S2	91.63	94.51	89.10	0.92	1.07	0.71	0.21	0.24	0.16	14.0	-	-	15.6	-9	-	14
C5	S1	97.55	95.85	87.40	1.26	1.00	1.03	0.23	0.18	0.19	2.5	4	-1.5	8.3	8	0.3	18
	S2	88.00	94.96	72.78	0.63	0.91	0.42	0.13	0.19	0.09	4.5	6	-1.5	11.6	11	0.6	19
C6	S1	89.65	94.07	81.02	0.77	1.05	0.53	0.13	0.18	0.09	6.7	7	-0.3	11.2	10	1.2	17
P1	S1	-	99.25	98.93	-	2.03	1.43	-	-	-	-	-	-	7.8	9	-1.2	17
P2	S2	97.89	96.22	92.41	1.95	1.09	0.7	0.21	0.11	0.07	12.7	4	8.7	7.3	10	-2.7	15
P3	S1	-	87.99	62.26	-	0.67	0.35	-	-	-	-	-	-	12.0	12	0.0	20
	S2	80.15	79.42	64.08	0.59	0.56	0.36	0.15	0.14	0.09	-2.8	-	-	15.7	-	-	30
Mean±s.d.		*90.47±6.93*	*93.06±4.87*	*81.59±13.51*	*0.95±0.41*	*1.01±0.35*	*0.66±0.31*	*0.18±0.04*	*0.20±0.10*	*0.13±0.08*	*5.7±5.1*	*5±1*	*0.5±3.9*	*10.5±2.7*	*10±1*	*0.0±1.0*	*19±3*

3.3.2 Control group-level analysis

In order to compare controls between the two sessions (premenstrual and midcycle), boxplots representing the distributions of the number of voxels with detected CVR (with a CVR in $\% > 0.3$) and the median CVR and delays are presented in figures 3.8 and 3.9. C6 was not included in this comparison analysis as she only performed one of the two sessions (the premenstrual one). In figure 3.8, a comparison is made for all the used methods, for controls C2 to C5 (who achieved valid $PetCO_2$ signals in both sessions). The mean $\Delta PetCO_2$ for the referred controls that is used for the conversion of CVR from $\%$ units to $\%$/mm Hg units is also represented in the figure 3.8. In turn, in figure 3.9 controls C1 to C5 were included, but CVR was only compared in $\%$ units (as C1 did not achieve a valid $PetCO_2$ signal in the midcycle session and therefore the $PetCO_2$ method was not used in the dataset C1-S2, with the consequent absence of a $\Delta PetCO_2$ measure to normalize CVR). Due to the small number of patients, comparison between ictal and interictal sessions at a group-level analysis was not developed.

The block model presented the highest number of voxels with detected CVR, the highest estimates of CVR and the least variability across the group, thus seeming once more to be the best model in fitting our BH BOLD-fMRI data. On the other hand, the sine-cosine model seems once more to be the worst method to model the datasets as it presents the lowest percentage of voxels with detected CVR, the lowest CVR estimates and the highest variability across the group.

The number of voxels with detected CVR (in $\%$) and the CVR (in $\%$) were found out to be increased in the premenstrual session in comparison to the midcycle session. A repeated measures Analysis of Variance (ANOVA) test using the statistics program JASP (https://jasp-stats.org/) was performed over the percentage of voxels with detected CVR that did not find significant effects of methods nor menstrual cycle phases. On the other hand, the test performed over the median CVR values revealed a significant main effect of methods ($p = 0.003$). However, the fact that the differences did not achieve statistical significance may be due to the reduced number of controls.

It can be seen that the normalization of the CVR measures can change their interpretation. In fact, CVR was shown to be increased in the premenstrual sessions in comparison to the midcycle sessions, although this relation was inverted when normalizing CVR measures, which can be explained by the increased mean $\Delta PetCO_2$ measures in the premenstrual sessions. The reason for this increase in $\Delta PetCO_2$ is not clear. It is not likely that it is a hormonal effect, so it may have been caused by the inherent unstable measure of $PetCO_2$, as referred in section 3.1.

Finally, lower delays were noticed in the premenstrual sessions (through the $PetCO_2$ and block analysis methods). A repeated measures ANOVA test in JASP was performed over the median delay values that revealed a significant main effect of methods ($p=0.001$), but not of the menstrual cycle phases. Once more, the fact that the differences did not achieve statistical significance may be due to the small sample of controls.

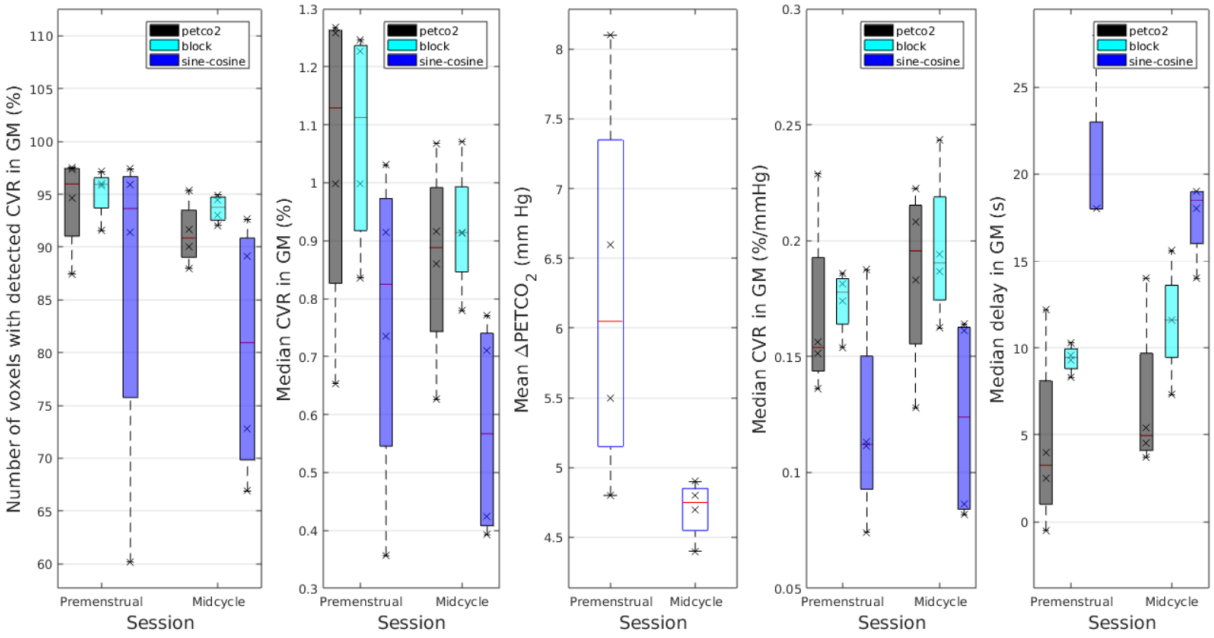

Figure 3.8: Boxplots representing the distributions of number of voxels with detected CVR (%), median CVR in %, mean $\Delta PetCO_2$ in mm Hg, median CVR in %/mm Hg and median delays in seconds (from left to right) in GM across controls C2-C5 for both sessions and the 3 analysis methods ($PetCO_2$ in gray, block in cyan and sine-cosine in blue). In the boxplots, the central mark is the median; the edges of the box are the 25th and 75th percentiles; the upper and lower extreme represent, respectively, the maximum and minimum values.

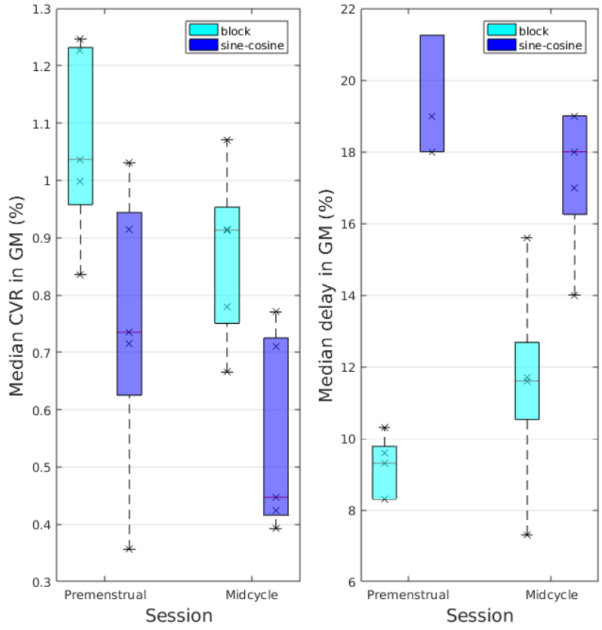

Figure 3.9: Boxplots representing the distributions of median CVR (%) (left) and delays (s) (right) in GM across controls C1-C5 for both sessions and two analysis methods (block in cyan and sine-cosine in blue). In the boxplots, the central mark is the median; the edges of the box are the 25th and 75th percentiles; the upper and lower extreme represent, respectively, the maximum and minimum values.

3.4 Region-specific analysis

Following control group (for controls C2 to C5) analysis in the whole-brain (more specifically, GM) of CVR and delay maps, a region-specific voxelwise analysis was performed in these maps in order to assess voxelwise differences of particular brain regions between premenstrual and midcycle sessions. Therefore, the cortical lobes frontal, temporal, parietal and occipital; the arterial flow territories supplied by the ICA and the VBA; and the subcortical regions brainstem, thalamus, pallidum, putamen, hippocampus and caudate, within GM for each subject and session (whose masks creation had been described in 2.4.1.3) were analysed.

3.4.1 Control group-level analysis

In order to compare controls between the two sessions (premenstrual and midcycle), the distributions of the median CVR in % and %/mm Hg and delays were analysed and are presented through boxplots in figures 3.10, 3.11 and 3.12, respectively. The median of the median CVR (in %) across controls C2 to C5 has shown to be increased in all ROIs in the premenstrual session when compared to the midcycle session, achieving the highest values in the case of the occipital lobe, putamen and caudate. In these regions, the CVR in the premenstrual session was increased when compared to the CVR in the global GM presented in 3.8 (1.2-1.4% in these ROIs vs 1.1-1.2% in the global GM). The visual cortex in the occipital lobe and the putamen had already shown to have increased CVR values when compared to the global GM resulting from a BH-task performance and using fMRI [94, 97]. In order to further investigate the differences between the premenstrual and midcycle phases, a repeated measures ANOVA test using the statistics program JASP was performed over the within ROIs median CVR values, for each ROI. The ANOVA test revealed a significant main effect of ROIs and analysis methods ($p<0.001$), but not of the menstrual cycle phases. Nevertheless, the fact that the differences did not achieve statistical significance may be due to the small sample of controls. Additionally, posthoc tests showed differences between block and sine-cosine models (uncorrected p = 0.04); however, these did not survive multiple comparison correction (Bonferroni corrected p = 0.12). As concerns the normalized CVR and the delays among the different ROIs, no differences were verified between the premenstrual and midcycle phases of the controls.

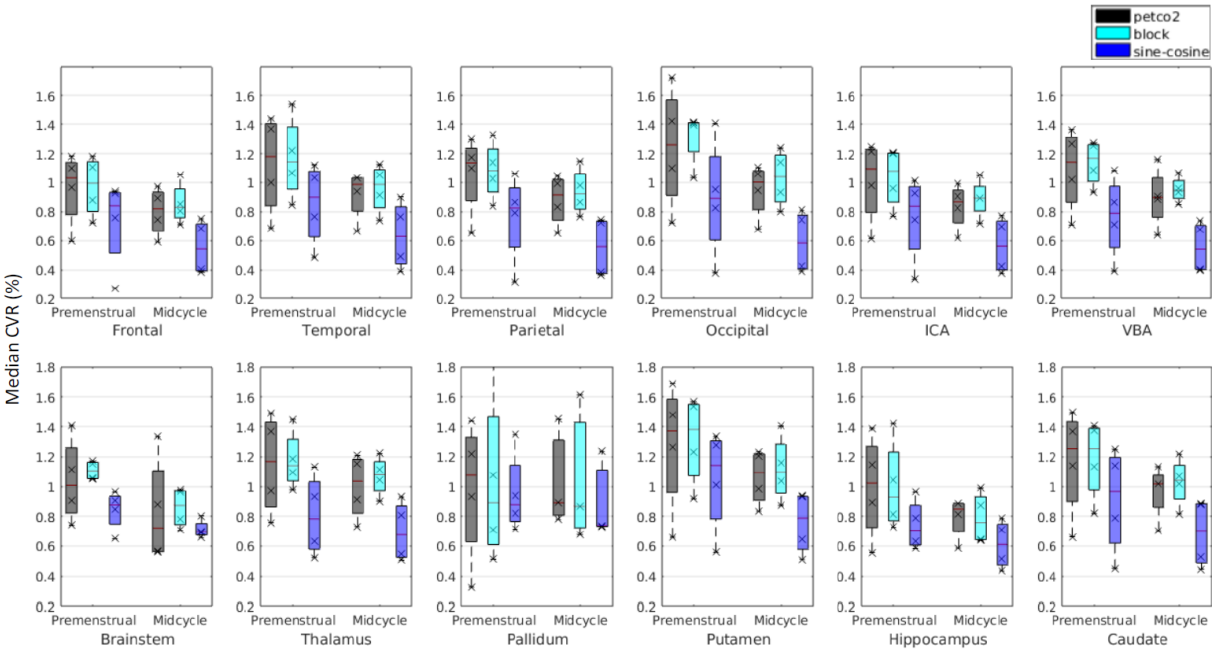

Figure 3.10: Boxplots representing the distributions of the median CVR (%) in different ROIs in GM (cerebral lobes and arterial flow territories ROIs above, subcortical ROIs below) across controls C2-C5 for both sessions and the 3 analysis methods ($PetCO_2$ in gray, block in cyan and sine-cosine in blue). In the boxplots, the central mark is the median; the edges of the box are the 25th and 75th percentiles; the upper and lower extreme represent, respectively, the maximum and minimum values.

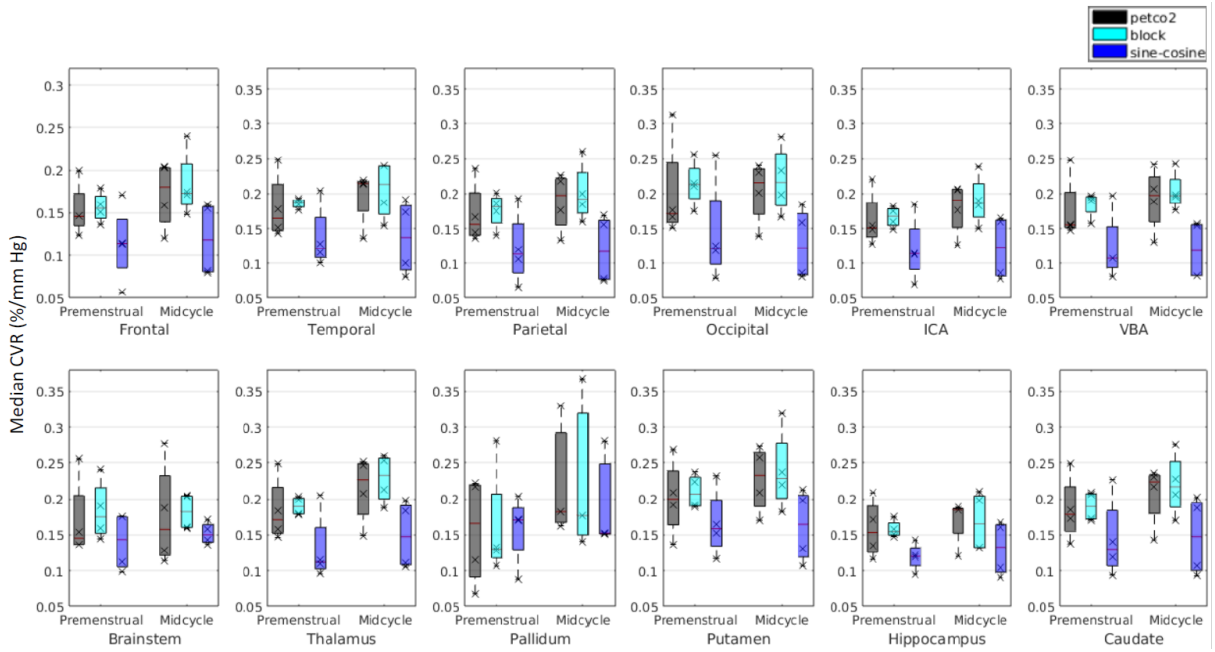

Figure 3.11: Boxplots representing the distributions of the median CVR (%/mm Hg) in different ROIs in GM (cerebral lobes and arterial flow territories ROIs above, subcortical ROIs below) across controls C1-C5 and for both sessions and the 3 analysis methods ($PetCO_2$ in gray, block in cyan and sine-cosine in blue). In the boxplots, the central mark is the median; the edges of the box are the 25th and 75th percentiles; the upper and lower extreme represent, respectively, the maximum and minimum values.

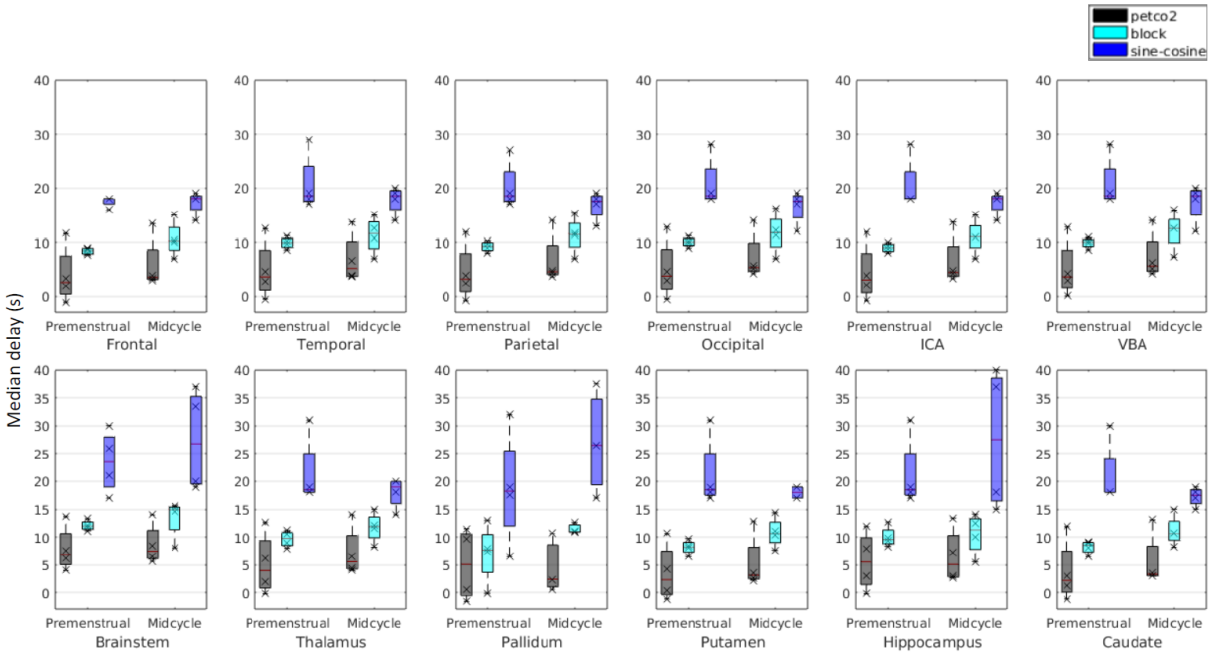

Figure 3.12: Boxplots representing the distributions of the median delays (s) in different ROIs in GM (cerebral lobes and arterial flow territories ROIs above, subcortical ROIs below) across controls C2-C5 and for the 3 analysis methods ($PetCO_2$ in gray, block in cyan and sine-cosine in blue). In the boxplots, the central mark is the median; the edges of the box are the 25th and 75th percentiles; the upper and lower extreme represent, respectively, the maximum and minimum values.

Chapter 4

Conclusions and future work

In the present study, CVR was investigated using a BH-task and BOLD-fMRI in a group of patients which was studied during the ictal (headache) and interictal phases of migraine and a group of hormonal controls which was studied during the premenstrual and midcycle phases of the menstrual cycle. In the control group, increased CVR (in $\%$) and reduced delays in GM were detected in the premenstrual phase when compared to the midcycle phase, although this difference did not achieve statistical significance. In previous studies, the PCA had already been reported to be reduced in migraineurs when compared to controls [15, 29, 31]. Furthermore, migrainous infarction had been shown to be more prone to happen in the occipital cortex [17, 61, 62, 65]. In a study from Sofia et al. [33] developed at Laseeb, CVR and TTP were found out to be increased in the occipital lobe during the ictal (headache) phase compared with the interictal phase in migraine patients. In the present work, control group delay maps showed alterations in the posterior area that included the occipital lobe region. Additionally, in controls, CVR in the occipital lobe was increased in the premenstrual sessions, when compared to the midcycle sessions (although not significant). This may imply that the alterations in the occipital region in migraineurs during the ictal phase described in previous studies [33] may in fact be associated with (possibly hormonal) alterations related to the menstrual cycle and not characteristic of the migraine disorder (that had been associated with an endothelial dysfunction of the posterior cerebral circulation [29, 33]). This enhances the importance of including appropriate controls in studies, even when following a longitudinal approach.

Three different analysis methods were implemented to characterize CVR: the iteratively shifted $PetCO_2$ regressors GLM, the iteratively shifted block regressors GLM and the sine-cosine GLM methods. The results obtained shows that the iteratively shifted block regressors GLM method was the most effective in modelling the BH BOLD-fMRI data as it produced the highest percentage of voxels with detected CVR and the highest CVR amplitude estimates. On the other hand, the relative underestimation of the iteratively shifted $PetCO_2$ regressors GLM methods seem to be due to incorrect CO_2 recording caused by experimental setup issues, namely to the use of an exclusively nasal cannula that did not

account for the CO_2 signal expired through the mouth. Nevertheless, both of these methods produced maps with the expected contrast between GM and WM and showed higher delays in the posterior region of the brain, according to the existing literature [3, 36, 88, 94, 130, 131]. In turn, the sine-cosine GLM model showed to be the worst in fitting the data, which can be justified by the incorrect number of harmonics. Additionally, the delay maps obtained through this method were the noisiest. As concerns the normalized CVR, this accounts for the variability in the task performance and allows to make a more accurate comparison between different subjects and sessions. However, the $\Delta PetCO_2$ in our case is prone to have misleading values due to experimental setup issues, which may introduce some errors and alter the results, so they must be dealt with caution.

4.1 Relation with the literature

Overall, the present work contributes with new evidence to the limited literature.

This dissertation was, as far as we know, the first work investigating CVR in both migraineurs and hormonal controls in a longitudinal approach (studying patients' ictal and interictal phases and controls' premenstrual and midcycle phases). In fact, only two studies have assessed CVR in menstrual migraine and did not include hormonal controls, with one scanning patients without accounting for the migraine cycle phase [72] and the other one employing a case-control approach for studying migraine only in the interictal phase [23]. Additionally, only two studies were found in literature that have evaluated CVR in the menstrual cycle following a longitudinal approach [25, 71]. All these used TCD and not fMRI, lacking spatial resolution.

Finally, this study also contributes for the scarce information about the BH paradigm design parameters, experimental setup, and analysis methods that can be used to model this type of data.

4.2 Limitations and future work

Regarding the breathing task paradigm parameters, the BH performed by the subjects in this study was preceded by an expiration and followed by periods of externally-paced breathing according to the subjects' natural breathing rate, according to what had been found in literature [3, 34–36, 87]. However, end-inspiration protocols are easier to perform and therefore could lead to better results when dealing with less cooperative patients (which is the case of this study patients in the ictal phase). However, if using an end-inspiration BH task, the amplitude of the BOLD response would also depend on the depth of the preparatory inspiration and so instructions during this period would be necessary. Using computer-paced breathing according to the subjects' natural breathing rate instead of self-paced breathing reduces possible inter- and intra-subjects CBF differences arising from CO_2 variations caused by subjects' venti-

lation and lung function [3,36]. However, this may induce deep breathing and its associated hypocapnia. Additionally, the natural breathing rate calculation might be affected by experimental setup issues.

The cause of the vascular response is the change in $PaCO_2$ levels associated with the BH challenge. Thus, measuring its surrogate $PetCO_2$ and using it as a regressor in the GLM analysis provides a complete model of the hypercapnia stimulus. This accounts for inter- and intrasubject variability caused by BH-task performance differences. In addition, it is possible to obtain a quantitative measure of CVR if the BOLD percent signal change (PSC) is normalized by the $\Delta PetCO_2$ [3]. However, CO_2 recording requires complex experimental setups. In fact, it could be concluded from this study that an exclusively nasal cannula does not get the expired CO_2 from the mouth, which frequently occurs even when instructions are given for subjects to breath mostly through their noses. Thus, a breathing mask seems to be necessary for a correct CO_2 acquisition and would probably improve the results obtained using the iteratively shifted $PetCO_2$ regressors GLM analysis method. However, it is often more uncomfortable and thus can lead to increased motion.

As concerns the sine-cosine GLM method, an analysis should be made assessing the appropriate number of harmonics that better fits the BH BOLD-fMRI considering the BH-task trials duration. Additionally, a better model could possibly be achieved by making the BH period duration more similar to the baseline period duration since it gets closer to a sinusoidal shape. Nevertheless, it is important to have in mind that this is still a paradigm-based model that does not account for task performance variability.

For the purpose of this dissertation, the number of participants was small, namely in the case of patients, in which a group analysis could not be developed. This limits the statistical power of the findings and consequently the generalization of the results. This was mainly due the COVID pandemic, that caused the interruption of the acquisitions until may 2021 and exacerbated the hospital logistics issues. Furthermore, patients participation was especially difficult since they had to be scanned during pain. Even when enrolled in the study, some patients withdrew or were not so collaborative in the ictal session, causing inter- and intrasubject variations in task performance. With more patients, a group-level analysis could have been done to compare their ictal and interictal phases. Moreover, migraine patients during other phases of the ictal period beyond the headache phase, such as the preictal, were not investigated, which would be interesting as a way to increase the limited knowledge on the mechanisms involved in the stages of ictal phase. In fact, patients' preictal phase usually happens in their premenstrual phase of the menstrual cycle and the interictal phase in the midcycle phase of their menstrual cycle [22–26]. Therefore, it would be interesting to compare patients' preictal and controls' premenstrual phases, such as patients' interictal and controls' midcycle phases between volunteers who share similar menstrual cycles and hormonal contraception. This is planned in the scope of the MIG_N2Treat project from which this study is part of (but was out of the scope of this dissertation).

Moreover, controlling for the menstrual cycle phase in both groups is important for comparison pur-

poses [23, 71]. The performance of blood tests to every woman in order to know the accurate ovulation time according to the hormones' concentrations in plasma would be ideal, but is inconvenient Thus, the calendar method was used (sometimes together with the basal temperature method). Nevertheless, this is not completely reliable [71]. Moreover, participants who were taking hormonal contraception were not excluded and so these may have limited the findings since previous studies reported that these may affect cerebrovascular function [23].

Finally, the BOLD-fMRI technique measures CBF in an indirect semiquantitative manner as the signal is influenced by other physiological parameters as CBV and blood oxygenation. In turn, ASL provides a direct quantitative measure of CBF and has shown to be superior to BOLD in terms of spatial localization [3, 36, 76, 77, 90]. Unfortunately, its intrinsically low signal-to-noise ratio (SNR) has limited its applicability to studies of CVR. Nevertheless, simultaneous ASL and BOLD imaging have shown promising results in CVR assessment based on breathing tasks and may increase the utility of ASL in future research [133].

Bibliography

[1] L. M. Cupini, I. Corbelli, and P. Sarchelli, “Menstrual migraine: what it is and does it matter?” *Journal of Neurology*, vol. 268, no. 7, pp. 2355–2363, 2021.

[2] J. E. Brian, “Carbon Dioxide and the Cerebral Circulation,” *Anesthesiology*, vol. 88, no. 5, pp. 1365–1386, 05 1998.

[3] J. Pinto, M. G. Bright, D. P. Bulte, and P. Figueiredo, “Cerebrovascular Reactivity Mapping Without Gas Challenges: A Methodological Guide,” *Frontiers in Physiology*, vol. 11, pp. 320–326, 2021.

[4] L. H. Schulte and A. May, “The migraine generator revisited: Continuous scanning of the migraine cycle over 30 days and three spontaneous attacks,” *Brain*, vol. 139, no. 7, pp. 1987–1993, 2016.

[5] L. J. Stovner, E. Nichols, T. J. Steiner, F. Abd-Allah, A. Abdelalim, R. M. Al-Raddadi, M. G. Ansha, A. Barac, I. M. Bensenor, L. P. Doan, D. Edessa, M. Endres, K. J. Foreman, F. G. Gankpe, G. Gopalkrishna, A. C. Goulart, R. Gupta, G. J. Hankey, S. I. Hay, M. I. Hegazy, E. H. Hilawe, A. Kasaeian, D. H. Kassa, I. Khalil, Y. H. Khang, J. Khubchandani, Y. J. Kim, Y. Kokubo, M. A. Mohammed, M. Moradi-Lakeh, H. L. T. Nguyen, Y. L. Nirayo, M. Qorbani, A. Ranta, K. T. Roba, S. Safiri, I. S. Santos, M. Satpathy, M. Sawhney, M. S. Shiferaw, I. Shiue, M. Smith, C. E. Szoeke, N. T. Truong, N. Venketasubramanian, K. G. Weldegwergs, R. Westerman, T. Wijeratne, B. X. Tran, N. Yonemoto, V. L. Feigin, T. Vos, and C. J. Murray, “Global, regional, and national burden of migraine and tension-type headache, 1990–2016: a systematic analysis for the Global Burden of Disease Study 2016,” *The Lancet Neurology*, vol. 17, no. 11, pp. 954–976, 2018.

[6] R. Pradeep, S. C. Nemichandra, S. Harsha, and K. Radhika, “Migraine Disability, Quality of Life, and Its Predictors,” *Annals of Neurosciences*, vol. 27, no. 1, pp. 18–23, 2020.

[7] T. J. Steiner, L. J. Stovner, R. Jensen, D. Uluduz, and Z. Katsarava, “Migraine remains second among the world’s causes of disability, and first among young women: findings from GBD2019,” *Journal of Headache and Pain*, vol. 21, no. 1, pp. 4–7, 2020.

[8] A. Charles, “The pathophysiology of migraine: implications for clinical management,” *The Lancet Neurology*, vol. 17, no. 2, pp. 174–182, 2018.

[9] K. G. Vetvik and E. A. MacGregor, “Menstrual migraine: a distinct disorder needing greater recognition,” *The Lancet Neurology*, vol. 20, no. 4, pp. 304–315, 2021.

[10] R. Burstein, R. Noseda, and D. Borsook, “Migraine: Multiple processes, complex pathophysiology,” *Journal of Neuroscience*, vol. 35, no. 17, pp. 6619–6629, 2015.

[11] P. J. Goadsby, P. R. Holland, M. Martins-Oliveira, J. Hoffmann, C. Schankin, and S. Akerman, “Pathophysiology of migraine: A disorder of sensory processing,” *Physiological Reviews*, vol. 97, no. 2, pp. 553–622, 2017.

[12] M. De Tommaso, A. Ambrosini, F. Brighina, G. Coppola, A. Perrotta, F. Pierelli, G. Sandrini, M. Valeriani, D. Marinazzo, S. Stramaglia, and J. Schoenen, “Altered processing of sensory stimuli in patients with migraine,” *Nature Reviews Neurology*, vol. 10, no. 3, pp. 144–155, 2014.

[13] F. Puledda, R. Messina, and P. J. Goadsby, “An update on migraine: current understanding and future directions,” *Journal of Neurology*, vol. 264, no. 9, pp. 2031–2039, 2017.

[14] D. W. Dodick, “A Phase-by-Phase Review of Migraine Pathophysiology,” *Headache*, vol. 58, pp. 4–16, 2018.

[15] M. J. Lee, S. Cho, S. Y. Woo, and C. S. Chung, “Paradoxical association between age and cerebrovascular reactivity in migraine: A cross-sectional study,” *Journal of the Neurological Sciences*, vol. 398, no. September 2018, pp. 204–209, 2019.

[16] S. Raut, U. Singh, D. Sarmah, A. Datta, F. Baidya, B. Shah, M. Bohra, P. Jagtap, A. Sarkar, K. Kalia, A. Borah, K. R. Dave, D. R. Yavagal, and P. Bhattacharya, “Migraine and Ischemic Stroke: Deciphering the Bidirectional Pathway,” *ACS Chemical Neuroscience*, vol. 11, no. 11, pp. 1525–1538, 2020.

[17] Y. Zhang, A. Parikh, and S. Qian, “Migraine and stroke,” *Stroke and Vascular Neurology*, vol. 2, no. 3, pp. 160–167, 2017.

[18] M. J. Lee, C. Lee, and C. S. Chung, “The migraine-stroke connection,” *Journal of Stroke*, vol. 18, no. 2, pp. 146–156, 2016.

[19] A. Saeed, K. F. Rana, Z. I. Warriach, M. A. Tariq, and B. H. Malik, “Association of Migraine and Ischemic Heart Disease: A Review,” *Cureus*, vol. 11, no. 9, 2019.

[20] A. N. Mahmoud, A. Mentias, A. Y. Elgendy, A. Qazi, A. F. Barakat, M. Saad, A. Mohsen, A. Abuzaid, H. Mansoor, M. K. Mojadidi, and I. Y. Elgendy, “Migraine and the risk of cardiovascular and cerebrovascular events: A meta-analysis of 16 cohort studies including 1 152 407 subjects,” *BMJ Open*, vol. 8, no. 3, pp. 1–10, 2018.

[21] L. R. Øie, L. R. Øie, T. Kurth, S. Gulati, S. Gulati, and D. W. Dodick, "Migraine and risk of stroke," *Journal of Neurology, Neurosurgery and Psychiatry*, vol. 91, no. 6, pp. 593–604, 2020.

[22] D. Chen, M. Willis-Parker, and G. P. Lundberg, "Migraine headache: Is it only a neurological disorder? Links between migraine and cardiovascular disorders," *Trends in Cardiovascular Medicine*, vol. 30, no. 7, pp. 424–430, 2020.

[23] J. S. A. Dzator, P. R. C. Howe, L. R. Griffiths, K. G. Coupland, and R. H. X. Wong, "Cerebrovascular Function in Hormonal Migraine: An Exploratory Study," *Frontiers in Neurology*, vol. 12, no. July, pp. 1–12, 2021.

[24] J. L. Brandes, "The influence of estrogen on migraine: A systematic review," *Journal of the American Medical Association*, vol. 295, no. 15, pp. 1824–1830, 2006.

[25] G. L. Peltonen, J. W. Harrell, B. P. Aleckson, K. M. LaPlante, M. K. Crain, and W. G. Schrage, "Cerebral blood flow regulation in women across menstrual phase: Differential contribution of cyclooxygenase to basal, hypoxic, and hypercapnic vascular tone," *American Journal of Physiology - Regulatory Integrative and Comparative Physiology*, vol. 311, no. 2, pp. R222–R231, 2016.

[26] A. H. Calhoun, "Understanding Menstrual Migraine," *Headache*, vol. 58, no. 4, pp. 626–630, 2018.

[27] J. S. Dzator, P. R. Howe, and R. H. Wong, "Profiling cerebrovascular function in migraine: A systematic review and meta-analysis," *Journal of Cerebral Blood Flow and Metabolism*, 2020.

[28] V. González-Quintanilla, M. Toriello, E. Palacio, M. A. González-Gay, J. Castillo, S. Montes, R. Martínez-Nieto, J. Fernandez, A. Rojo, S. Gutiérrez, E. Pons, and A. Oterino, "Systemic and cerebral endothelial dysfunction in chronic migraine. A case-control study with an active comparator," *Cephalalgia*, vol. 36, no. 6, pp. 552–560, 2016.

[29] R. Rajan, D. Khurana, and V. Lal, "Interictal cerebral and systemic endothelial dysfunction in patients with migraine: A case-control study," *Journal of Neurology, Neurosurgery and Psychiatry*, vol. 86, no. 11, pp. 1253–1257, 2014.

[30] M. Silvestrini, M. Matteis, E. Troisi, L. M. Cupini, and G. Bernardi, "Cerebrovascular reactivity in migraine with and without aura," *Headache*, vol. 36, no. 1, pp. 37–40, 1996.

[31] D. Perko, J. Pretnar-Oblak, M. Šabovič, B. Žvan, and M. Zaletel, "Cerebrovascular reactivity to l-arginine in the anterior and posterior cerebral circulation in migraine patients," *Acta Neurologica Scandinavica*, vol. 124, no. 4, pp. 269–274, 2011.

[32] S. T. Chan, K. C. Evans, T. Y. Song, R. Gupta, B. R. Rosen, A. Singhal, and K. K. Kwong, "Functional magnetic resonance imaging of regional impaired cerebrovascular reactivity for migraineurs in the interictal state," *bioRxiv*, vol. 7194, no. 617, 2019.

[33] S. Cotrim, R. Gil-Gouveia, J. Pinto, P. Vilela, M. I. Pavão, and P. Figueiredo, "Increased cerebrovascular reactivity during spontaneous migraine attacks compared to pain-free periods," *Proc. 37th Annual Scientific Meeting of the European Society for Magnetic Resonance in Medicine and Biology (ESMRMB 2020)*, 2020.

[34] I. Lipp, K. Murphy, X. Caseras, and R. G. Wise, "Agreement and repeatability of vascular reactivity estimates based on a breath-hold task and a resting state scan," *NeuroImage*, vol. 113, pp. 387–396, 2015.

[35] M. G. Bright and K. Murphy, "Reliable quantification of BOLD fMRI cerebrovascular reactivity despite poor breath-hold performance," *NeuroImage*, vol. 83, pp. 559–568, 2013.

[36] A. L. Urback, B. J. MacIntosh, and B. I. Goldstein, "Cerebrovascular reactivity measured by functional magnetic resonance imaging during breath-hold challenge: A systematic review," *Neuroscience and Biobehavioral Reviews*, vol. 79, pp. 27–47, 2017.

[37] B. Jacobs and G. Dussor, "Neurovascular contributions to migraine: Moving beyond vasodilation," *Neuroscience*, vol. 338, pp. 130–144, 2016.

[38] A. May, "Understanding migraine as a cycling brain syndrome: reviewing the evidence from functional imaging," *Neurological Sciences*, vol. 38, pp. 125–130, 2017.

[39] A. B. Gago-Veiga, J. Pagán, K. Henares, P. Heredia, N. González-García, M. I. De Orbe, J. L. Ayala, M. Sobrado, and J. Vivancos, "To what extent are patients with migraine able to predict attacks?" *Journal of Pain Research*, vol. 11, pp. 2083–2094, 2018.

[40] J. Olesen, "Headache Classification Committee of the International Headache Society (IHS) The International Classification of Headache Disorders, 3rd edition," *Cephalalgia*, vol. 38, no. 1, pp. 1–211, 2018.

[41] G. L. Onderwater, J. Dool, M. D. Ferrari, and G. M. Terwindt, "Premonitory symptoms in glyceryl trinitrate triggered migraine attacks: a case-control study," *Pain*, vol. 161, no. 9, pp. 2058–2067, 2020.

[42] A. B. Gago-Veiga, J. Vivancos, and M. Sobrado, "Fase premonitoria, una etapa clave en la migraña," *Neurologia*, 2017.

[43] F. H. Maniyar, T. Sprenger, T. Monteith, C. J. Schankin, and P. J. Goadsby, "The premonitory phase of migraine - What can we learn from it?" *Headache*, vol. 55, no. 5, pp. 609–620, 2015.

[44] N. Karsan, P. Bose, and P. J. Goadsby, "The Migraine Premonitory Phase," *CONTINUUM Lifelong Learning in Neurology*, vol. 24, no. 4-Headache, pp. 996–1008, 2018.

[45] N. Karsan and P. J. Goadsby, “Imaging the Premonitory Phase of Migraine,” *Frontiers in Neurology*, vol. 11, 2020.

[46] L. H. Schulte and K. P. Peng, “Current understanding of premonitory networks in migraine: A window to attack generation,” *Cephalalgia*, vol. 39, no. 13, pp. 1720–1727, 2019.

[47] M. J. Marmura, “Triggers, Protectors, and Predictors in Episodic Migraine,” *Current Pain and Headache Reports*, vol. 22, no. 12, 2018.

[48] J. M. Hansen and C. J. Schankin, “Cerebral hemodynamics in the different phases of migraine and cluster headache,” *Journal of Cerebral Blood Flow and Metabolism*, vol. 39, no. 4, pp. 595–609, 2019.

[49] R. Gil-Gouveia, A. G. Oliveira, and I. P. Martins, “Subjective cognitive symptoms during a migraine attack: A prospective study of a clinic-based sample,” *Pain Physician*, vol. 19, no. 1, pp. E137–E150, 2016.

[50] D. J. Hodkinson, S. L. Wilcox, R. Veggeberg, R. Noseda, R. Burstein, D. Borsook, and L. Becerra, “Increased amplitude of thalamocortical low-frequency oscillations in patients with migraine,” *Journal of Neuroscience*, vol. 36, no. 30, pp. 8026–8036, 2016.

[51] J. Hoffmann, S. M. Baca, and S. Akerman, “Neurovascular mechanisms of migraine and cluster headache,” *Journal of Cerebral Blood Flow and Metabolism*, vol. 39, no. 4, pp. 573–594, 2019.

[52] R. Noseda, V. Kainz, D. Borsook, and R. Burstein, “Neurochemical pathways that converge on thalamic trigeminovascular neurons: Potential substrate for modulation of migraine by sleep, food intake, stress and anxiety,” *PLoS ONE*, vol. 9, no. 8, 2014.

[53] S. Magon, A. May, A. Stankewitz, P. J. Goadsby, A. R. Tso, M. Ashina, F. M. Amin, C. L. Seifert, M. M. Chakravarty, J. Müller, and T. Sprenger, “Morphological abnormalities of thalamic subnuclei in migraine: A multicenter MRI study at 3 tesla,” *Journal of Neuroscience*, vol. 35, no. 40, pp. 13 800–13 806, 2015.

[54] S. Younis, A. Hougaard, R. Noseda, and M. Ashina, “Current understanding of thalamic structure and function in migraine,” *Cephalalgia*, vol. 39, no. 13, pp. 1675–1682, 2019.

[55] J. Olesen, R. Burstein, M. Ashina, and P. Tfelt-Hansen, “Origin of pain in migraine: evidence for peripheral sensitisation,” *The Lancet Neurology*, vol. 8, no. 7, pp. 679–690, 2009.

[56] O. Summ, A. R. Charbit, A. P. Andreou, and P. J. Goadsby, “Modulation of nocioceptive transmission with calcitonin gene-related peptide receptor antagonists in the thalamus,” *Brain*, vol. 133, no. 9, pp. 2540–2548, 2010.

[57] A. S. Wattiez, L. P. Sowers, and A. F. Russo, “Calcitonin gene-related peptide (CGRP): role in migraine pathophysiology and therapeutic targeting,” *Expert Opinion on Therapeutic Targets*, vol. 24, no. 2, pp. 91–100, 2020.

[58] A. F. Russo, “CGRP as a neuropeptide in migraine: Lessons from mice,” *British Journal of Clinical Pharmacology*, vol. 80, no. 3, pp. 403–414, 2015.

[59] J. T. Spector, S. R. Kahn, M. R. Jones, M. Jayakumar, D. Dalal, and S. Nazarian, “analysis,” vol. 123, no. 7, pp. 612–624, 2011.

[60] C. Tzourio, S. Iglesias, J. B. Hubert, J. M. Visy, A. Alperovitch, A. Tehindrazanarivelo, V. Biousse, F. Woimant, and M. G. Bousser, “Migraine and risk of ischaemic stroke: A case control study,” *British Medical Journal*, vol. 307, no. 6899, pp. 289–292, 1993.

[61] Y. Abanoz, Y. Gülen Abanoz, A. Gündüz, D. Uludüz, B. İnce, B. Yavuz, and B. Göksan, “Migraine as a risk factor for young patients with ischemic stroke: a case–control study,” *Neurological Sciences*, vol. 38, no. 4, pp. 611–617, 2017.

[62] E. C. Agostoni and M. Longoni, “Migraine and cerebrovascular disease: still a dangerous connection?” *Neurological Sciences*, vol. 39, pp. 33–37, 2018.

[63] A. Caminero and M. Sánchez Del Río González, “Migraine as a cerebrovascular risk factor,” *Neurología (English Edition)*, vol. 27, no. 2, pp. 103–111, 2012.

[64] S. Sacco, S. Ricci, D. Degan, and A. Carolei, “Migraine in women: The role of hormones and their impact on vascular diseases,” *Journal of Headache and Pain*, vol. 13, no. 3, pp. 177–189, 2012.

[65] M. C. Kruit, L. J. Launer, M. D. Ferrari, and M. A. Van Buchem, “Infarcts in the posterior circulation territory in migraine. The population-based MRI CAMERA study,” *Brain*, vol. 128, no. 9, pp. 2068–2077, 2005.

[66] J. E. Deanfield, J. P. Halcox, and T. J. Rabelink, “Endothelial function and dysfunction: Testing and clinical relevance,” *Circulation*, vol. 115, no. 10, pp. 1285–1295, 2007.

[67] K. Heshmat-Ghahdarijani, S. H. Javanmard, S. A. Sonbolestan, M. Saadatnia, and S. A. Sonbolestan, “Endothelial function in patients with migraine without aura during the interictal period,” *International Journal of Preventive Medicine*, vol. 2015-Janua, 2015.

[68] A. Yilmaz Avci, M. H. Akkucuk, E. Torun, S. Arikan, U. Can, and M. A. Tekindal, “Migraine and subclinical atherosclerosis: endothelial dysfunction biomarkers and carotid intima-media thickness: a case-control study,” *Neurological Sciences*, vol. 40, no. 4, pp. 703–711, 2019.

[69] X. Rodríguez-Osorio, T. Sobrino, D. Brea, F. Martínez, J. Castillo, and R. Leira, "Endothelial progenitor cells: A new key for endothelial dysfunction in migraine," *Neurology*, vol. 79, no. 5, pp. 474–479, 2012.

[70] T. G. Liman, K. Bachelier-Walenta, L. Neeb, J. Rosinski, U. Reuter, M. Böhm, and M. Endres, "Circulating endothelial microparticles in female migraineurs with aura," *Cephalalgia*, vol. 35, no. 2, pp. 88–94, 2015.

[71] J. Krejza, W. Rudzinski, M. Arkuszewski, O. Onuoha, and E. R. Melhem, "Cerebrovascular reactivity across the menstrual cycle in young healthy women," *Neuroradiology Journal*, vol. 26, no. 4, pp. 413–419, 2013.

[72] S. Tasdemir, H. Akgun, S. Mazman, E. Eroglu, S. Alay, M. Yucel, O. Oz, U. Ulas, and S. Demirkaya, "Evaluation of Cerebral Hemodynamics of Patients with Menstrual Migraine," *Cephalgia*, vol. 33, no. 8, p. 166, 2013.

[73] K. J. Brackley, M. M. Ramsay, F. Broughton Pipkin, and P. C. Rubin, "The effect of the menstrual cycle on human cerebral blood flow: studies using doppler ultrasound," *Ultrasound in Obstetrics & Gynecology*, vol. 14, no. 1, pp. 52–57, 1999.

[74] M. Dubol, C. N. Epperson, J. Sacher, B. Pletzer, B. Derntl, R. Lanzenberger, I. Sundström-Poromaa, and E. Comasco, "Neuroimaging the menstrual cycle: A multimodal systematic review," *Frontiers in Neuroendocrinology*, vol. 60, 2021.

[75] O. Nevo, J. F. Soustiel, and I. Thaler, "Cerebral blood flow is increased during controlled ovarian stimulation," *American Journal of Physiology - Heart and Circulatory Physiology*, vol. 293, no. 6, pp. 3265–3269, 2007.

[76] P. Liu, Y. Li, M. Pinho, D. C. Park, B. G. Welch, and H. Lu, "Cerebrovascular reactivity mapping without gas challenges Corresponding author HHS Public Access," *Neuroimage*, vol. 146, pp. 320–326, 2017.

[77] S. J. Catchlove, A. Pipingas, M. E. Hughes, and H. Macpherson, "Magnetic resonance imaging for assessment of cerebrovascular reactivity and its relationship to cognition: A systematic review," *BMC Neuroscience*, vol. 19, no. 1, pp. 1–15, 2018.

[78] E. Sleight, M. S. Stringer, I. Marshall, J. M. Wardlaw, and M. J. Thrippleton, "Cerebrovascular Reactivity Measurement Using Magnetic Resonance Imaging: A Systematic Review," *Frontiers in Physiology*, vol. 12, 2021.

[79] R. Aaslid, T. M. Markwalder, and H. Nornes, “Noninvasive transcranial Doppler ultrasound recording of flow velocity in basal cerebral arteries,” *Journal of Neurosurgery*, vol. 57, no. 6, pp. 769–774, 1982.

[80] T. D. Thomas, G. J. Harpold, and B. T. Troost, “Cerebrovascular Reactivity in Migraineurs as Measured by Transcranial Doppler,” *Cephalalgia*, vol. 10, no. 2, pp. 95–99, 1990.

[81] H. W. Schytz, F. M. Amin, J. Selb, and D. A. Boas, “Non-invasive methods for measuring vascular changes in neurovascular headaches,” *Journal of Cerebral Blood Flow and Metabolism*, vol. 39, no. 4, pp. 633–649, 2019.

[82] A. A. Bhogal, J. C. Siero, J. A. Fisher, M. Froeling, P. Luijten, M. Philippens, and H. Hoogduin, “Investigating the non-linearity of the BOLD cerebrovascular reactivity response to targeted hypo/hypercapnia at 7T,” *NeuroImage*, vol. 98, pp. 296–305, 2014.

[83] N. K. Logothetis and B. A. Wandell, “Interpreting the BOLD signal,” *Annual Review of Physiology*, vol. 66, pp. 735–769, 2004.

[84] S. G. Kim and P. Bandetyini, “Principles of BOLD Functional MRI,” *Functional Neuroradiology: Principles and Clinical Applications*, pp. 103–111, 2012.

[85] P. M. Matthews and P. Jezzard, “Functional magnetic resonance imaging,” *Journal of Neurology, Neurosurgery & Psychiatry*, vol. 75, no. 1, pp. 6–12, 2004.

[86] S. D. Goode, S. Krishan, C. Alexakis, R. Mahajan, and D. P. Auer, “Precision of cerebrovascular reactivity assessment with use of different quantification methods for hypercapnia functional MR imaging,” *American Journal of Neuroradiology*, vol. 30, no. 5, pp. 972–977, 2009.

[87] K. Murphy, A. D. Harris, and R. G. Wise, “Robustly measuring vascular reactivity differences with breath-hold: Normalising stimulus-evoked and resting state BOLD fMRI data,” *NeuroImage*, vol. 54, no. 1, pp. 369–379, 2011.

[88] J. Pinto, J. Jorge, I. Sousa, P. Vilela, and P. Figueiredo, “Fourier modeling of the BOLD response to a breath-hold task: Optimization and reproducibility,” *NeuroImage*, vol. 135, pp. 223–231, 2016.

[89] H. A. Kontos, E. P. Wei, A. Jarrell Raper, and J. L. Patterson, “Local mechanism of CO2 action on cat pial arterioles,” *Stroke*, vol. 8, no. 2, pp. 226–229, 1977.

[90] R. F. Leoni, K. C. Mazzetto-Betti, A. C. Silva, A. C. dos Santos, D. B. de Araujo, J. P. Leite, and O. M. Pontes-Neto, “Assessing Cerebrovascular Reactivity in Carotid Steno-Occlusive Disease Using MRI BOLD and ASL Techniques,” *Radiology Research and Practice*, vol. 2012, pp. 1–10, 2012.

[91] F. C. Moreton, K. A. Dani, C. Goutcher, K. O'Hare, and K. W. Muir, "Respiratory challenge MRI: Practical aspects," *NeuroImage: Clinical*, vol. 11, pp. 667–677, 2016.

[92] J. Fierstra, O. Sobczyk, A. Battisti-Charbonney, D. M. Mandell, J. Poublanc, A. P. Crawley, D. J. Mikulis, J. Duffin, and J. A. Fisher, "Measuring cerebrovascular reactivity: What stimulus to use?" *Journal of Physiology*, vol. 591, no. 23, pp. 5809–5821, 2013.

[93] P. Liu, C. Xu, Z. Lin, S. Sur, Y. Li, S. Yasar, P. Rosenberg, M. Albert, and H. Lu, "Cerebrovascular reactivity mapping using intermittent breath modulation," *NeuroImage*, vol. 215, no. April, p. 116787, 2020.

[94] S. Moia, R. C. Stickland, A. Ayyagari, M. Termenon, C. Caballero-Gaudes, and M. G. Bright, "Voxelwise optimization of hemodynamic lags to improve regional CVR estimates in breath-hold fMRI," *Proceedings of the Annual International Conference of the IEEE Engineering in Medicine and Biology Society, EMBS*, vol. 2020-July, pp. 1489–1492, 2020.

[95] F. B. Tancredi and R. D. Hoge, "Comparison of cerebral vascular reactivity measures obtained using breath-holding and CO 2 inhalation," *Journal of Cerebral Blood Flow and Metabolism*, vol. 33, no. 7, pp. 1066–1074, 2013.

[96] E. Prisman, M. Slessarev, J. Han, J. Poublanc, A. Mardimae, A. Crawley, J. Fisher, and D. Mikulis, "Comparison of the effects of independently-controlled end-tidal PCO_2 and PO_2 on Blood Oxygen Level-Dependent (BOLD) MRI," *Journal of Magnetic Resonance Imaging*, vol. 27, no. 1, pp. 185–191, 2008.

[97] M. G. Bright, M. J. Donahue, J. H. Duyn, P. Jezzard, and D. P. Bulte, "The effect of basal vasodilation on hypercapnic and hypocapnic reactivity measured using magnetic resonance imaging," *Journal of Cerebral Blood Flow and Metabolism*, vol. 31, no. 2, pp. 426–438, 2011.

[98] F. Geranmayeh, R. J. Wise, R. Leech, and K. Murphy, "Measuring vascular reactivity with breath-holds after stroke: A method to aid interpretation of group-level BOLD signal changes in longitudinal fMRI studies," *Human Brain Mapping*, vol. 36, no. 5, pp. 1755–1771, 2015.

[99] R. C. Stickland, K. M. Zvolanek, S. Moia, A. Ayyagari, C. Caballero-Gaudes, and M. G. Bright, "A practical modification to a resting state fMRI protocol for improved characterization of cerebrovascular function," *NeuroImage*, vol. 239, 2021.

[100] M. Jenkinson and M. Chappell, *Short Introduction to the General Linear Model for Neuroimaging*. Oxford University Press, 2018.

[101] ——, *Introduction to Neuroimaging Analysis*. Oxford University Press, 2018.

[102] R. M. Birn, M. A. Smith, T. B. Jones, and P. A. Bandettini, "The respiration response function: The temporal dynamics of fMRI signal fluctuations related to changes in respiration," *Neuroimage*, vol. 40, no. 2, pp. 644–654, 2008.

[103] K. M. Vogt, J. W. Ibinson, P. Schmalbrock, and R. H. Small, "Comparison between end-tidal CO2 and respiration volume per time for detecting BOLD signal fluctuations during paced hyperventilation," *Magnetic Resonance Imaging*, vol. 29, no. 9, pp. 1186–1194, 2011.

[104] S. S. Kannurpatti, M. A. Motes, B. Rypma, and B. B. Biswal, "Increasing measurement accuracy of age-related BOLD signal change: Minimizing vascular contributions by resting-state-fluctuation-of-amplitude scaling," *Human Brain Mapping*, vol. 32, no. 7, pp. 1125–1140, 2011.

[105] C. Chang, M. E. Thomason, and G. H. Glover, "Mapping and correction of vascular hemodynamic latency in the BOLD signal," *NeuroImage*, vol. 43, no. 1, pp. 90–102, 2008.

[106] C. H. B. van Niftrik, M. Piccirelli, O. Bozinov, A. Pangalu, A. Valavanis, L. Regli, and J. Fierstra, "Fine tuning breath-hold-based cerebrovascular reactivity analysis models," *Brain and Behavior*, vol. 6, no. 2, pp. 1–13, 2016.

[107] M. Silvestrini, L. M. Cupini, E. Troisi, M. Matteis, and G. Bernardi, "Estimation of cerebrovascular reactivity in migraine without aura," *Stroke*, vol. 26, no. 1, pp. 81–83, 1995.

[108] F. Sakai and J. S. Meyer, "Abnormal Cerebrovascular Reactivity in Patients with Migraine and Cluster Headache," *Headache: The Journal of Head and Face Pain*, vol. 19, no. 5, pp. 257–266, 1979.

[109] C. Harer and R. Kummer, "Cerebrovascular CO_2 reactivity in migraine: assessment by transcranial Doppler ultrasound," *Journal of Neurology*, vol. 238, pp. 23–26, 1991.

[110] R. Ornello, I. Frattale, V. Caponnetto, F. Pistoia, and S. Sacco, "Cerebral vascular reactivity and the migraine-stroke relationship: A narrative review," *Journal of the Neurological Sciences*, vol. 414, no. May, 2020.

[111] S. Harris and A. Rasyid, "Objective Diagnosis of Migraine without Aura with Migraine Vascular Index: A Novel Formula to Assess Vasomotor Reactivity," *Ultrasound in Medicine and Biology*, vol. 46, no. 6, pp. 1359–1364, 2020.

[112] A. Podgorac, I. Petrušić, A. Radojičić, and J. Zidverc-Trajković, "Breath holding index in episodic primary headaches," *Vojnosanitetski Pregled*, vol. 75, no. 4, pp. 347–351, 2018.

[113] H. M. El-Khawas, A. S. Shalash, A. M. Said, and R. G. Zaki, "Multimodal visual functions and cerebrovascular reactivity in migraine patients between attacks," *Egyptian Journal of Neurology, Psychiatry and Neurosurgery*, vol. 47, no. 4, pp. 655–664, 2010.

[114] A. Arjona, L. A. P. D. Torres, and P. J. Serrano-castro, “Letter to the Editor Diagnosis of Broncho-Pleural Fistula: Is There a Role for Sonography?” 2007.

[115] M. Silvestrini, R. Baruffaldi, M. Bartolini, F. Vernieri, C. Lanciotti, M. Matteis, E. Troisi, and L. Provinciali, “Basilar and Middle Cerebral Artery Reactivity in Patients with Migraine,” *Headache*, vol. 44, no. 1, pp. 29–34, 2004.

[116] B. Dora and S. Balkan, “Exaggerated interictal cerebrovascular reactivity but normal blood flow velocities in migraine without aura,” *Cephalalgia*, vol. 22, no. 4, pp. 288–290, 2002.

[117] A. Kastrup, C. Thomas, C. Hartmann, and M. Schabet, “Cerebral blood flow and CO_2 reactivity in interictal migraineurs: a transcranial Doppler study,” *Headache*, vol. 38, no. 8, pp. 608–613, 1998.

[118] R. Totaro, C. Marini, G. Matteis, M. Napoil, and A. Carolei, “Cerebrovascular reactivity in migraine during headache-free intervals,” *Cephalalgia*, vol. 17, no. 3, pp. 191–194, 1997.

[119] A. Valikovics, L. Oláh, B. Fulesdi, Z. Káposzta, A. Ficzere, D. Bereczki, and L. Csiba, “Cerebrovascular reactivity measured by transcranial Doppler in migraine,” *Headache*, vol. 36, no. 5, pp. 323–328, 1996.

[120] G. Fiermonte, F. Pierelli, F. Pauri, F. I. Cosentino, R. Soccorsi, and P. Giacomini, “Cerebrovascular CO2 reactivity in migraine with aura and without aura. A transcranial doppler study,” *Acta Neurologica Scandinavica*, vol. 92, no. 2, pp. 166–169, 1995.

[121] L. L. Thomsen, H. K. Iversen, and J. Olesen, “Increased Cerebrovascular pCO_2 Reactivity in Migraine with Aura- a Transcranial Doppler Study During Hyperventilation,” *Cephalalgia*, vol. 15, no. 3, pp. 211–215, 1995.

[122] C. P. Zwetsloot, J. F. Caekebeke, J. C. Jansen, J. Odink, and M. D. Ferrari, “Blood flow velocities in the vertebrobasilar system during migraine attacks - A transcranial Doppler study,” *Cephalalgia*, vol. 12, no. 1, pp. 29–32, 1992.

[123] C. P. Zwetsloot, J. F. Caekebeke, J. Odink, and M. D. Ferrari, “Vascular Reactivity During Migraine Attacks: A Transcranial Doppler Study,” *Headache: The Journal of Head and Face Pain*, vol. 31, no. 9, pp. 593–595, 1991.

[124] A. Kastrup, V. Happe, C. Hartmann, and M. Schabet, “Gender-related effects of indomethacin on cerebrovascular CO_2 reactivity,” *Journal of the Neurological Sciences*, vol. 162, no. 2, pp. 127–132, 1999.

[125] R. A. Poldrack, J. A. Mumford, and T. E. Nichols, *Handbook of funtional MRI data analysis*. Cambridge University Press, 2011.

[126] “Improved Optimization for the Robust and Accurate Linear Registration and Motion Correction of Brain Images,” *NeuroImage*, vol. 17, no. 2, pp. 825–841, 2002.

[127] S. M. Smith and J. M. Brady, “SUSAN - A new approach to low level image processing,” *International Journal of Computer Vision*, vol. 23, no. 1, pp. 45–78, 1997.

[128] J. M. Soares, R. Magalhães, P. S. Moreira, A. Sousa, E. Ganz, A. Sampaio, V. Alves, P. Marques, and N. Sousa, “A Hitchhiker’s guide to functional magnetic resonance imaging,” *Frontiers in Neuroscience*, vol. 10, no. November, pp. 1–35, 2016.

[129] “Donahue lab,” https://www.vumc.org/donahue-lab/software.

[130] R. B. Buxton, “Introduction to Functional Magnetic Resonance Imaging: Principles and Techniques,” *Cambridge University Press*, 2009.

[131] A. Kastrup, T.-q. Li, A. Takahashi, G. H. Glover, and M. E. Moseley, “Short Communications Cerebral Blood Oxygenation Changes,” pp. 2641–2645, 1998.

[132] F. H. Van der Zande, P. A. Hofman, and W. H. Backes, “Mapping hypercapnia-induced cerebrovascular reactivity using BOLD MRI,” *Neuroradiology*, vol. 47, no. 2, pp. 114–120, 2005.

[133] A. Cohen and Y. Wang, “Improving the assessment of breath-holding induced cerebral vascular reactivity using a multiband multi-echo asl/bold sequence,” *Scientific Reports*, vol. 9, p. 5079, 03 2019.

Appendix A

Annex 1

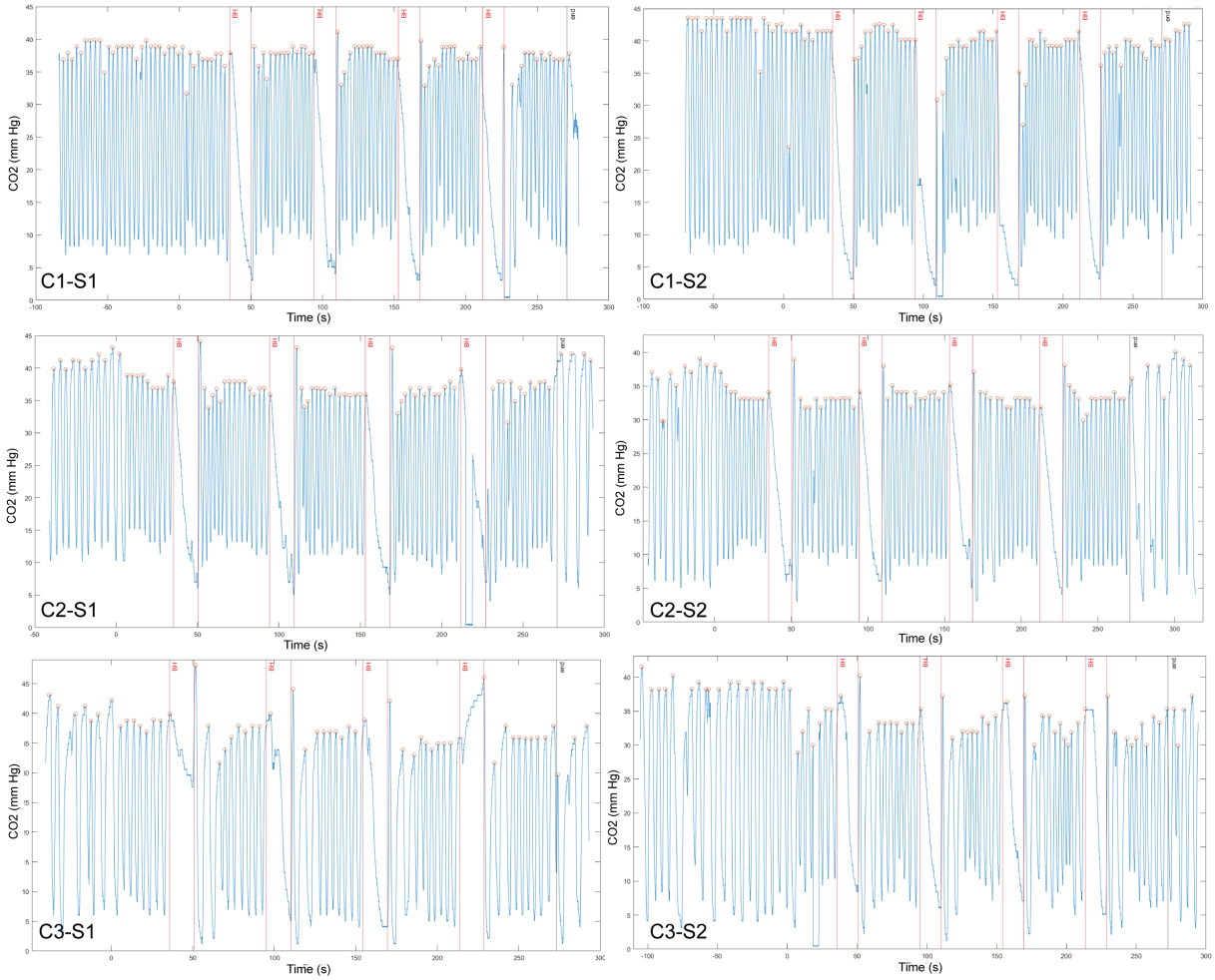

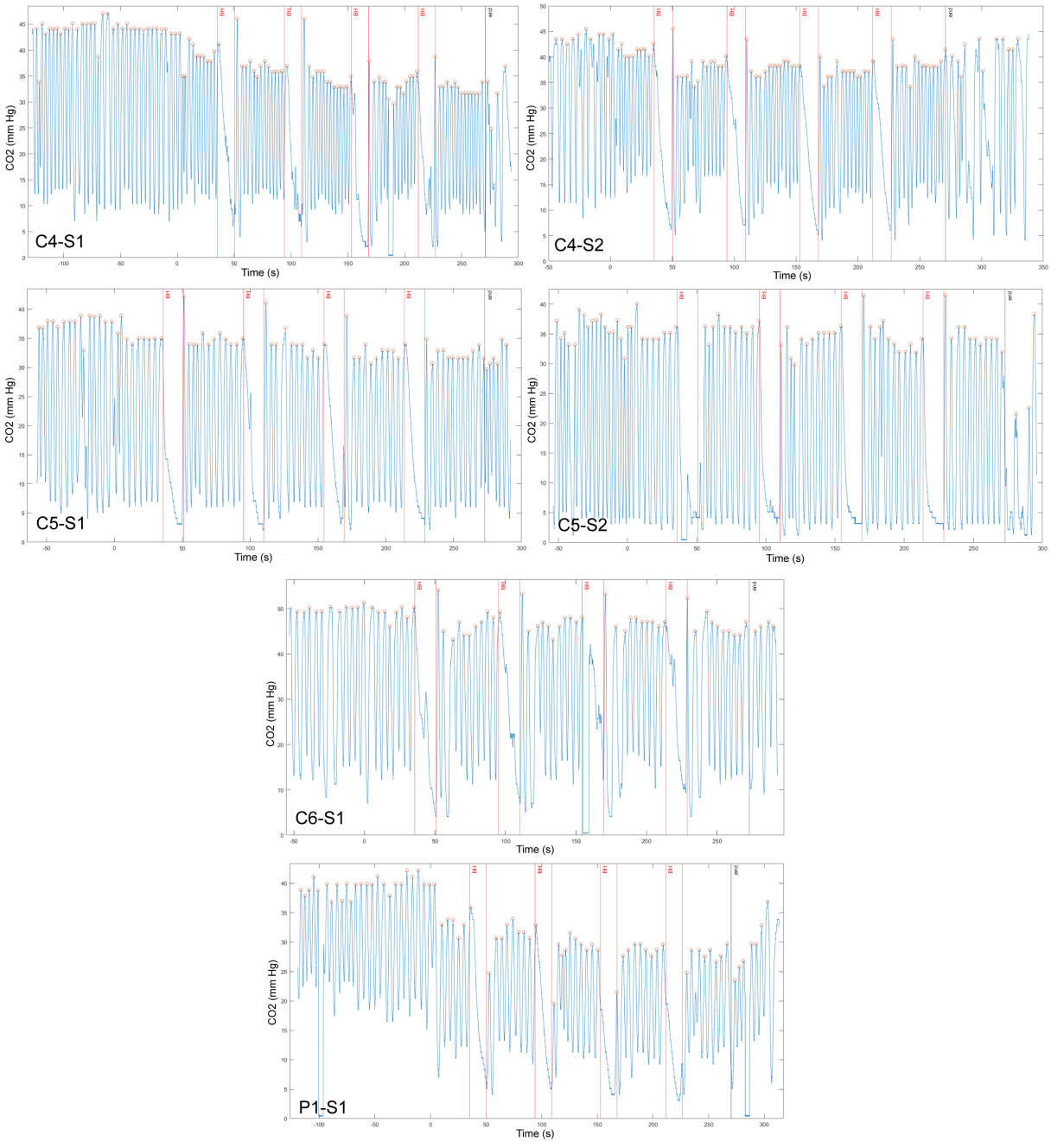
C4-S1
C4-S2
C5-S1
C5-S2
C6-S1
P1-S1
CO2 (mm Hg)
Time (s)
BH
BHL
end

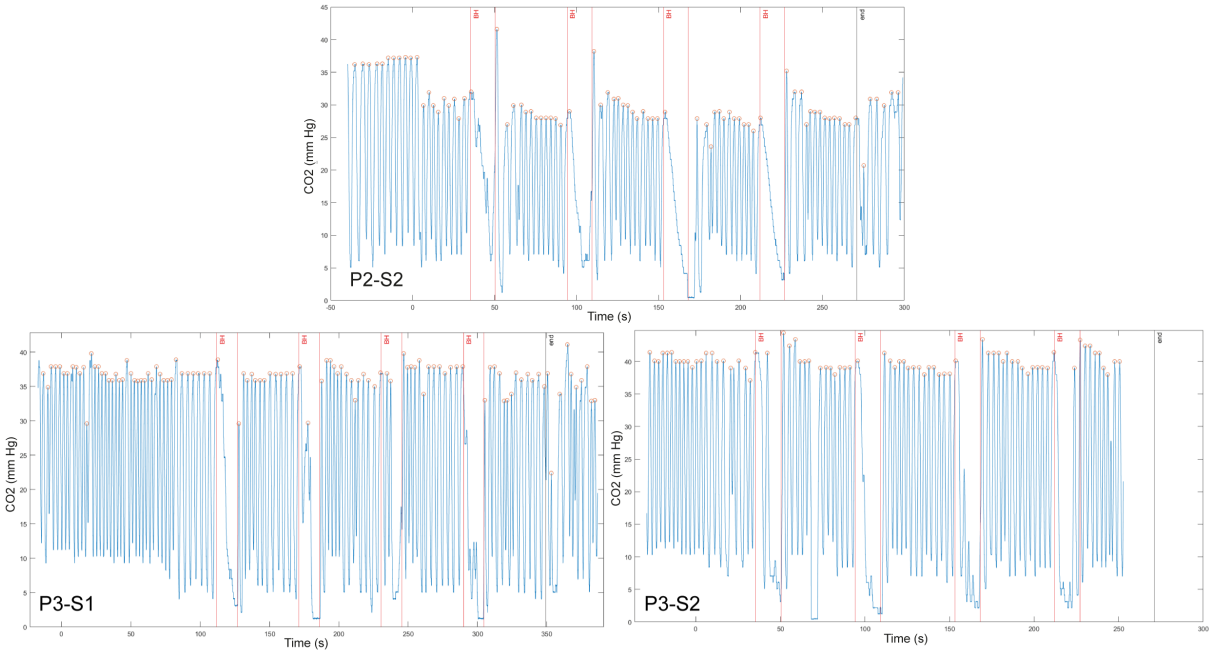

Figure A.1: CO_2 signal (mm Hg) recorded during the BH BOLD-fMRI corrected for the delay introduced by the tubing system, for each participant and session. C1-S2, P1-S1 and P2-S2 obtained low quality CO_2 traces and so were excluded from further $PetCO_2$ analysis. Lines in red represent the BH periods according to the instructions' timings given and the ones in black the end of the task. C: controls; P: patients; S1: premenstrual/ictal session; S2: midcycle/interictal session (for controls/patients)

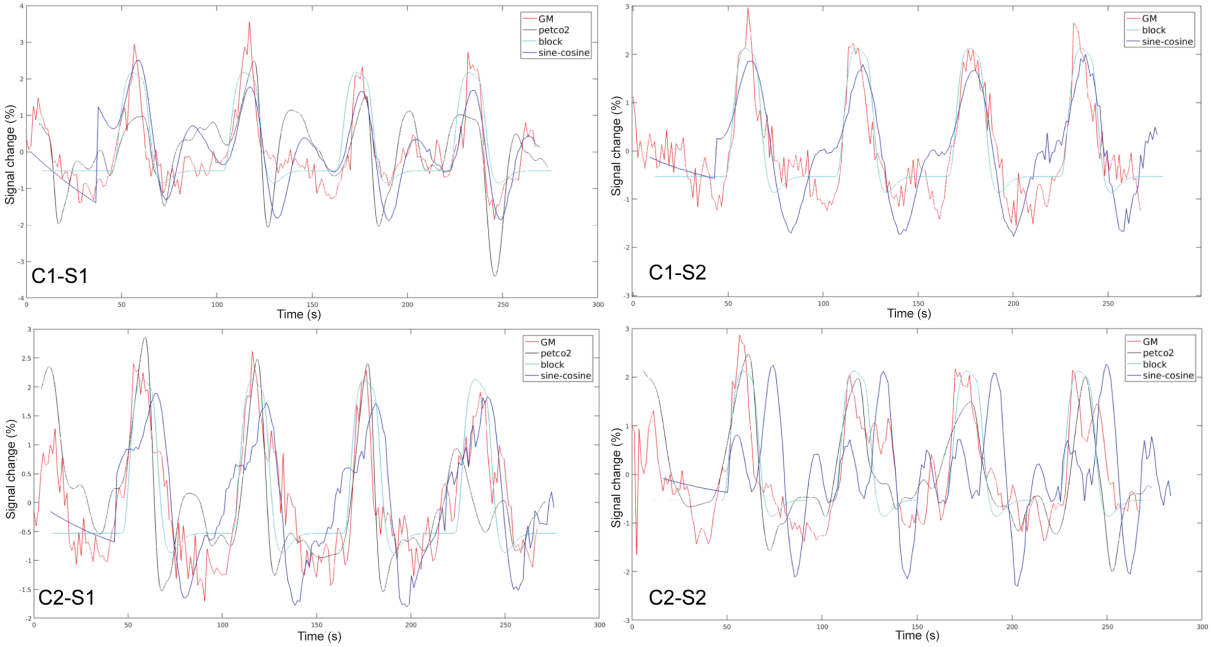

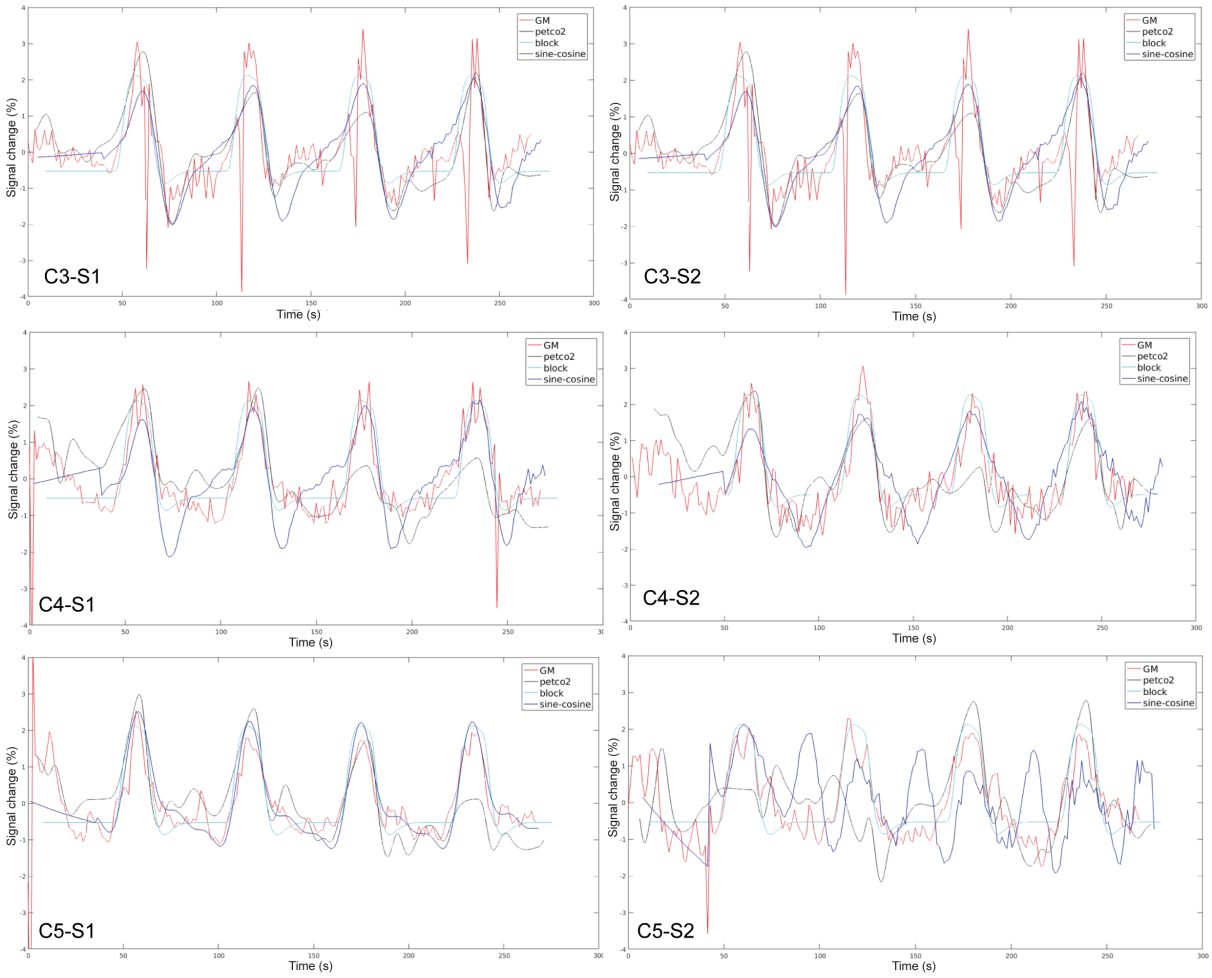
GM
petco2
block
sine-cosine
Signal change (%)
Time (s)
C3-S1
C3-S2
C4-S1
C4-S2
C5-S1
C5-S2

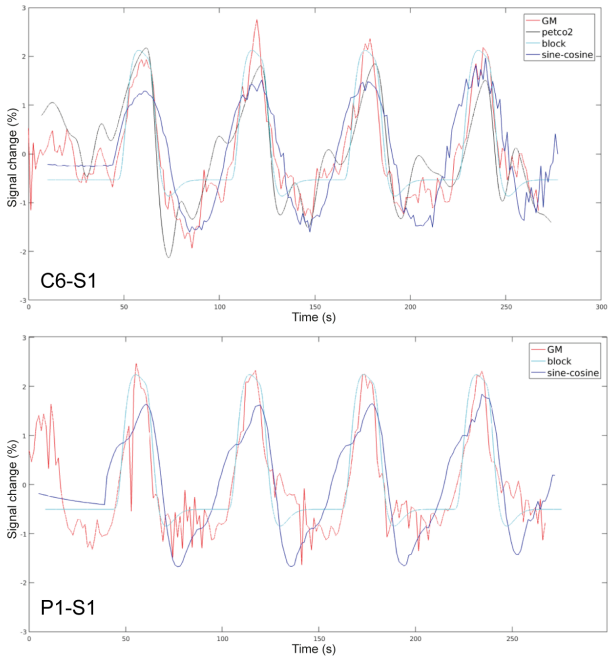
GM
petco2
block
sine-cosine
Signal change (%)
Time (s)
C6-S1
P1-S1

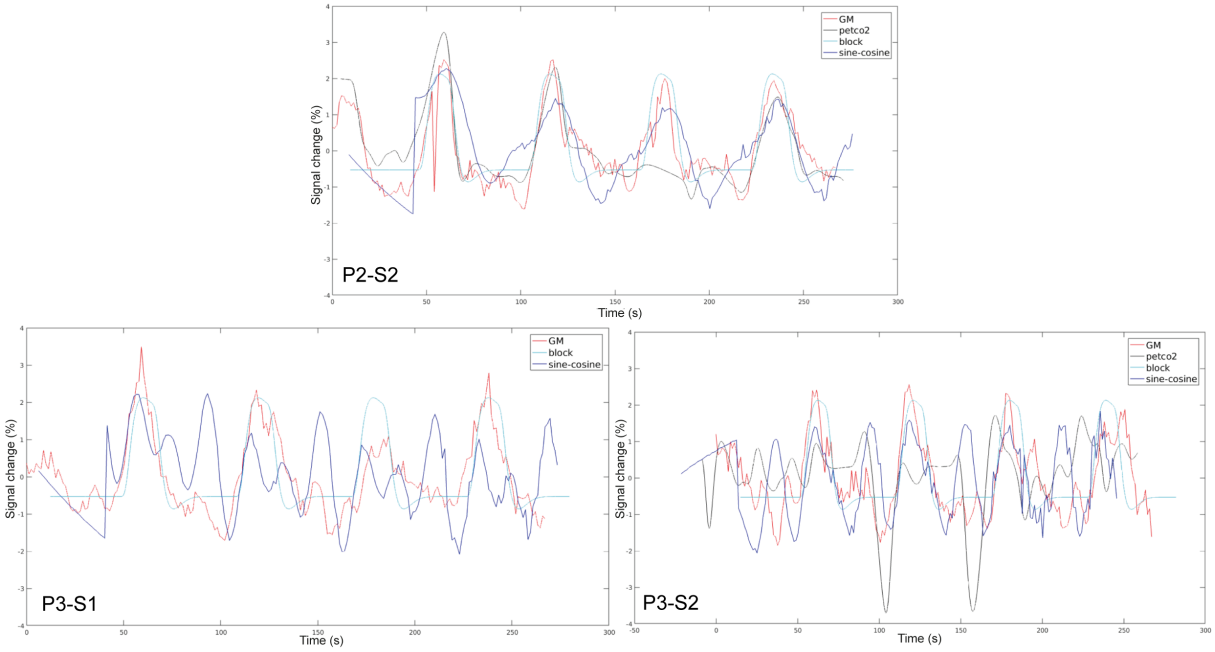

Figure A.2: Regressors $PETCO_2$, block and the mean sine-cosine model aligned with the GM BOLD-fMRI mean time course according to the maximum correlation between each regressor and the GM, for each participant and session (GM in red, $PETCO_2$ in black, block in cyan and sine-cosine in blue). C: controls; P: patients; S1: premenstrual/ictal session; S2: midcycle/interictal session (for controls/patients)